(2)

MISCELLANEOUS PAPER CERC-91-

PRELIMINARY ESTIMATES OF FREQUENCY-DIRECTION SPECTRA DERIVED FROM THE SAMSON PRESSURE GAGE ARRAY NOVEMBER 1990 TO MAY 1991

by

Charles E. Long

Coastal Engineering Research Center

DEPARTMENT OF THE ARMY
Waterways Experiment Station, Corps of Engineers
3909 Halls Ferry Road, Vicksburg, Mississippi 39180-6199

Robert T. Guza and Thomas H. C. Herbers

Center for Coastal Studies

Scripps Institution of Oceanography
University of California, San Diego
La Jolla, California 92093-0209

and

Joan M. Oltman-Shay

Applied Physics Division
Quest Integrated, Inc.
21414 68th Avenue South
Kent, Washington 98032

September 1991
Draft Report

Prepared for DEPARTMENT OF THE ARMY
US Army Corps of Engineers
Washington, DC 20314-1000
Under Civil Works Research Work Unit 32484

ABSTRACT

In the course of the SAMSON (Sources of Ambient Micro-Seismic Noise) Experiment conducted by researchers from Scripps Institution of Oceanography at the Coastal Engineering Research Center (CERC) Field Research Facility (FRF) near Duck, NC, a two-dimensional array of 24 bottom-mounted pressure sensors was deployed near the 13-m depth contour to detect the attenuated pressure signal arising from the interaction of directionally opposed wave trains.

The geometry of the array was ideal for wind wave directional spectral estimation in the 0.05 to 0.24 Hz frequency band. The formal SAMSON experiment took place in October and early November 1990, but data collection continued until June 1991. Data from this post-experiment period were made available to CERC and were subsequently processed with a 360-degree Maximum Likelihood Estimation algorithm to determine the general character of the local wave field, including specifically any indications of significant seaward-propagating wind wave energy.

This report contains a description of the SAMSON array, the type of data collected, and the analysis algorithm. It contains displays, both graphic and tabular, of relevant wind wave parameters deduced from the analysis. A means of acquiring the processed data, available to the general public after June 1994, is also described.

Key Words: Frequency-direction spectra
Maximum Likelihood Estimation
Wave climate
Wind waves

Preface

This paper provides a summary of a series of wind-wave frequency-direction spectral observations made with a two-dimensional, high-resolution directional wave gage of opportunity, being the result of data shared by researchers from Scripps Institution of Oceanography (SIO) in execution of the SAMSON experiment. The work was motivated by an opportunity to conduct a 360-degree analysis of data from a 24-gage array ~~and thus find an extraordinary observation set of directionally distributed wave energy~~ to augment understanding and modeling of nearshore processes which affect coastal engineering projects. This effort was authorized by Headquarters, US Army Corps of Engineers (HQUSACE), under Civil Works Research Work Unit 32484, Directionality of Waves in Shallow Water, Coastal Flooding Program. Funds were provided through the Coastal Engineering Research Center (CERC), US Army Engineer Waterways Experiment Station (WES), under the program management of Mr. Charles C. Calhoun, CERC. Messrs. John H. Lockhart, Jr.; John G. Housley; Robert H. Campbell; and James E. Crews were HQUSACE Technical Monitors.

This data summary was prepared by Dr. Charles E. Long at CERC's Field Research Facility (FRF) in Duck, NC, under the direct supervision of Mr. William A. Birkemeier, Chief, FRF, and Mr. Thomas W. Richardson, Chief, Engineering Development Division, CERC; and under the general supervision of Dr. James R. Houston and Mr. Charles C. Calhoun, Jr., Chief and Assistant Chief, CERC, respectively.

The SAMSON experiment, including the directional array, was planned and executed by Drs. Robert T. Guza and Thomas H. C. Herbers of SIO. Data processing and testing software was written by Dr. Joan M. Oltman-Shay of QUEST Integrated, Inc., Seattle, WA. The concept of continued data collection after the primary SAMSON experiment is credited to Dr. C. Linwood Vincent, CERC. This document was edited by Ms. Lee Byrne, Information Technology Laboratory, WES.

Commander and Director of WES during the publication of this report was COL Larry B. Fulton, EN. Dr. Robert W. Whalin was Technical Director.

Contents

PRELIMINARY ESTIMATES OF FREQUENCY-DIRECTION SPECTRA DERIVED FROM THE SAMSON PRESSURE GAGE ARRAY, NOVEMBER 1990 TO MAY 1991

Introduction

1. During October and early November 1990, an experiment involving the detection of interacting wave trains was conducted at the Coastal Engineering Research Center (CERC) Field Research Facility (FRF). Known as SAMSON (Sources of Ambient Micro-Seismic Ocean Noise), the experiment was designed to detect relatively unattenuated near-bottom pressure signals arising from nonlinear interactions of wind wave trains traveling in opposing directions. These small but detectable pressure signals are believed to initiate ocean bottom seismic waves that can propagate long distances and appear frequently in seismograms worldwide. In detecting both presence of interacting wave trains and resulting pressure signals, results of the SAMSON experiment can be used to test hypotheses concerning the initiation of such seismic waves near a coast where nearshore bathymetry can act as a partial reflector of ocean wind waves and thereby induce the requisite opposing wave trains. The experiment was designed and executed under the direction of Drs. Robert T. Guza and Thomas H. C. Herbers of the Center for Coastal Studies (CCS) at Scripps Institution of Oceanography (SIO), University of California, San Diego (UCSD), with experiment site, staging area and logistical support provided by the FRF.

2. The primary instrument in the SAMSON experiment was a two-dimensional array of 24 bottom-mounted pressure gages located in a nominal water depth of 13 m. By design, this depth is deeper than is normally used for measurement of ocean wind waves. The idea was to let the water column act as a filter for pressure signals arising directly from wind waves above a certain cut-off frequency. In that way, any detectable pressure signal above the cut-off frequency could be interpreted as being from the wave-wave interactions sought in the experiment. At frequencies below the cut-off, the pressure gages could readily detect wind wave signals. As a result, the array of gages was an excellent directional detector for waves in the lower part of the wind wave frequency band, from about 0.05 to 0.24 Hz.

3. The SAMSON pressure gage array was deployed in September 1990 and the formal experiment took place in October and early November. Scheduling

recovery of the gages immediately after the experiment was deemed unwise because of the onset of winter and the high likelihood of poor working conditions. Hence, the gages were left in place until the following spring and, because it was a fully functioning instrument set, data were collected for as long as the gages continued to function, though this was not expected to be for very long given the harshness of the environment, ~~in which they were deployed.~~ ~~Curiously~~ Fortunately, 22 of the 24 gages continued to function perfectly until the first part of June 1991, at which time the gages were recovered. Data from this post-experiment phase of instrument deployment, mid-November 1990 to the end of May 1991, have been made available to the FRF for directional analysis. This report addresses the ~~nature~~ analysis methods and results ~~of that analysis~~.

4. Because of the volume of data involved, considerable time has been saved by performing a preliminary, fairly rudimentary analysis to obtain the general character of the observed directional energy distributions, as described by a few simple parameters. More detailed analysis can be performed at a later date on individual cases or sequences of cases that are of most interest. The high-resolution directional estimation algorithm known as Maximum Likelihood Estimation (MLE) (Davis and Regier, 1977) is used here for the preliminary analysis because it is rather quick to compute and is adequate to describe the general directional nature of the observations. A more refined but more time-consuming algorithm, such as Iterative Maximum Likelihood Estimation (IMLE) (Pawka, 1983), can be used later to increase resolution on select cases.

5. Because the SAMSON array is two-dimensional, it can detect wave energy propagating in any direction. This allows estimation of energy propagating seaward and avoids the 180-degree ambiguity present in analysis of data from the FRF linear array directional wave gage reported previously (Long and Oltman-Shay 1991, Long 1991a, 1991b). In this report, seaward propagating energy is called "reflected" energy because reflections of incident waves from nearshore bathymetry is its most likely cause, ~~though other processes may possibly be present~~ given the short fetch between shore and the array. Determination of reflected directional spectra is of enormous interest in coastal research because of myriad processes that are possible theoretically if significant reflection is present. Hence, this report is the first to describe a well-resolved estimation of the full 360-degree wave climate at the FRF.

6. The beginning text of this document describes and clarifies the substantial information contained in the appendices. A brief overview is given of the measurement site, instrumentation, data collection, and method of directional spectral estimation. These subjects are described in other publications to which the reader is referred for greater detail. Following the overview is a description of the archived frequency-direction spectra and some characterizing bulk parameters that can be derived from them. Appendix A is a listing of these characterizing parameters and is intended to be used as a kind of catalog of the set of spectra. Appendix B contains graphs of time series of some of these parameters as a pictorial augmentation of the information in Appendix A. Appendix C is a derivation of the MLE used in this analysis. It is intended to augment the somewhat brief derivations normally found in the literature, and thereby perhaps augment the reader's understanding of this method of directional estimation.

Measurement Site

7. As shown in Figure 1, the FRF is located on the barrier island chain of coastal North Carolina. A detailed description of the layout, function, and capabilities of the FRF is given by Birkemeier et al. (1985). A detailed, quantitative description of the climate at the FRF, as determined from its arsenal of instrumentation and for the ten years of its existence, is given by Leffler et al. (1990). Of particular relevance to directional wave studies are the wave-steering bathymetry and wave-generating winds.

8. As regards the former, the coastline in the vicinity of the FRF is nearly straight for several tens of kilometers north and south (Figure 1). It is oriented such that a shore-normal line (directed seaward) is very nearly 70 deg from true north. Waves and onshore winds can approach this site along an easterly 180-deg arc from 340 to 160 deg true. The adjacent continental shelf is wide, relatively shallow, and of somewhat complex bathymetry. The direction of nearest approach of the 100-m isobath, which indicates the shelf break, is 10 to 15 deg south of east and is about 80 km distant. A typical bottom slope for the shelf is 1 m/km, but this is interrupted by numerous features of 1- to 10-km horizontal scales and 10-m vertical scales scattered irregularly across the shelf.

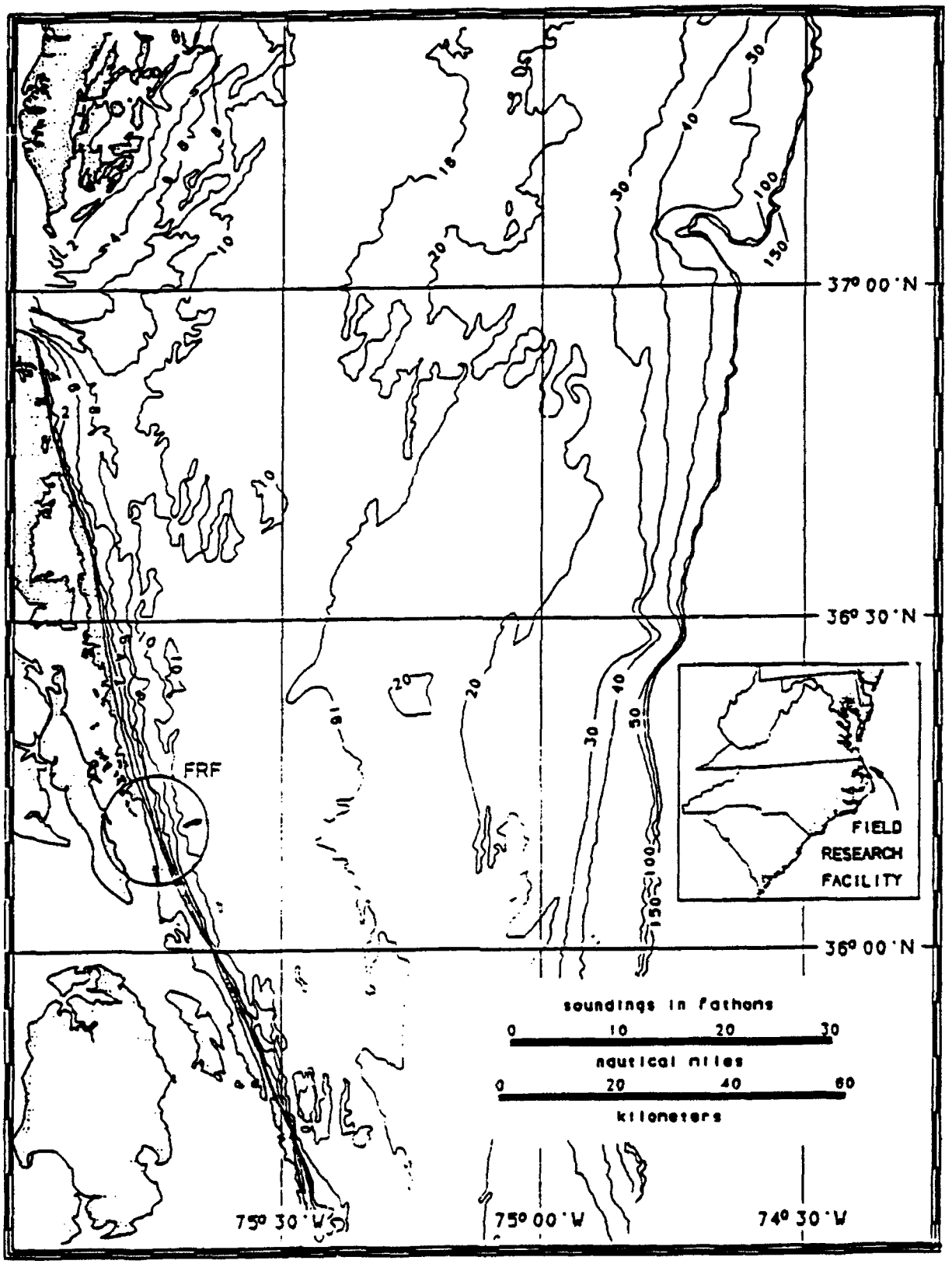

Figure 1. Location and offshore bathymetry of the FRF

9. Within a few kilometers of the FRF, the offshore bathymetry is more regular, with isobaths nearly shore-parallel and a bottom slope of about 2 m/km (Figure 2). Some irregularities exist. Within about 300 m of the shore, there exists a complex and mobile bar system (Birkemeier 1984). Waves and currents have created some irregular bathymetry in the vicinity of the FRF research pier which extends about 600 m offshore (Miller, Birkemeier, and DeWall 1983).

10. The site is subject to a variety of climates which gives rise to a diverse set of directional wave conditions. Primary sources of high-energy waves are winds associated with hurricanes and frontal passages. Though Hurricane Lily moved up the middle Atlantic Ocean during the formal SAMSON experiment, no other hurricanes affected the FRF wave climate in the period covered by this report. Low-pressure weather fronts, of which several crossed

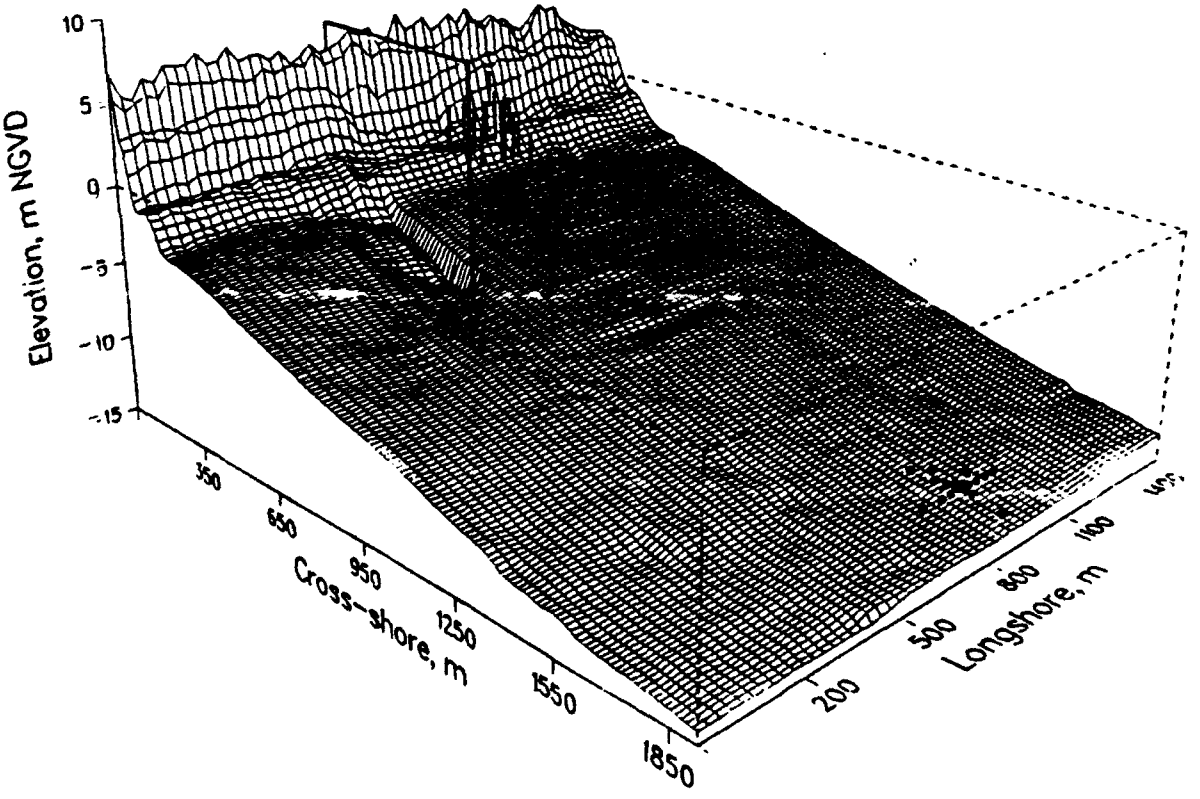

Figure 2. Approximate nearshore bathymetry and SAMSON array location (seawardmost set of dots)

the FRF site during this reporting period, were typically oriented northeast-southwest, with strong wave-generating winds coming from the northeast.

11. As a consequence of the complex offshore bathymetry and the close proximity of wave-generating wind systems, it is expected that directional wave spectra will exhibit a rather broad, complex structure. This expectation has been realized in studies at the FRF using a linear array directional wave gage in 8 m water depth (Long and Oltman-Shay, 1991). Excepting well-sorted waves from distant storms and waves in the initial growth stages under strong steady local winds, most directional spectra were found to be rather broad. Because of the 180-degree ambiguity inherent in a linear array, it is possible that part of this broadness could be due to reflected wave energy, which is folded over to appear as incident wave energy in the linear array data processing algorithm. The ability to perform a 360-degree wave analysis with the SAMSON array will help to ascertain the extent of the error induced by the 180-degree ambiguity of the linear array, in addition to estimating the amount of seaward propagating energy.

Instrumentation

12. The primary instrument in this study was a high-resolution, two-dimensional array directional wave gage. It consisted of two parts. The first was an array of sensors that sampled sea-surface displacement at several points in (horizontal) space. The second, described in the following section on data processing and in Appendix C, is the mathematical treatment of these data to obtain estimates of wave directionality.

Basic array

13. The SAMSON array consisted of 24 pressure gages buried about 0.1 m below the bottom in the vicinity of the 13-m isobath about 1700 m offshore and slightly to the north of the research pier. This is shown in Figure 2 as the seawardmost set of dots. ~~In addition to the design requirements mentioned above,~~ Its location satisfies three constraints. First, it is generally outside the surf zone so that linear wave theory is applicable in data processing. Second, it is in water shallow enough that signals from 4-sec waves are detectable above background noise at the bottom-mounted gages. Third, it is away from the irregular isobaths around the pier and in the

nearshore bar system, which helps minimize bathymetrically induced inhomogeneities in the wave field.

14. Figure 3 is an enlarged view of the array layout and shows gage spacing as well as the gage numbering scheme. Spacing between the gages in the array corresponds reasonably well to the array-design criterion posed by Davis and Regier (1977) that every gage pair have a unique separation or spatial lag. There are a large number of redundant lags built into the array so that multiple estimates of cross-spectral densities can be made to check

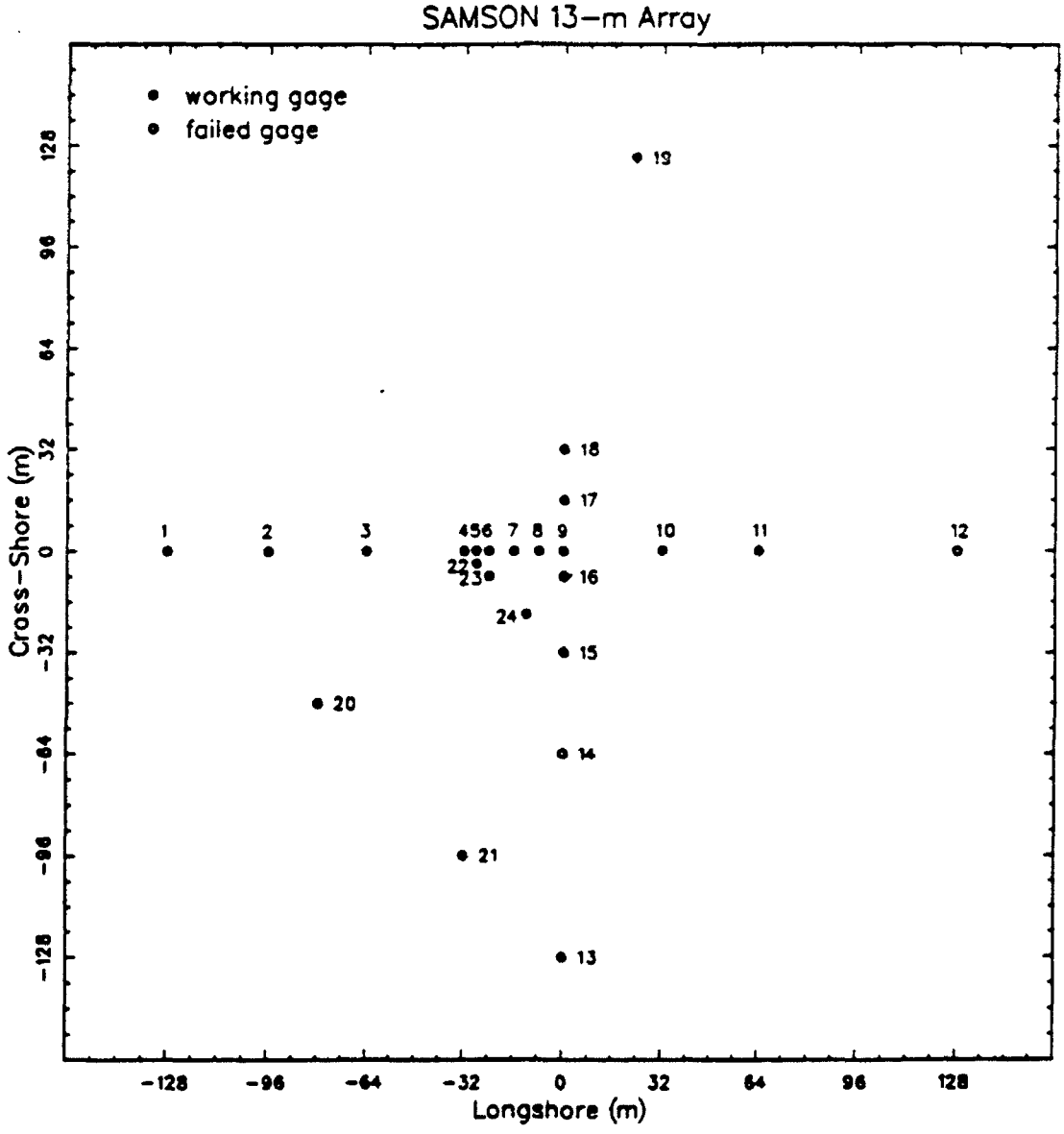

Figure 3. Layout and numbering scheme for SAMSON array

for spatial inhomogeneity in the wave field and to reduce system noise. There are a much greater number of unique lags with which to fill in the spatial cross-spectral matrix from which wave direction estimates are made. Minimum gage spacing is 4 m, maximum spacing (the greatest dimension of the array) is 256 m, and intermediate gage spacings are in multiples of 4 m. Unfortunately, gages 12 and 14 were inoperative, and the loss of gage 12 reduced the long-shore dimension of the array to 192 m, at some cost to direction resolving ability for the longest (0.05 Hz) waves measured. It is noted that gage 19 appears to be offline from the basic gage pattern, and it was, in fact, slightly misplaced. However, this does not make it ineffective. In MLE processing, it is only necessary for the true gage positions to be known, and not that they conform to any particular pattern. The SAMSON gage positions were surveyed to an accuracy of better than 1 m after the gages were in place. At worst, this uncertainty would result in an error of about 1.8 degrees for the shortest (0.24 Hz) waves considered and about 0.6 deg for the longest (0.05 Hz).

Sub-arrays

15. At sufficiently large lags, signals from a natural wave field tend to become uncorrelated. As a result, cross-spectra between widely spaced gages tend to become mostly noise. At very small lags, correlations and cross-spectra are difficult to discern from those at zero lag and so tend to become somewhat redundant. The terms large and small are generally related to the wavelengths of waves under consideration. To avoid both redundancy at small lags and the problem of noise at large lags, the SAMSON array data were processed by using subsets of gages, or sub-arrays, based on ranges of wavelengths being considered.

16. Figure 4 illustrates the sub-arrays and the ranges of wave frequency used with each sub-array used in the present analysis. Note that gages 12 and 14, from which reliable data were not obtained, are not shown. For the longest waves, all the working gages were used except those which introduced the shortest (4-m) lags, i.e., gages 5 and 22. This left 20 gages for processing data in the frequency f range $0.05 < f\ (\text{Hz}) < 0.10$ or wavelength λ range $103 < \lambda\ (\text{m}) < 220$ (assuming a nominal water depth of 13 m), and included the longest possible lags.

17. For shorter wavelengths, the selection criterion was that the longest dimension of the sub-array not exceed about three wavelengths of the

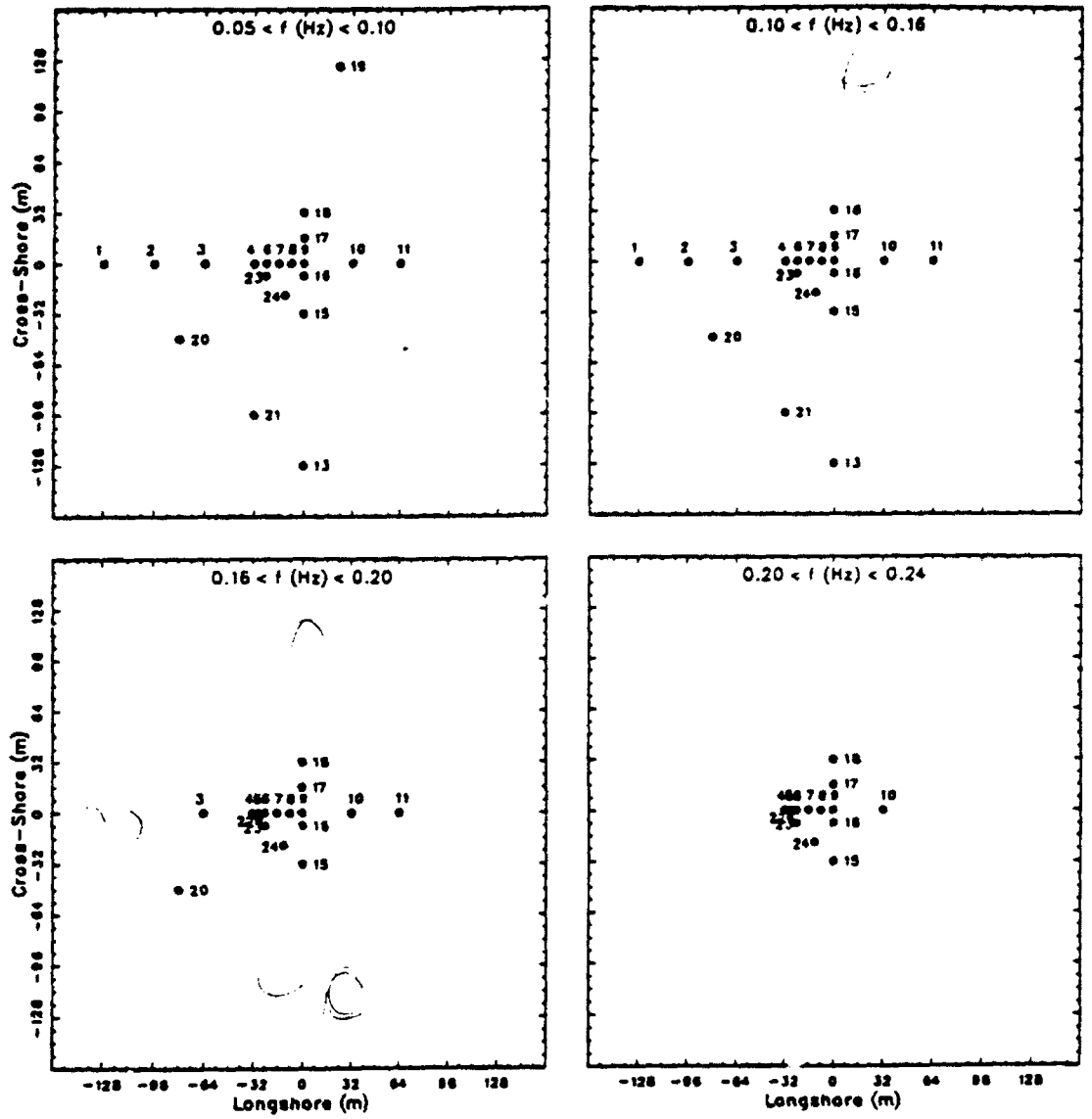

Figure 4. Sub-arrays and their associated frequency bands

shortest waves in a given band. For the low mid-range of frequencies, $0.10 < f\ (Hz) < 0.16$, corresponding to wavelengths $55 < \lambda\ (m) < 103$, this procedure eliminated gage 19 from analysis, leaving 19 gages in the sub-array. For the high mid-range of frequencies $0.16 < f\ (Hz) < 0.20$, or $38 < \lambda\ (m) < 55$, gages 1, 2, 13, and 21 were eliminated, but the short-lag gages 5 and 24 were included for a total of 17 gages. For the highest frequencies, $0.20 < f\ (Hz) < 0.24$, $27 < \lambda\ (m) < 38$, gages 3, 11, and 20 were excluded from the previous set, leaving 14 gages.

Pressure gages and data collection hardware

18. Each pressure gage is a Setra Systems Model 280E capacitive-type transducer having a range of 0 to 50 psia. The manufacturer's specifications indicate an accuracy of 0.11% of full scale or the pressure equivalent of ±0.037 m of water. Analog pressure signals were collected in an underwater terminal where they were discretized to 12-bit binary form, multiplexed, and encoded for transmission down a single data line. Digitization of the signal to 12-bit binary form resulted in a discretization uncertainty of the equivalent of 0.002 m of water. At the landward end of the data line, the encoded signal was decoded and sent to a parallel port on an AST 286 personal computer for data acquisition. During the post-experiment period, data files from the personal computer were periodically transferred to the higher-capacity hard disks of the FRF VAX 11/750 computer for accumulation and eventual archiving on magnetic media.

Data Collection

19. Signals from each of the 24 pressure gages were sampled at 4 Hz, and stored in records of 768 samples. A total of 1,280 records or 10,240 data points were collected for each gage for an elapsed time of 2 hr 50 min 40 sec for each collection. Starting times for collections during the main SAMSON experiment were daily at 0100, 0400, 0700, 1000, 1300, 1600, 1900, and 2200 Eastern Standard Time (EST) and this pattern was continued into the post-experiment period until 1 December 1990. At that time, collection start times were set to coincide with routine FRF observations (Birkemeier et al. 1985), which occur daily at 0100, 0700, 1300, and 1900 EST. This collection pattern was maintained until the gages were disconnected for retrieval on 1 Jun 1991.

20. In the analysis presented here, only the first 2 hr 16 min 32 sec (eight records of 4,096 points) of data from each collection was used. This procedure resulted in data sets that coincided both in start times and duration with other permanent directional wave gages at the FRF. It also allowed consistency in processing some collections that were terminated early to allow time for file transfers from the data collection computer to the FRF VAX 11/750 hard disks.

Data Processing

21. Conversion of measured time series to estimates of frequency-direction spectra requires products of frequency spectral estimates from all the various gages in the array. For final results to be accurate, raw input data must be of exceptionally high quality so that spiky or drifty data from one gage do not contaminate products of results from the other gages. Hence, the procedure for data processing is to check the raw data for errors, estimate the frequency-direction spectrum, and then compute some bulk parameters with which to characterize results.

Error checking

22. Because multiple gages were deployed in an (assumed) uniform sea, certain properties of raw data from the pressure gages should be identical. A convenient method of error checking is to compute frequency spectra of the raw time series from each of the 22 functioning gages and overplot the results on a single graph. ~~This method was used by Drs. Guza and Herbers during the main experiment and has also been incorporated for the present analysis.~~ Because of the depth at which the SAMSON gages were deployed, very little direct wind wave signal is expected in the frequency range from about 0.3 Hz out to the Nyquist frequency of 2.0 Hz. The frequency spectrum in this frequency band should primarily indicate system noise, which should be about the same for each gage. Excessively spiky data from one gage will raise the noise level for that gage relative to the noise levels from the other gages so that its signature will be distinct in a collection of overplotted spectra. Strong drifts in the signal can appear in a variety of ways in corresponding spectra, but will generally give a distinct signal at low frequencies. In the pass band of wind wave frequencies for which directional estimates are computed (here 0.05 to 0.24 Hz), one expects the frequency spectra to be nearly identical.

23. Figure 5 is an example of one set of overplotted frequency spectra. Semi-logarithmic coordinates have been used and pressure gage voltages have been converted to equivalent heights of a static water column, but no other transformations have been used. As can be seen, signals in the wind wave frequency pass band are all very nearly alike, indicating that all gages are functioning reasonably well. The noise floor at high frequencies is very low relative to the wind wave signal and is nearly uniform for all gages. The

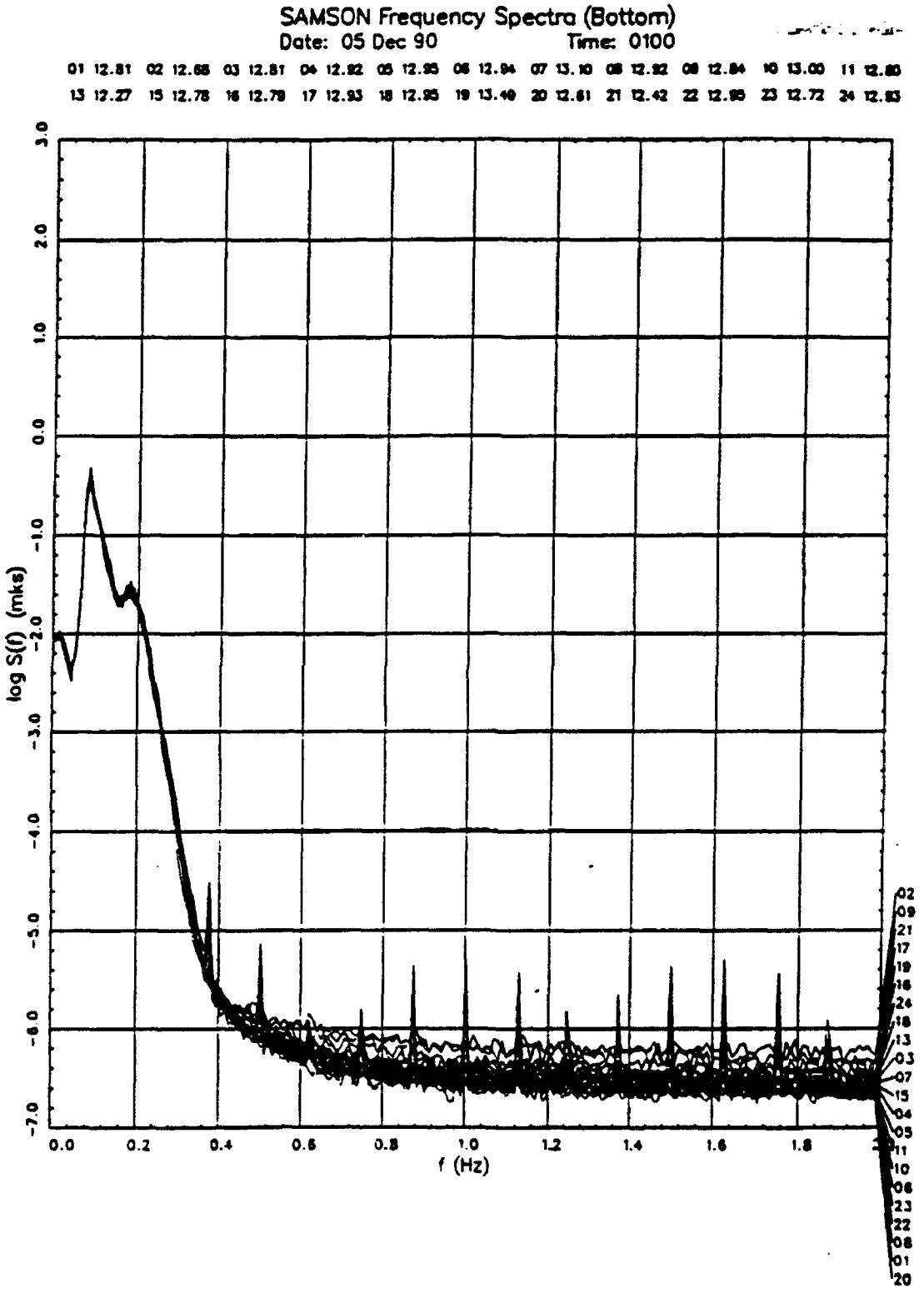

Figure 5. Example of overplotted frequency spectra

spikes in the spectra at high frequencies are due to low levels of commercial 60 Hz power line noise present in the system. The column of numbers in the right margin is the gage number associated with each spectrum. If a particular gage becomes more noisy than the others, its identifying number can then be readily determined. Because the signal mean is removed prior to spectral estimation, it would not normally appear in a spectral plot. Signal means are also useful indicators of misbehaving gages, so they are written out in the two rows of numbers below the plot header.

24. Initial tests with this kind of checking routine indicated that the SAMSON gages and data collection system were extremely reliable. Consequently, overplotted spectra were not computed for every run, but were computed for the first run of each day. At no time during the post-experiment period were any of the 22 functioning gages found to have any significant errors.

Frequency-direction spectra

25. Estimation of frequency-direction spectra is done in four parts. First, time series of pressure data from each gage are Fourier transformed to the frequency domain. Second, these transforms are converted to sea-surface displacement transforms. Third, cross-spectra of sea-surface displacement are computed between all unique gage pairs for each frequency. Finally, an estimate is made of a directional distribution of wave energy that corresponds to the computed spatial variation in cross-spectral density for each frequency.

26. The Fourier transform is conventional. A 32,768-point time series is divided into 15 half-overlapping segments of 4,096 points. Segments are tapered with a Kaiser-Bessel window (a modified Bessel function of the first kind, compensated uniformly for loss of variance due to windowing) and fast Fourier transformed. An intermediate-resolution transform is found by averaging the 15 transformed segments, frequency by frequency. Final transforms are found by then averaging results over 10 adjacent frequency bands. Final resolution bandwidth is 0.00976 Hz, and degrees of freedom are at least 150 (assuming 8 contiguous segments and ignoring any gain from lapped segments). Transform estimates are retained for 20 frequency bands with band-center frequency ranging from 0.054 to 0.240 Hz.

27. Conversion of pressure signals at depth to water-surface displacement is done through the linear wave theory pressure response factor as described in the Shore Protection Manual (SPM) (1984). After this conversion,

complex cross-spectra in the form of coincident and quadrature spectra are computed in the conventional way (Bendat and Piersol 1971, Jenkins and Watts 1968) between all unique gage pairs. Cross-spectral estimates at a given frequency are then stored in a matrix of complex numbers, the indices of which can be used to address data arrays containing gage position for the computation of gage separation distance, or lag space, in preparation for directional spectral estimation at that frequency.

28. In this preliminary analysis of the SAMSON data, conversion of cross-spectral patterns in lag space to directional spectra is done with the Maximum Likelihood Estimation (MLE) algorithm described by Davis and Regier (1977). The algorithm is also described in application to data from heave-pitch-roll buoys by Oltman-Shay and Guza (1984). Neither of these two references includes all the steps in the derivation, so, for pedantic completeness, a more complete outline of the derivation of MLE is given in Appendix C.

29. The algorithm used here made a spectral estimate for every 1 deg of azimuthal direction. These were smoothed over 2-deg arcs to create 180 bins covering a complete circle with which to describe the directional distribution of wave energy.

30. The primary result of data processing is an estimate of the discrete frequency-direction spectrum $S(f_n,\theta_m)$, which represents* the variance of sea-surface displacement per frequency resolution bandwidth df (= 0.00976 Hz) per direction resolution arc $d\theta$ (= 2 deg), where f_n is the n^{th} of N = 20 discrete frequencies and θ_m is the m^{th} of M = 180 discrete directions. In this work, direction is considered to be the angle from which wave energy is coming, measured counterclockwise from shore normal. Also, it is pointed out that parametric definitions below are given in terms of these discrete definitions rather than in terms of the continuous functions they approximate.

31. Numerical values of $S(f_n,\theta_m)$ can range over many orders of magnitude, depending on the amount of energy in a given frequency band and direction arc, and this can require space-consuming formats for archiving data. To simplify this problem, frequency-direction spectra can be saved in

---

* For convenience, symbols and abbreviations are listed in the Notation (Appendix D).

the form of directional distribution functions $D(f_n, \theta_m)$ defined by

$$D(f_n, \theta_m) = \frac{S(f_n, \theta_m)}{S(f_n)} \tag{1}$$

where $S(f_n)$ is the frequency spectral density at frequency f_n. The directional distribution function has units of deg^{-1}, and its integral with respect to direction over all directions is unity.

32. The frequency spectrum in Equation 1 represents the total over all directions of sea-surface variance per frequency bandwidth and is defined in terms of the frequency-direction spectrum by

$$S(f_n) = \sum_{m=1}^{M} S(f_n, \theta_m)\, d\theta \tag{2}$$

Note that this is the same thing as a conventional frequency spectrum that would result from a time series of sea-surface displacements at a single point in space. Because it is an integral of the frequency-direction spectrum, it is called the integrated frequency spectrum.

33. A directional analog of the frequency spectrum is the integrated direction spectrum, found by summing the frequency-direction spectrum over all frequencies for a fixed direction arc. It is computed from

$$S(\theta_m) = \sum_{n=1}^{N} S(f_n, \theta_m)\, df \tag{3}$$

Figure 6 shows one way to display the frequency-direction spectrum and the corresponding integrated frequency and integrated direction spectra.

Bulk parameters

34. Several parameters have been computed to characterize the observed spectra. Five elementary types of parameter have been used here: water depth, characteristic wave height, peak frequency (or its inverse, peak period), peak direction, and reflection coefficient. There is more than one way to define some of these parameters, so definitions are presented here.

35. Water depth. Water depth is found from the average of the mean depths from all 22 gages in the array. It represents a water level that varies with low frequency processes like tides. Because variations in mean water level adjust intersections of the water surface with nearshore bathymetry, it may be an important variable in accounting for the amount of observed reflected energy.

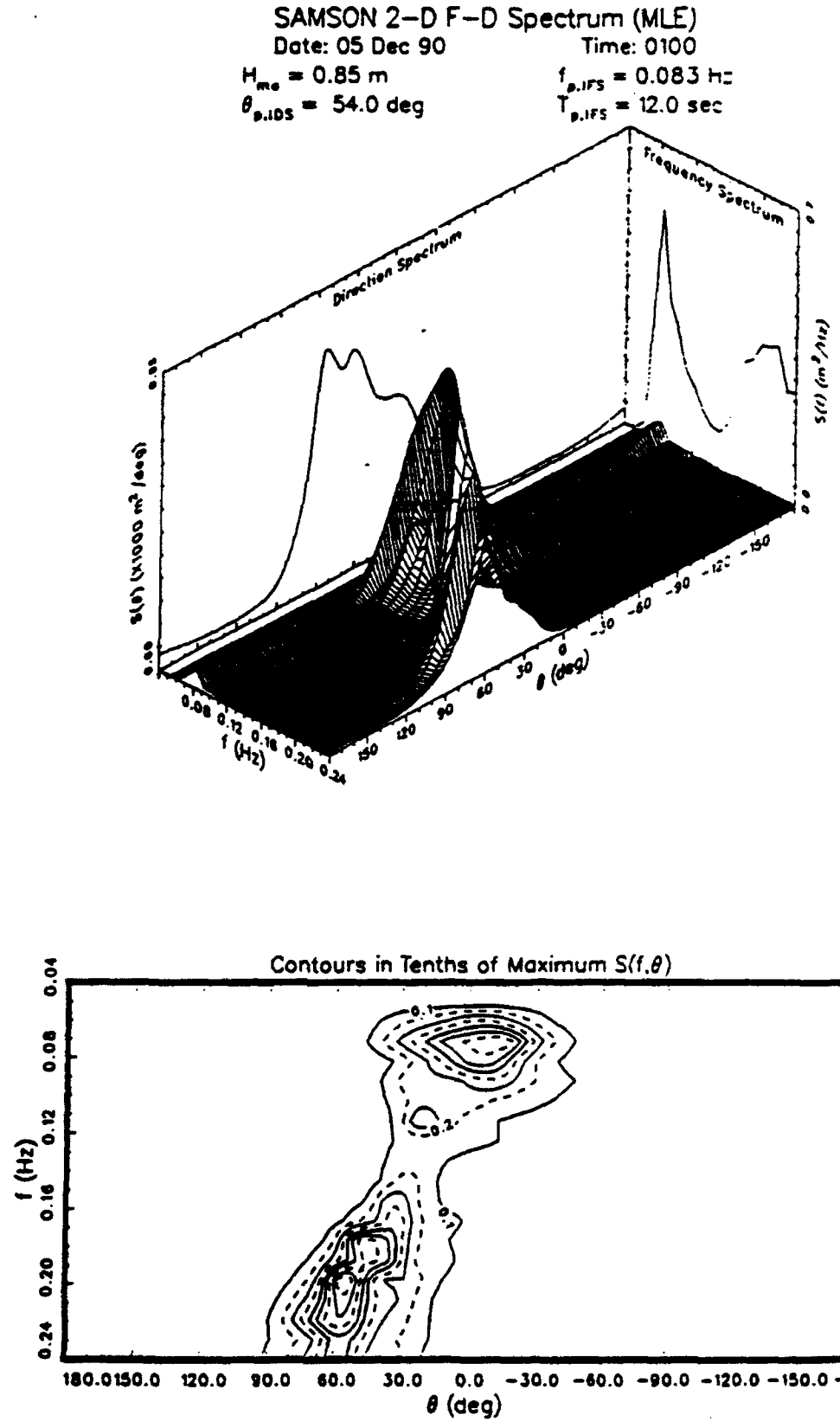

Figure 6. Sample displays of frequency spectrum, direction spectrum, and frequency-direction spectrum

36. Characteristic wave height. Characteristic wave heights from spectral observations are most frequently given as H_{mo}, which is four times the standard deviation of sea-surface displacement. It can be determined from the volume under the frequency-direction spectrum by the equation

$$H_{mo}^2 = 16 \sum_{n=1}^{N} \sum_{m=1}^{M} S(f_n, \theta_m)\, d\theta\, df \tag{4}$$

It can be found equivalently from the integrated frequency spectrum by

$$H_{mo}^2 = 16 \sum_{n=1}^{N} S(f_n)\, df \tag{5}$$

which is its conventional definition, or from the integrated direction spectrum by

$$H_{mo}^2 = 16 \sum_{m=1}^{M} S(\theta_m)\, d\theta \tag{6}$$

37. Because the analysis yields a 360-deg distribution of wave energy, it is reasonable to distinguish between incident wave energy and outgoing wave energy, which here is arbitrarily called reflected wave energy. A characteristic incident wave height $H_{mo,i}$ can be identified from the volume under the frequency-direction spectrum for waves approaching from directions in the range $-90 \text{ deg} < \theta < 90 \text{ deg}$ or, equivalently, the area under the integrated direction spectrum over the same range of directions. Discrete directions in the present analysis are defined by

$$\theta_m = 180 - 2(m - 1) \tag{7}$$

If half the energy in the 90-deg and -90-deg bins and all the energy in the intervening directional bins is attributed to incident energy, a characteristic incident wave height is

$$H_{mo,i}^2 = \frac{1}{2} S(\theta_{46})\, d\theta + \sum_{m=47}^{135} S(\theta_m)\, d\theta + \frac{1}{2} S(\theta_{136})\, d\theta \tag{8}$$

If the other half of the energy in the 90-deg and -90-deg bins and the remainder of the offshore propagating energy is attributed to reflected energy, a characteristic reflected wave height $H_{mo,r}$ is given by

$$H^2_{mo,r} = \sum_{m=1}^{45} S(\theta_m)\,d\theta + \frac{1}{2}S(\theta_{46})\,d\theta + \frac{1}{2}S(\theta_{136})\,d\theta + \sum_{m=137}^{180} S(\theta_m)\,d\theta \qquad (9)$$

38. Peak frequency. Peak frequency, which has the generic notation f_p, can be defined at least two ways. One way is to find the frequency (and direction) at which the frequency-direction spectrum is maximum. Another way is to find the frequency at which the integrated frequency spectrum is maximum. This is the more conventional definition and is the basic definition used here. As with characteristic wave height, a distinction is made between peak frequencies associated with incident and reflected wave energy. The peak frequency of the incident wave spectrum $f_{p,i}$ is defined as the frequency of the maximum of the integrated incident frequency spectrum $S_i(f_n)$ defined following the notation above for H_{mo} as

$$S_i(f_n) = \frac{1}{2}S(f_n,\theta_{46})\,d\theta + \sum_{m=47}^{135} S(f_n,\theta_m)\,d\theta + \frac{1}{2}S(f_n,\theta_{136})\,d\theta \qquad (10)$$

In a similar manner, the peak frequency of the reflected wave spectrum $f_{p,r}$ is defined as the frequency of the maximum of the integrated reflected frequency spectrum $S_r(f_n)$ given by

$$S_r(f_n) = \sum_{m=1}^{45} S(f_n,\theta_m)\,d\theta + \frac{1}{2}S(f_n,\theta_{46})\,d\theta + \frac{1}{2}S(f_n,\theta_{136}) + \sum_{m=137}^{180} S(f_n,\theta_m)\,d\theta \qquad (11)$$

The distinction between $f_{p,i}$ and $f_{p,r}$ may be important. Unless there are very strong reflections, the incident peak frequency is virtually the same as the peak frequency one would obtain from a time series at a single point in space. If the beach is uniformly reflective (the same for all frequencies), reflected peak frequency will be the same as incident peak frequency. If the two frequencies are not equal, the beach may be significantly more reflective for certain frequencies other than the peak, a situation of no small dynamic importance in nearshore processes.

39. Peak period. Peak period T_p is the characteristic wave period associated with spectral peak frequency. As simply inverses of peak frequencies, there are two peak periods associated with a directional spectrum corresponding to the two peak frequencies defined above. The incident peak period is $T_{p,i} = 1/f_{p,i}$ and the reflected peak period is $T_{p,r} = 1/f_{p,r}$.

40. Peak direction. Peak direction is the direction at which the most energy occurs. Given the generic symbol θ_p, it is defined analogously to

peak frequency through the integrated direction spectrum. As with the other parameters there is an incident peak direction $\theta_{p,i}$ and a reflected peak direction $\theta_{p,r}$. Incident peak direction is the direction of the maximum of the integrated incident direction spectrum, which is Equation 3 restricted to those directions for which $-90 \text{ deg} < \theta < 90 \text{ deg}$ or for which index m is in the range $46 < m < 136$. Reflected peak direction is the maximum of the integrated reflected direction spectrum, again Equation 3 but now restricted to offshore propagation directions. This restriction leads to two ranges (in the present definition) of direction $-180 \text{ deg} < \theta < -90 \text{ deg}$ and $90 \text{ deg} < \theta < 180 \text{ deg}$ or of direction indices $1 < m < 46$ and $136 < m < 180$. These measures of peak direction indicate only the single direction cells in each direction range that contain the most energy. If much depth- and frequency-dependent refraction is occurring (as appears to be occurring in Figure 6, e.g.), the integrated direction spectra are somewhat smeared across the direction axis. Peak directions thus found may not correspond then with any peaks in the full frequency-direction spectrum. Hence, these parameters, while adequate for preliminary analysis, must be considered as very rough characterizations.

41. Reflection coefficient. Following notation and definitions given in SPM, reflection coefficients χ are generally defined as ratios of reflected to incident wave heights. Coefficients indicating ratios of energy would then vary as the squares of height-based coefficients defined here. Three reflection coefficients are identified. The first is a bulk parameter that characterizes total reflected to total incident energy. These two energies are the volumes under the reflected and incident spectra, respectively, and are the sources of the definitions of $H_{mo,r}$ and $H_{mo,i}$, respectively. Because it is a wave height ratio that is used in the definition, a bulk reflection coefficient χ_{mo} is simply

$$\chi_{mo} = \frac{H_{mo,r}}{H_{mo,i}} \qquad (12)$$

It should be pointed out that $H_{mo,r}$ is limited in freq - it does not increase for $> 0.24^{+}$

The other two reflection coefficients are frequency specific. One is based on the square root of the ratio of reflected to incident energy at the peak frequency of the incident spectrum and suggests how much of the energy at the frequency spectral peak is reflected. Denoted $\chi_{p,i}$, it is defined from the incident and reflected frequency spectra given by Equations 10 and 11,

respectively, as

$$\chi_{p,i} = \left[\frac{S_r(f_{p,i})}{S_i(f_{p,i})}\right]^{\frac{1}{2}} \tag{13}$$

Because the peak in the reflected energy may not occur at the peak frequency of the incident spectrum, a third reflection coefficient is defined from the ratio of frequency spectral energies at the peak frequency of the reflected spectrum. Denoted $\chi_{p,r}$, it is defined by

$$\chi_{p,r} = \left[\frac{S_r(f_{p,r})}{S_i(f_{p,r})}\right]^{\frac{1}{2}} \tag{14}$$

42. Together, these parameters give a bulk characterization of some properties of a frequency-direction spectrum. There are, of course, many other parameters that can be defined, but the present set is simple and is adequate for this preliminary analysis.

Archived Results

43. A magnetic tape containing the set of observed frequency-direction spectra has been prepared for copying and distribution. These spectra are immediately available to researchers within the USACE and are available to the general public after June 1994. They can be obtained by communicating with:

Chief, Field Research Facility
1261 Duck Road
Kitty Hawk, NC 27949-4471
Phone: (919) 261-3511
Fax: (919) 261-4432

44. Appendix A contains a listing of the date, starting time, and the characterizing parameters defined previously for each case. It is intended to be used as a kind of index or catalog of the set of cases. Dates are given in the form yymmdd where yy is a two-digit year indicator (e.g., 90 means 1990), mm is the numeric index of the calendar month (i.e, 01 is January, 12 is December, etc.), and dd is day of the month. All times are Eastern Standard Time. A 24-hr clock is used.

45. Some of the bulk parameters defined above are plotted as functions of time in Appendix B. One graph is shown for each month of the post-

experiment period. Shown are H_{mo} , $H_{mo,i}$, $H_{mo,r}$, depth, $\theta_{p,i}$, a modified form of $\theta_{p,r}$, $T_{p,i}$, $T_{p,r}$, χ_{mo} , $\chi_{p,i}$, and $\chi_{p,r}$. The modification to $\theta_{p,r}$ involved a shift of 180 deg so that, in the figures, this variable represents direction toward which reflected waves propagate. The variable $\theta_{p,i}$ continues to represent direction from which incident waves arrive.

Discussion

46. The intent of this report is to indicate that additional frequency-direction spectral observations have been added to the already extensive FRF data base and to characterize these observations with some simple parameters. There is clearly much more work to be done with this extraordinary data set, including scientific interpretation, but that is beyond the scope of this document. The descriptive parameters used here are defined simply to be preliminary indicators of the nature of the data. Close examination of the parameters displayed in Appendix B indicates that the rudimentary definitions used here may be somewhat misleading. Hence, there are a few *caveatae* for the reader.

47. In plots of characteristic wave height, it is clear that most of the total wave energy, characterized by H_{mo} , is in the incident spectrum which is characterized by $H_{mo,i}$. The so-called reflected energy, indicated by $H_{mo,r}$ is small, but is very seldom zero. It is possible that some energy always reflects from the FRF beach, but there are (at least) two other reasons for this indication of reflection that is not related to reflection at all. One reason is that there is usually some low-level, broad band background noise in the data, which the MLE algorithm tends to distribute uniformly around the horizon. Integration of the spectra with respect to direction then tends to suggest more reflected (and incident, but to a lesser extent) energy than is actually present. A second misleading indicator occurs if the tails of directional distributions for incoming waves extend beyond the arbitrarily assigned 90-deg limit for incident energy. In the definitions used here, the energy represented by these extended tails becomes associated with reflection when it is more likely part of an onshore distribution of energy where the peak is at a large, but less than 90-deg, angle to shore normal. Figure 6 illustrates both these effects. A low level of energy is perceived at all

directions in the integrated direction spectrum and high-frequency waves have a high angle of attack, with energy distribution tails that exceed 90 deg.

48. These effects have consequences in some of the other parameters, as well. If there is significant energy in distribution tails that cross one of the 90-deg boundaries, the search algorithm will likely find one of those tails and the corresponding 90-deg boundary as the peak energy point for the reflected spectrum. Hence, there will be a number of cases where $\theta_{p,r}$ is 90 deg or -90 deg. This is seen to be the case in the figures in Appendix B. Though not as obvious, peak reflected periods $T_{p,r}$ derived from peak reflected frequencies $f_{p,r}$ are also affected.

49. Finally, reflection coefficients, deduced from the integral properties of the spectra, are also somewhat biased. This is especially noticeable when low incident wave conditions exist. When the low, but persistent, background levels of the so-called reflected energies are divided by low incident wave energies, the ratio can become of order 1, which is unrealistically high.

50. These observations do not entirely preclude the usefulness of the parameters defined here. High energy conditions are readily identified, as are primary directions and periods. In some high energy conditions, reflected wave heights rise above the background level and suggest the existence of legitimate reflected energy. The point here is that brute parameter definition, even though reasonable at some low level of reliability, can mislead. Clearly, more elegant definitions are required for sound scientific interpretation, a task reserved for future work.

Summary

51. Data from the post-experiment period of the SAMSON project has provided an opportunity to add to the FRF data base of high-resolution, directional-spectral observations. Processed data have been put in a form that will be highly accessible to researchers interested in nearshore processes. Directional gage, directional analysis algorithms, and definitions of characterizing parameters are described. The parameters used here are crude, but adequate for case distinction in this preliminary analysis. More refined parametric definitions will be necessary for proper scientific interpretation of the data.

References

Bendat, J. S., and Piersol, A. G. 1971. Random Data: Analysis and Measurement Procedures, Wiley-Interscience, New York.

Birkemeier, W. A. 1984. "Time Scales of Nearshore Profile Changes," Proceedings of the 19th Coastal Engineering Conference, American Society of Civil Engineers, 3-7 September 1984, Houston, TX, pp 1507-1521.

Birkemeier, W. A., Miller, H. C., Wilhelm, S. D., DeWall, A. E., and Gorbics, C. S. 1985. "A User's Guide to the Coastal Engineering Research Center's (CERC's) Field Research Facility," Technical Report CERC-85-1, US Army Engineer Waterways Experiment Station, Vicksburg, MS.

Davis, R. E., and Regier, L. A. 1977. "Methods for Estimating Directional Wave Spectra from Multi-Element Arrays," Journal of Marine Research, Vol 35, pp 453-477.

Hildebrand, F. B. 1965. Advanced Calculus for Applications, Prentice-Hall, Englewood Cliffs, NJ.

Jenkins, G. M., and Watts, D. G. 1968. Spectral Analysis and Its Applications, Holden-Day, Oakland, CA.

Leffler, M. W., Hathaway, K. K., Scarborough, B. L., Baron, C. F., and Miller, H. C. 1990. "Annual Data Summary for 1988, CERC Field Research Facility," Technical Report CERC-90-13, US Army Engineer Waterways Experiment Station, Vicksburg, MS.

Long, C. E. 1991a. "Index and Bulk Parameters for Frequency-Direction Spectra Measured at CERC Field Research Facility, September 1986 to August 1987," Miscellaneous Paper CERC-91-6, US Army Engineer Waterways Experiment Station, Vicksburg, MS.

_____. 1991b. "Index and Bulk Parameters for Frequency-Direction Spectra Measured at CERC Field Research Facility, September 1987 to August 1988," Miscellaneous Paper CERC-91-7, US Army Engineer Waterways Experiment Station, Vicksburg, MS.

Long, C. E., and Oltman-Shay, J. M. 1991. "Directional Characteristics of Waves in Shallow Water," Technical Report CERC-91-1, US Army Engineer Waterways Experiment Station, Vicksburg, MS.

Miller, H. C., Birkemeier, W. A., and DeWall, A. E. 1983. "Effects of CERC Research Pier on Nearshore Processes," Proceedings of Coastal Structures '83, American Society of Civil Engineers, March 9-11, 1983, Arlington, VA, pp 769-784.

Munk, W., Miller, G., Snodgrass, F., and Barber, N. 1963. "Directional Recording of Swell from Distant Storms," Proceedings of the Royal Society of London, Series A, Vol 255, pp 505-584.

Oltman-Shay, J., and Guza, R. T. 1984. "A Data-Adaptive Ocean Wave Directional-Spectrum Estimator for Pitch and Roll Type Measurements," Journal of Physical Oceanography, Vol 14, pp 1800-1810.

Pawka, S. S. 1983. "Island Shadows in Wave Directional Spectra," Journal of Geophysical Research, Vol 88, pp 2579-2591.

Shore Protection Manual. 1984. 4th Edition, 2 Vols, US Army Engineer Waterways Experiment Station, Coastal Engineering Research Center, US Government Printing Office, Washington, DC.

Appendix A: Table of Collection Times and Bulk Parameters

Bulk Parameters of Observed Frequency-Direction Spectra*

Date	Time EST	Wave Height H_{mo} m	$H_{mo,i}$ m	$H_{mo,r}$ m	Direction $\theta_{p,i}$ deg	$\theta_{p,r}$ deg	Frequency $f_{p,i}$ Hz	$f_{p,r}$ Hz	Reflection X_{mo}	$X_{p,i}$	$X_{p,r}$	Depth m
901112	1600	0.68	0.65	0.18	20.0	90.0	0.132	0.132	0.280	0.278	0.278	13.44
901112	1900	0.66	0.64	0.17	24.0	90.0	0.152	0.171	0.262	0.192	0.346	12.85
901112	2200	0.70	0.68	0.17	18.0	90.0	0.123	0.123	0.244	0.227	0.227	12.76
901113	0100	1.03	1.01	0.20	28.0	90.0	0.132	0.132	0.196	0.208	0.208	13.40
901113	0400	1.21	1.19	0.25	24.0	90.0	0.152	0.171	0.207	0.167	0.234	13.71
901113	0700	1.10	1.08	0.21	26.0	90.0	0.152	0.142	0.197	0.149	0.213	13.15
901113	1600	1.07	1.04	0.25	30.0	90.0	0.152	0.142	0.242	0.219	0.262	13.54
901113	1900	0.91	0.89	0.19	34.0	90.0	0.152	0.152	0.216	0.197	0.197	13.12
901114	0100	1.35	1.32	0.25	32.0	90.0	0.152	0.132	0.193	0.182	0.196	13.41
901114	0400	1.43	1.40	0.30	42.0	90.0	0.152	0.142	0.216	0.153	0.260	13.93
901114	0700	1.48	1.45	0.31	28.0	90.0	0.132	0.240	0.210	0.163	0.323	13.51
901114	1300	1.35	1.32	0.26	28.0	90.0	0.132	0.113	0.200	0.169	0.249	13.25
901114	1600	1.24	1.20	0.31	26.0	90.0	0.123	0.113	0.259	0.211	0.266	13.70
901114	1900	1.05	1.01	0.29	18.0	90.0	0.123	0.113	0.286	0.281	0.314	13.38
901114	2200	0.92	0.89	0.21	18.0	178.0	0.132	0.123	0.235	0.180	0.247	12.91
901115	0100	0.79	0.76	0.21	20.0	-170.0	0.132	0.132	0.280	0.252	0.252	13.30
901115	0400	0.70	0.67	0.21	20.0	-164.0	0.142	0.132	0.312	0.301	0.359	13.95
901115	0700	0.57	0.54	0.18	20.0	-180.0	0.152	0.191	0.332	0.232	0.412	13.69
901115	1000	0.49	0.46	0.15	18.0	-178.0	0.142	0.103	0.335	0.196	0.437	12.98
901115	1300	0.46	0.44	0.14	12.0	176.0	0.113	0.113	0.326	0.353	0.353	13.06
901115	1600	0.42	0.40	0.13	6.0	178.0	0.123	0.113	0.337	0.344	0.409	13.61
901115	1900	0.34	0.32	0.12	2.0	176.0	0.123	0.113	0.355	0.317	0.350	13.42
901115	2200	0.32	0.30	0.12	-2.0	178.0	0.123	0.113	0.390	0.277	0.523	12.85
901116	0100	0.31	0.29	0.11	-14.0	-180.0	0.132	0.113	0.398	0.249	0.459	13.04
901116	0400	0.28	0.26	0.11	-16.0	-176.0	0.123	0.113	0.418	0.407	0.475	13.71
901116	0700	0.25	0.23	0.10	-2.0	-176.0	0.123	0.113	0.445	0.333	0.532	13.64
901116	1900	0.20	0.18	0.09	-36.0	-176.0	0.113	0.064	0.520	0.498	0.811	13.37
901116	2200	0.19	0.17	0.08	-30.0	-134.0	0.123	0.064	0.475	0.419	0.603	12.83
901117	0100	0.19	0.16	0.10	-28.0	-176.0	0.064	0.064	0.601	0.850	0.850	12.85
901117	0400	0.20	0.17	0.10	-46.0	178.0	0.064	0.064	0.627	0.782	0.782	13.55
901117	0700	0.20	0.16	0.11	-50.0	-132.0	0.064	0.064	0.658	0.958	0.958	13.79
901117	1000	0.95	0.91	0.28	58.0	90.0	0.201	0.201	0.310	0.332	0.332	13.21
901117	1300	1.30	1.25	0.34	50.0	90.0	0.181	0.181	0.272	0.280	0.280	12.98
901117	1600	1.40	1.34	0.38	42.0	90.0	0.162	0.171	0.285	0.209	0.300	13.57
901117	1900	1.70	1.65	0.44	38.0	90.0	0.162	0.171	0.267	0.196	0.293	13.83
901117	2200	2.23	2.16	0.54	30.0	90.0	0.142	0.230	0.250	0.138	0.383	13.45
901118	0100	2.35	2.28	0.59	26.0	90.0	0.142	0.191	0.259	0.182	0 329	13.27
901118	0400	2.28	2.18	0.66	24.0	90.0	0.152	0.181	0.303	0.246	0.372	13.91
901118	0700	2.32	2.21	0.71	20.0	90.0	0.162	0.191	0.319	0.293	0.376	14.31
901118	1000	2.27	2.18	0.65	14.0	90.0	0.152	0.162	0.298	0.219	0.317	13.79
901118	1300	2.04	1.97	0.54	20.0	90.0	0.152	0.240	0.272	0.190	0.401	13.33
901118	1600	1.86	1.80	0.45	18.0	90.0	0.103	0.093	0.252	0.220	0.322	13.63
901118	1900	1.86	1.80	0.46	24.0	90.0	0.103	0.093	0.257	0.283	0.297	13.99
901118	2200	1.83	1.79	0.40	20.0	90.0	0.103	0.103	0.223	0.223	0.223	13.63
901119	0100	1.87	1.81	0.43	18.0	-174.0	0.103	0.093	0.240	0.245	0.256	13.29
901119	0400	1.90	1.85	0.44	12.0	-174.0	0.093	0.093	0.237	0.252	0.252	13.72
901119	0700	1.84	1.78	0.46	14.0	-174.0	0.083	0.074	0.262	0.235	0.312	14.22
901119	1300	1.90	1.82	0.55	16.0	-174.0	0.083	0.074	0.303	0.267	0.337	13.21
901119	1600	1.81	1.74	0.49	14.0	-176.0	0.083	0.083	0.281	0.282	0.282	13.42

(Continued)

* See Notation (Appendix D) for definitions of terms

(Continued)

Date	Time EST	Wave Height H_{mo} m	$H_{mo,i}$ m	$H_{mo,r}$ m	Direction $\theta_{p,i}$ deg	$\theta_{p,r}$ deg	Frequency $f_{p,i}$ Hz	$f_{p,r}$ Hz	Reflection X_{mo}	$X_{p,i}$	$X_{p,r}$	Depth m
901119	1900	1.48	1.41	0.42	14.0	-178.0	0.083	0.083	0.298	0.269	0.269	13.85
901119	2200	1.33	1.25	0.44	16.0	-176.0	0.083	0.083	0.354	0.364	0.364	13.61
901120	0100	1.20	1.13	0.38	12.0	-176.0	0.083	0.083	0.334	0.339	0.339	13.22
901120	0400	1.12	1.05	0.39	14.0	-178.0	0.093	0.083	0.371	0.347	0.479	13.53
901120	0700	1.07	0.97	0.45	16.0	-168.0	0.103	0.093	0.469	0.441	0.644	14.12
901120	1000	0.93	0.88	0.32	14.0	-172.0	0.093	0.093	0.359	0.396	0.396	13.91
901120	1300	0.95	0.91	0.27	18.0	-174.0	0.093	0.083	0.300	0.276	0.366	13.30
901120	1600	0.99	0.96	0.27	18.0	-176.0	0.093	0.093	0.279	0.390	0.390	13.32
901120	1900	1.02	0.98	0.27	24.0	-172.0	0.093	0.093	0.279	0.388	0.388	13.77
901120	2200	1.05	1.02	0.26	22.0	-176.0	0.181	0.093	0.258	0.200	0.323	13.70
901121	0100	1.24	1.21	0.28	26.0	90.0	0.171	0.093	0.228	0.193	0.313	13.28
901121	0400	1.17	1.14	0.26	26.0	90.0	0.171	0.103	0.228	0.175	0.289	13.39
901121	0700	1.14	1.11	0.26	28.0	-168.0	0.171	0.103	0.233	0.204	0.359	13.95
901121	1000	1.03	1.00	0.26	24.0	-174.0	0.162	0.103	0.260	0.197	0.344	13.91
901121	1300	1.04	1.01	0.26	24.0	-172.0	0.142	0.123	0.252	0.215	0.322	13.32
901121	1600	1.02	0.99	0.24	20.0	-170.0	0.152	0.152	0.239	0.236	0.236	13.22
901121	1900	0.88	0.84	0.23	22.0	-168.0	0.162	0.123	0.273	0.244	0.381	13.61
901121	2200	0.77	0.74	0.22	28.0	-170.0	0.152	0.113	0.298	0.317	0.378	13.65
901122	0100	0.70	0.67	0.20	20.0	-164.0	0.103	0.113	0.292	0.308	0.351	13.25
901122	0400	0.67	0.64	0.19	14.0	-166.0	0.113	0.113	0.306	0.353	0.353	13.21
901122	0700	0.65	0.61	0.22	16.0	-164.0	0.113	0.113	0.357	0.533	0.533	13.71
901122	1000	0.61	0.58	0.18	16.0	-172.0	0.113	0.113	0.315	0.378	0.378	13.86
901122	1300	0.56	0.53	0.18	10.0	-154.0	0.113	0.113	0.331	0.352	0.352	13.36
901122	1600	0.54	0.51	0.16	12.0	-172.0	0.123	0.123	0.320	0.354	0.354	13.11
901122	1900	0.54	0.51	0.18	6.0	-150.0	0.132	0.123	0.362	0.345	0.395	13.47
901122	2200	0.49	0.47	0.15	8.0	-174.0	0.132	0.132	0.331	0.386	0.386	13.68
901123	0100	0.47	0.44	0.16	10.0	-152.0	0.123	0.113	0.374	0.355	0.404	13.32
901123	0400	0.48	0.45	0.16	4.0	-176.0	0.132	0.103	0.358	0.286	0.527	13.11
901123	0700	0.51	0.47	0.19	8.0	-152.0	0.132	0.103	0.402	0.338	0.542	13.51
901123	1000	0.47	0.44	0.17	10.0	-178.0	0.113	0.123	0.377	0.373	0.391	13.80
901123	1300	0.43	0.39	0.17	8.0	176.0	0.113	0.113	0.437	0.495	0.495	13.42
901123	1600	0.42	0.38	0.18	8.0	-174.0	0.123	0.113	0.476	0.407	0.557	13.04
901123	1900	0.46	0.42	0.18	6.0	-156.0	0.123	0.113	0.436	0.389	0.519	13.27
901123	2200	0.40	0.37	0.15	14.0	-176.0	0.113	0.103	0.401	0.354	0.473	13.62
901124	0100	0.34	0.31	0.13	2.0	-174.0	0.113	0.093	0.403	0.384	0.485	13.40
901124	0400	0.29	0.27	0.11	12.0	-178.0	0.093	0.103	0.420	0.404	0.474	13.06
901124	0700	0.28	0.25	0.12	6.0	-176.0	0.093	0.093	0.489	0.594	0.594	13.34
901124	1000	0.30	0.27	0.13	4.0	-172.0	0.093	0.093	0.481	0.614	0.614	13.75
901124	1300	0.31	0.28	0.14	20.0	-170.0	0.093	0.093	0.502	0.566	0.566	13.49
901124	1600	0.32	0.29	0.15	6.0	-172.0	0.093	0.093	0.522	0.529	0.529	13.01
901124	1900	0.34	0.29	0.17	20.0	-176.0	0.093	0.093	0.590	0.635	0.635	13.08
901124	2200	0.34	0.29	0.16	20.0	-172.0	0.093	0.093	0.558	0.597	0.597	13.47
901125	0100	0.30	0.28	0.13	12.0	-174.0	0.093	0.093	0.459	0.467	0.467	13.38
901125	0400	0.29	0.26	0.13	16.0	-174.0	0.093	0.093	0.503	0.557	0.557	12.95
901125	0700	0.25	0.22	0.12	4.0	-178.0	0.093	0.103	0.543	0.569	0.686	12.97
901125	1000	0.24	0.22	0.11	6.0	-174.0	0.103	0.093	0.503	0.545	0.671	13.39
901125	1300	0.24	0.22	0.10	-56.0	-172.0	0.093	0.083	0.439	0.412	0.626	13.40
901125	1600	0.25	0.23	0.10	-58.0	-90.0	0.103	0.103	0.426	0.478	0.478	12.93
901125	1900	0.26	0.24	0.11	-58.0	-90.0	0.103	0.064	0.467	0.603	0.755	12.83
901125	2200	0.28	0.26	0.10	-56.0	-90.0	0.103	0.064	0.404	0.462	0.741	13.31
901126	0100	0.26	0.24	0.09	-54.0	-90.0	0.162	0.064	0.388	0.352	0.710	13.49
901126	0400	0.25	0.23	0.10	-56.0	-90.0	0.152	0.064	0.434	0.315	0.768	13.11

(Continued)

(Continued)

Date	Time EST	Wave Height H_{mo} m	$H_{mo,i}$ m	$H_{mo,r}$ m	Direction $\theta_{p,i}$ deg	$\theta_{p,r}$ deg	Frequency $f_{p,i}$ Hz	$f_{p,r}$ Hz	Reflection X_{mo}	$X_{p,i}$	$X_{p,r}$	Depth m
901126	0700	0.25	0.22	0.12	-26.0	-178.0	0.064	0.064	0.526	0.642	0.642	12.92
901126	1000	0.26	0.23	0.13	-54.0	-172.0	0.064	0.054	0.534	0.729	0.889	13.33
901126	1300	0.30	0.26	0.15	-28.0	-176.0	0.054	0.054	0.563	0.876	0.876	13.55
901126	1600	0.32	0.27	0.16	-26.0	-174.0	0.054	0.054	0.605	0.761	0.761	13.15
901126	1900	0.33	0.27	0.18	-24.0	-176.0	0.054	0.054	0.665	0.780	0.780	12.85
901126	2200	0.39	0.32	0.23	4.0	-172.0	0.054	0.054	0.727	0.895	0.895	13.30
901127	0100	0.40	0.33	0.22	-6.0	-174.0	0.054	0.054	0.651	0.742	0.742	13.71
901128	0100	0.45	0.40	0.21	6.0	-170.0	0.074	0.064	0.515	0.684	0.811	13.72
901128	0400	0.44	0.40	0.18	2.0	-172.0	0.074	0.064	0.462	0.544	0.711	13.59
901128	0700	0.46	0.42	0.18	14.0	-90.0	0.074	0.074	0.435	0.582	0.582	13.02
901128	1000	0.55	0.51	0.21	-58.0	-90.0	0.191	0.074	0.404	0.277	0.649	13.03
901128	1300	0.55	0.50	0.21	2.0	-90.0	0.191	0.074	0.409	0.340	0.675	13.53
901128	1600	0.58	0.54	0.21	-54.0	-90.0	0.191	0.064	0.382	0.368	0.732	13.48
901128	1900	0.48	0.45	0.17	-52.0	-90.0	0.074	0.064	0.379	0.431	0.717	12.82
901128	2200	0.47	0.43	0.19	-56.0	-90.0	0.201	0.074	0.437	0.341	0.724	12.83
901129	0100	0.54	0.51	0.18	-56.0	-90.0	0.191	0.074	0.353	0.270	0.541	13.54
901129	0400	0.56	0.52	0.20	-52.0	-90.0	0.191	0.074	0.384	0.348	0.404	13.69
901129	0700	0.52	0.49	0.18	-50.0	-90.0	0.171	0.074	0.375	0.300	0.586	13.03
901129	1000	1.13	1.08	0.34	52.0	90.0	0.191	0.240	0.315	0.250	0.440	12.80
901129	1300	1.72	1.67	0.39	38.0	90.0	0.162	0.181	0.235	0.190	0.261	13.45
901129	1600	1.68	1.62	0.46	36.0	90.0	0.171	0.171	0.282	0.263	0.263	13.76
901129	1900	1.78	1.71	0.48	34.0	90.0	0.171	0.181	0.279	0.262	0.297	13.27
901129	2200	1.96	1.90	0.50	34.0	90.0	0.162	0.171	0.261	0.184	0.282	13.03
901130	0100	2.38	2.31	0.60	32.0	90.0	0.142	0.240	0.261	0.143	0.453	13.76
901130	0400	2.15	2.07	0.58	36.0	90.0	0.142	0.240	0.282	0.171	0.405	14.30
901130	0700	1.88	1.81	0.48	28.0	90.0	0.152	0.240	0.265	0.197	0.381	13.79
901130	1000	1.69	1.65	0.36	30.0	90.0	0.142	0.191	0.221	0.158	0.275	13.09
901130	1300	1.48	1.45	0.31	26.0	90.0	0.142	0.240	0.217	0.167	0.312	13.37
901130	1600	1.31	1.27	0.32	30.0	90.0	0.142	0.142	0.256	0.260	0.260	13.91
901130	1900	1.13	1.10	0.27	22.0	90.0	0.123	0.103	0.249	0.190	0.311	13.46
901130	2200	1.01	0.99	0.21	22.0	90.0	0.123	0.123	0.214	0.210	0.210	12.84
901201	0100	0.89	0.85	0.25	24.0	-166.0	0.142	0.123	0.295	0.218	0.359	13.36
901201	0400	0.76	0.72	0.26	22.0	-164.0	0.142	0.113	0.366	0.295	0.542	14.18
901201	0700	0.64	0.59	0.23	16.0	-170.0	0.132	0.142	0.384	0.383	0.425	13.84
901201	1300	0.52	0.49	0.17	16.0	180.0	0.142	0.103	0.357	0.264	0.417	12.88
901201	1900	0.46	0.42	0.19	10.0	-176.0	0.103	0.103	0.466	0.464	0.464	13.44
901202	0100	0.48	0.43	0.20	10.0	-178.0	0.093	0.093	0.467	0.500	0.500	12.88
901202	0700	0.41	0.37	0.19	0.0	-174.0	0.103	0.093	0.509	0.418	0.547	13.97
901202	1300	0.39	0.36	0.15	4.0	-176.0	0.103	0.103	0.429	0.383	0.383	12.66
901202	1900	0.41	0.36	0.19	0.0	-170.0	0.103	0.093	0.531	0.526	0.538	13.71
901203	0100	0.46	0.42	0.19	2.0	-176.0	0.103	0.083	0.447	0.387	0.539	12.88
901203	0700	1.03	1.00	0.22	8.0	-90.0	0.201	0.083	0.224	0.172	0.350	14.33
901203	1300	1.10	1.07	0.24	8.0	-90.0	0.171	0.093	0.223	0.152	0.328	12.84
901203	1900	1.38	1.32	0.40	-10.0	-90.0	0.132	0.132	0.300	0.349	0.349	13.92
901204	0100	1.53	1.45	0.49	2.0	-90.0	0.132	0.064	0.337	0.271	0.354	12.71
901204	0700	1.63	1.51	0.59	-2.0	-90.0	0.123	0.064	0.392	0.372	0.524	14.12
901204	1300	1.09	1.02	0.37	0.0	176.0	0.074	0.074	0.366	0.341	0.341	12.83
901204	1900	0.79	0.72	0.32	10.0	-176.0	0.074	0.074	0.445	0.523	0.523	13.84
901205	0100	0.85	0.82	0.25	54.0	90.0	0.083	0.083	0.301	0.358	0.358	12.93
901205	0700	0.87	0.84	0.24	32.0	90.0	0.162	0.113	0.293	0.224	0.523	14.04

(Continued)

(Continued)

Date	Time EST	Wave Height H_{mo} m	$H_{mo,i}$ m	$H_{mo,r}$ m	Direction $\theta_{p,i}$ deg	$\theta_{p,r}$ deg	Frequency $f_{p,i}$ Hz	$f_{p,r}$ Hz	Reflection X_{mo}	$X_{p,i}$	$X_{p,r}$	Depth m
901205	1300	0.80	0.78	0.20	32.0	90.0	0.162	0.083	0.262	0.214	0.354	13.03
901205	1900	0.58	0.55	0.17	36.0	90.0	0.171	0.093	0.312	0.336	0.396	13.54
901206	0100	0.50	0.47	0.17	28.0	180.0	0.083	0.083	0.361	0.370	0.370	12.97
901206	0700	0.48	0.45	0.18	14.0	-180.0	0.093	0.074	0.389	0.379	0.521	13.62
901206	1300	0.46	0.41	0.19	-6.0	-178.0	0.074	0.064	0.460	0.503	0.617	13.14
901206	1900	0.41	0.37	0.18	-2.0	-180.0	0.074	0.074	0.485	0.498	0.498	13.16
901207	0100	0.38	0.34	0.17	-6.0	-172.0	0.074	0.074	0.497	0.493	0.493	13.20
901207	0700	0.36	0.32	0.17	0.0	-180.0	0.074	0.074	0.521	0.608	0.608	13.36
901207	1300	0.37	0.34	0.16	-2.0	-178.0	0.083	0.074	0.476	0.366	0.573	13.54
901207	1900	0.40	0.36	0.16	-6.0	-172.0	0.083	0.074	0.458	0.376	0.594	13.24
901208	0100	0.72	0.71	0.15	22.0	90.0	0.230	0.240	0.214	0.159	0.167	13.78
901208	0700	1.57	1.54	0.35	2.0	90.0	0.191	0.191	0.226	0.229	0.229	13.39
901208	1300	2.08	2.01	0.50	8.0	90.0	0.171	0.181	0.249	0.213	0.273	13.88
901208	1900	2.05	2.00	0.42	14.0	90.0	0.142	0.152	0.207	0.151	0.163	13.32
901209	0100	2.06	2.02	0.43	22.0	90.0	0.152	0.142	0.211	0.167	0.191	14.05
901209	0700	2.10	2.05	0.44	22.0	90.0	0.142	0.240	0.217	0.146	0.368	13.37
901209	1300	1.74	1.69	0.40	16.0	-170.0	0.123	0.103	0.239	0.173	0.314	13.96
901209	1900	1.27	1.23	0.29	18.0	-176.0	0.113	0.093	0.237	0.217	0.298	13.12
901210	0100	0.95	0.89	0.34	16.0	-172.0	0.113	0.103	0.382	0.280	0.490	13.88
901210	0700	0.72	0.69	0.22	14.0	-176.0	0.113	0.093	0.318	0.238	0.386	13.04
901210	1300	0.54	0.49	0.23	16.0	-180.0	0.103	0.093	0.478	0.315	0.518	13.57
901210	1900	0.51	0.47	0.20	12.0	-90.0	0.103	0.083	0.426	0.301	0.539	12.84
901211	0100	1.29	1.27	0.24	40.0	90.0	0.181	0.181	0.193	0.199	0.199	13.77
901211	0700	1.26	1.24	0.25	38.0	90.0	0.162	0.171	0.204	0.148	0.186	13.19
901211	1300	1.19	1.16	0.26	28.0	90.0	0.152	0.132	0.225	0.215	0.257	13.62
901211	1900	0.91	0.89	0.21	24.0	-174.0	0.142	0.074	0.238	0.191	0.381	13.04
901212	0100	0.74	0.71	0.21	18.0	-170.0	0.171	0.074	0.292	0.206	0.423	13.72
901212	0700	0.59	0.56	0.19	16.0	-168.0	0.083	0.074	0.343	0.316	0.537	13.20
901212	1300	0.50	0.46	0.18	10.0	-172.0	0.074	0.083	0.383	0.353	0.494	13.41
901212	1900	0.43	0.39	0.16	8.0	-176.0	0.074	0.074	0.409	0.505	0.505	13.05
901213	0100	0.46	0.43	0.16	-2.0	-90.0	0.083	0.083	0.380	0.468	0.468	13.45
901213	0700	0.41	0.38	0.16	-18.0	-90.0	0.162	0.162	0.431	0.435	0.435	13.11
901213	1300	0.40	0.37	0.16	-18.0	-170.0	0.162	0.083	0.434	0.432	0.679	13.11
901213	1900	0.34	0.32	0.13	-28.0	-144.0	0.152	0.152	0.402	0.391	0.391	13.10
901214	0100	1.11	1.07	0.29	56.0	90.0	0.201	0.220	0.266	0.224	0.264	13.45
901214	0700	2.17	2.12	0.44	34.0	90.0	0.142	0.220	0.206	0.130	0.303	13.79
901214	1300	1.56	1.54	0.27	24.0	90.0	0.142	0.240	0.178	0.150	0.251	13.35
901214	1900	1.24	1.22	0.24	20.0	90.0	0.123	0.123	0.194	0.184	0.184	13.48
901215	0100	1.21	1.19	0.23	16.0	90.0	0.181	0.152	0.195	0.175	0.249	13.33
901215	0700	1.01	0.98	0.26	10.0	90.0	0.181	0.201	0.262	0.242	0.415	13.70
901215	1300	1.03	1.01	0.22	4.0	-90.0	0.162	0.162	0.219	0.229	0.229	13.02
901215	1900	1.09	1.04	0.31	0.0	-90.0	0.152	0.152	0.293	0.279	0.279	13.45
901216	0100	0.83	0.79	0.23	-6.0	-90.0	0.142	0.152	0.288	0.276	0.301	13.01
901216	0700	0.63	0.58	0.24	-26.0	-126.0	0.142	0.142	0.409	0.441	0.441	13.62
901216	1300	0.36	0.34	0.13	-26.0	-124.0	0.142	0.132	0.374	0.315	0.358	12.79
901216	1900	0.48	0.47	0.12	36.0	90.0	0.240	0.240	0.255	0.204	0.204	13.51
901217	0100	0.52	0.51	0.12	14.0	90.0	0.240	0.240	0.226	0.177	0.177	13.02

(Continued)

(Sheet 4 of 18)

(Continued)

Date	Time EST	Wave Height H_{mo} m	$H_{mo,i}$ m	$H_{mo,r}$ m	Direction $\theta_{p,i}$ deg	$\theta_{p,r}$ deg	Frequency $f_{p,i}$ Hz	$f_{p,r}$ Hz	Reflection X_{mo}	$X_{p,i}$	$X_{p,r}$	Depth m
901217	0700	0.76	0.74	0.19	34.0	90.0	0.171	0.171	0.253	0.237	0.237	13.82
901217	1300	0.63	0.62	0.13	24.0	90.0	0.171	0.152	0.204	0.141	0.253	12.79
901217	1900	0.59	0.57	0.16	18.0	90.0	0.171	0.152	0.290	0.250	0.390	13.48
901218	0100	0.55	0.53	0.14	10.0	-176.0	0.152	0.152	0.267	0.240	0.240	12.83
901218	0700	0.46	0.44	0.14	-10.0	-176.0	0.132	0.123	0.314	0.275	0.314	13.78
901218	1300	0.41	0.38	0.14	-12.0	-90.0	0.123	0.074	0.355	0.264	0.586	12.69
901218	1900	0.55	0.52	0.18	-38.0	-90.0	0.240	0.240	0.354	0.443	0.443	13.34
901219	0100	0.54	0.51	0.17	-46.0	-90.0	0.123	0.093	0.326	0.223	0.365	12.68
901219	0700	0.53	0.50	0.19	-38.0	-90.0	0.103	0.103	0.375	0.475	0.475	13.73
901219	1300	0.51	0.49	0.13	-10.0	-90.0	0.103	0.093	0.264	0.210	0.318	12.90
901219	1900	1.05	1.02	0.23	8.0	90.0	0.201	0.181	0.222	0.155	0.239	13.68
901220	0100	1.17	1.15	0.21	16.0	90.0	0.181	0.181	0.186	0.185	0.185	13.07
901220	0700	1.46	1.44	0.28	16.0	90.0	0.171	0.181	0.197	0.165	0.189	13.99
901220	1300	1.53	1.51	0.24	12.0	90.0	0.162	0.181	0.162	0.130	0.185	13.16
901220	1900	1.58	1.55	0.32	8.0	90.0	0.152	0.142	0.203	0.158	0.244	13.71
901221	0100	1.56	1.53	0.30	12.0	-90.0	0.152	0.123	0.196	0.131	0.198	13.17
901221	0700	1.52	1.48	0.35	0.0	-174.0	0.142	0.132	0.237	0.213	0.255	13.83
901221	1300	1.55	1.52	0.31	-6.0	-90.0	0.123	0.123	0.203	0.150	0.150	13.16
901222	0100	1.35	1.32	0.30	-14.0	-90.0	0.123	0.113	0.227	0.159	0.189	13.22
901222	0700	1.34	1.30	0.31	-4.0	-90.0	0.123	0.103	0.239	0.191	0.293	13.58
901222	1300	1.05	1.01	0.27	-8.0	-90.0	0.123	0.142	0.263	0.206	0.270	13.21
901222	1900	1.03	1.00	0.25	-4.0	-90.0	0.142	0.123	0.251	0.223	0.242	13.34
901223	0100	0.89	0.86	0.26	-2.0	-90.0	0.113	0.083	0.306	0.234	0.439	13.28
901223	0700	1.11	1.06	0.31	0.0	-90.0	0.152	0.152	0.294	0.272	0.272	13.24
901223	1300	1.01	0.96	0.31	0.0	-90.0	0.142	0.152	0.320	0.308	0.350	13.18
901223	1900	0.91	0.88	0.24	-6.0	-90.0	0.093	0.093	0.270	0.243	0.243	13.00
901224	0100	0.82	0.76	0.29	-2.0	-140.0	0.093	0.093	0.385	0.328	0.328	13.27
901224	0700	0.91	0.86	0.29	-24.0	-90.0	0.093	0.093	0.332	0.283	0.283	12.95
901224	1300	0.93	0.88	0.28	-14.0	90.0	0.093	0.093	0.322	0.258	0.258	13.30
901224	1900	1.87	1.84	0.34	30.0	90.0	0.152	0.210	0.187	0.106	0.273	13.18
901225	0100	1.56	1.52	0.35	30.0	90.0	0.152	0.240	0.231	0.151	0.350	13.73
901225	0700	1.18	1.15	0.25	30.0	90.0	0.181	0.240	0.221	0.186	0.290	13.07
901225	1300	1.09	1.06	0.27	32.0	90.0	0.093	0.093	0.253	0.289	0.289	13.49
901225	1900	1.05	1.02	0.25	-8.0	90.0	0.083	0.083	0.241	0.186	0.186	12.89
901226	0100	1.02	0.96	0.34	-10.0	-168.0	0.083	0.083	0.358	0.390	0.390	13.77
901226	0700	0.94	0.90	0.27	-14.0	-172.0	0.083	0.083	0.295	0.303	0.303	13.07
901226	1300	1.17	1.14	0.29	6.0	90.0	0.083	0.083	0.255	0.293	0.293	13.69
901226	1900	1.21	1.18	0.26	6.0	90.0	0.191	0.201	0.218	0.191	0.207	12.97
901227	0100	1.38	1.35	0.30	16.0	90.0	0.191	0.093	0.220	0.175	0.289	13.97
901227	0700	1.67	1.63	0.34	16.0	90.0	0.181	0.191	0.209	0.174	0.211	13.19
901227	1300	1.91	1.87	0.38	12.0	90.0	0.162	0.162	0.202	0.170	0.170	13.74
901227	1900	1.79	1.77	0.29	12.0	90.0	0.152	0.152	0.166	0.143	0.143	13.06
901228	0100	1.90	1.84	0.44	14.0	-90.0	0.132	0.123	0.237	0.178	0.209	13.97
901228	0700	1.60	1.56	0.39	12.0	-172.0	0.113	0.123	0.248	0.212	0.223	13.33
901228	1300	1.29	1.23	0.39	14.0	-170.0	0.113	0.103	0.317	0.270	0.300	13.67
901228	1900	1.01	0.98	0.27	14.0	180.0	0.113	0.103	0.279	0.243	0.321	13.17
901229	0100	1.04	0.97	0.37	10.0	-180.0	0.103	0.103	0.379	0.452	0.452	13.82

(Continued)

(Sheet 5 of 18)

(Continued)

Date	Time EST	Wave Height H_{mo} m	$H_{mo,i}$ m	$H_{mo,r}$ m	Direction $\theta_{p,i}$ deg	$\theta_{p,r}$ deg	Frequency $f_{p,i}$ Hz	$f_{p,r}$ Hz	Reflection x_{mo}	$x_{p,i}$	$x_{p,r}$	Depth m
901229	0700	1.08	1.02	0.35	16.0	180.0	0.103	0.103	0.341	0.317	0.317	13.60
901229	1300	1.16	1.11	0.32	10.0	-176.0	0.093	0.093	0.287	0.254	0.254	13.43
901229	1900	1.06	1.01	0.32	2.0	-176.0	0.093	0.093	0.316	0.311	0.311	13.31
901230	0100	1.00	0.95	0.31	8.0	-90.0	0.093	0.083	0.323	0.252	0.400	13.38
901230	0700	0.89	0.81	0.37	-8.0	-90.0	0.093	0.093	0.457	0.525	0.525	13.64
901230	1300	0.83	0.78	0.27	-2.0	-90.0	0.093	0.093	0.344	0.324	0.324	12.85
901230	1900	0.75	0.69	0.29	-10.0	-132.0	0.093	0.093	0.424	0.373	0.373	13.23
901231	0100	0.67	0.62	0.23	-12.0	176.0	0.093	0.093	0.376	0.342	0.342	12.72
901231	1300	1.67	1.64	0.33	36.0	90.0	0.162	0.240	0.199	0.127	0.287	12.82
901231	1900	1.46	1.42	0.33	22.0	90.0	0.152	0.210	0.230	0.151	0.277	13.79
910101	0100	1.38	1.35	0.31	20.0	90.0	0.201	0.240	0.226	0.227	0.317	12.91
910101	0700	1.41	1.37	0.35	18.0	90.0	0.181	0.171	0.253	0.199	0.274	14.26
910101	1300	1.16	1.13	0.23	12.0	90.0	0.162	0.093	0.207	0.150	0.229	12.87
910101	1900	1.18	1.14	0.29	10.0	90.0	0.181	0.093	0.256	0.202	0.331	13.95
910102	0100	1.03	1.00	0.24	4.0	-90.0	0.093	0.093	0.235	0.231	0.231	12.82
910102	0700	1.15	1.10	0.34	4.0	-166.0	0.162	0.162	0.305	0.331	0.331	14.28
910102	1300	1.16	1.13	0.28	18.0	90.0	0.230	0.230	0.252	0.281	0.281	12.89
910102	1900	1.27	1.22	0.36	16.0	-174.0	0.171	0.181	0.295	0.248	0.295	13.96
910103	0100	0.93	0.91	0.20	16.0	-90.0	0.171	0.181	0.225	0.187	0.243	12.85
910103	0700	0.78	0.74	0.25	14.0	-174.0	0.171	0.103	0.341	0.286	0.460	14.08
910103	1300	0.63	0.61	0.18	4.0	-90.0	0.123	0.103	0.288	0.238	0.305	12.92
910103	1900	0.73	0.69	0.22	8.0	-178.0	0.123	0.103	0.311	0.303	0.380	13.81
910104	0100	0.57	0.54	0.18	6.0	-180.0	0.103	0.103	0.326	0.327	0.327	13.07
910104	0700	1.22	1.19	0.26	34.0	90.0	0.201	0.191	0.220	0.165	0.215	13.99
910104	1300	1.34	1.32	0.27	34.0	90.0	0.171	0.171	0.205	0.174	0.174	13.26
910104	1900	1.05	1.03	0.22	20.0	90.0	0.181	0.181	0.209	0.185	0.185	13.67
910105	0100	1.05	1.03	0.20	20.0	90.0	0.181	0.240	0.197	0.154	0.196	13.40
910105	0700	1.18	1.15	0.24	14.0	90.0	0.201	0.201	0.209	0.199	0.199	13.65
910105	1300	1.03	1.00	0.24	8.0	-90.0	0.181	0.181	0.234	0.215	0.215	13.40
910105	1900	0.97	0.94	0.24	2.0	-90.0	0.152	0.152	0.251	0.261	0.261	13.39
910106	0100	0.75	0.71	0.24	6.0	-176.0	0.152	0.152	0.340	0.347	0.347	13.56
910106	0700	0.61	0.58	0.19	8.0	-90.0	0.162	0.162	0.332	0.310	0.310	13.25
910106	1300	0.47	0.44	0.18	-8.0	-178.0	0.103	0.113	0.415	0.408	0.438	13.44
910106	1900	0.50	0.46	0.18	-2.0	-90.0	0.113	0.113	0.396	0.457	0.457	13.10
910107	0100	0.52	0.48	0.21	-8.0	-176.0	0.113	0.113	0.427	0.456	0.456	13.70
910107	0700	0.50	0.46	0.19	0.0	-178.0	0.113	0.103	0.413	0.404	0.445	13.25
910107	1300	1.98	1.93	0.44	36.0	90.0	0.152	0.162	0.228	0.170	0.196	13.87
910107	1900	2.92	2.87	0.52	10.0	90.0	0.123	0.240	0.179	0.130	0.334	13.47
910108	0100	3.00	2.93	0.63	12.0	90.0	0.123	0.113	0.213	0.177	0.198	14.22
910108	0700	2.75	2.70	0.49	10.0	90.0	0.113	0.240	0.183	0.154	0.327	13.50
910108	1300	3.01	2.97	0.54	14.0	90.0	0.123	0.132	0.182	0.143	0.169	14.00
910108	1900	2.84	2.79	0.48	6.0	90.0	0.093	0.240	0.172	0.131	0.394	13.39
910109	0100	3.11	3.05	0.59	0.0	90.0	0.093	0.093	0.195	0.137	0.137	14.19
910109	0700	2.69	2.64	0.54	2.0	90.0	0.083	0.240	0.207	0.132	0.509	13.48
910109	1300	2.61	2.55	0.52	0.0	90.0	0.083	0.083	0.203	0.126	0.126	13.91
910109	1900	1.83	1.78	0.44	-16.0	-180.0	0.083	0.083	0.246	0.215	0.215	13.35
910110	0100	1.69	1.60	0.52	22.0	-174.0	0.093	0.093	0.327	0.335	0.335	14.04

(Continued)

(Continued)

Date	Time EST	Wave Height H_{mo} m	$H_{mo,i}$ m	$H_{mo,r}$ m	Direction $\theta_{p,i}$ deg	$\theta_{p,r}$ deg	Frequency $f_{p,i}$ Hz	$f_{p,r}$ Hz	Reflection x_{mo}	$x_{p,i}$	$x_{p,r}$	Depth m
910110	0700	1.51	1.44	0.46	18.0	-176.0	0.103	0.103	0.321	0.368	0.368	13.50
910110	1300	1.49	1.43	0.44	22.0	-172.0	0.093	0.093	0.309	0.482	0.482	13.77
910110	1900	1.15	1.09	0.37	16.0	-174.0	0.093	0.093	0.337	0.435	0.435	13.32
910111	0100	1.47	1.42	0.39	20.0	90.0	0.191	0.103	0.276	0.264	0.418	13.91
910111	0700	1.64	1.59	0.41	16.0	-180.0	0.152	0.152	0.261	0.243	0.243	13.55
910111	1300	1.56	1.50	0.45	12.0	178.0	0.142	0.132	0.302	0.234	0.304	13.53
910111	1900	2.00	1.92	0.56	0.0	-90.0	0.123	0.123	0.293	0.282	0.282	13.31
910112	0100	2.39	2.28	0.70	0.0	-90.0	0.113	0.113	0.305	0.313	0.313	13.57
910112	0700	1.66	1.52	0.66	0.0	-172.0	0.103	0.103	0.431	0.490	0.490	13.57
910112	1300	1.41	1.27	0.60	0.0	-174.0	0.113	0.103	0.469	0.491	0.549	13.37
910112	1900	1.16	1.04	0.52	0.0	-172.0	0.113	0.113	0.501	0.494	0.494	13.44
910113	0100	1.16	1.05	0.49	14.0	-172.0	0.113	0.113	0.463	0.531	0.531	13.54
910113	0700	1.43	1.35	0.46	26.0	90.0	0.181	0.181	0.342	0.313	0.313	13.85
910113	1300	1.14	1.09	0.32	32.0	90.0	0.171	0.181	0.289	0.254	0.321	13.32
910113	1900	1.08	1.02	0.35	30.0	166.0	0.171	0.171	0.342	0.362	0.362	13.61
910114	0100	0.87	0.83	0.25	28.0	-174.0	0.171	0.171	0.300	0.283	0.283	13.41
910114	0700	0.74	0.69	0.27	30.0	166.0	0.171	0.171	0.398	0.468	0.468	13.91
910114	1300	0.55	0.51	0.20	-2.0	-178.0	0.103	0.064	0.393	0.368	0.649	13.07
910114	1900	0.53	0.48	0.22	0.0	-174.0	0.103	0.064	0.485	0.390	0.733	13.49
910115	0100	0.49	0.45	0.21	-4.0	-174.0	0.064	0.064	0.475	0.593	0.593	12.99
910115	0700	0.45	0.41	0.19	-8.0	-170.0	0.064	0.064	0.479	0.487	0.487	13.78
910115	1300	0.46	0.41	0.21	-4.0	-176.0	0.064	0.064	0.524	0.708	0.708	12.89
910115	1900	0.46	0.41	0.20	-12.0	-174.0	0.123	0.064	0.492	0.308	0.720	13.63
910116	0100	0.45	0.41	0.18	-8.0	-174.0	0.074	0.074	0.433	0.550	0.550	13.01
910116	0700	1.75	1.62	0.65	-10.0	-126.0	0.123	0.113	0.401	0.346	0.428	13.90
910116	1300	1.42	1.33	0.49	-8.0	-110.0	0.113	0.103	0.369	0.330	0.364	12.86
910116	1900	1.08	0.97	0.47	-12.0	-128.0	0.123	0.123	0.484	0.500	0.500	13.73
910117	0100	0.78	0.72	0.30	-16.0	-112.0	0.113	0.113	0.412	0.415	0.415	12.94
910117	0700	0.65	0.56	0.33	-14.0	-142.0	0.103	0.103	0.586	0.653	0.653	13.94
910117	1300	0.45	0.41	0.18	-12.0	-178.0	0.113	0.113	0.450	0.431	0.431	12.88
910117	1900	0.43	0.39	0.17	-6.0	-174.0	0.113	0.113	0.447	0.484	0.484	13.74
910118	0100	0.36	0.33	0.15	-2.0	-180.0	0.113	0.103	0.446	0.405	0.510	12.86
910118	0700	0.37	0.34	0.13	32.0	-180.0	0.103	0.103	0.387	0.422	0.422	13.78
910118	1300	0.30	0.27	0.12	32.0	178.0	0.093	0.093	0.436	0.483	0.483	12.74
910118	1900	0.25	0.22	0.11	-2.0	180.0	0.103	0.054	0.501	0.561	0.861	13.57
910119	0100	0.18	0.17	0.08	-10.0	-178.0	0.103	0.054	0.498	0.456	0.698	12.76
910119	0700	0.21	0.18	0.10	-26.0	-176.0	0.162	0.054	0.553	0.371	0.909	13.63
910119	1300	0.24	0.23	0.09	14.0	180.0	0.103	0.054	0.408	0.435	0.692	12.78
910119	1900	0.28	0.26	0.11	14.0	-180.0	0.162	0.103	0.414	0.235	0.530	13.41
910120	0100	0.25	0.23	0.10	0.0	-180.0	0.103	0.054	0.447	0.439	0.908	12.87
910120	0700	0.46	0.44	0.15	32.0	90.0	0.240	0.240	0.335	0.251	0.251	13.57
910120	1300	0.78	0.75	0.19	20.0	90.0	0.220	0.220	0.260	0.206	0.206	13.00
910120	1900	0.63	0.58	0.24	20.0	-136.0	0.220	0.083	0.416	0.221	0.638	13.49
910121	0100	0.54	0.47	0.26	-4.0	-138.0	0.093	0.093	0.562	0.597	0.597	13.25
910121	0700	0.46	0.41	0.22	-6.0	-140.0	0.093	0.103	0.548	0.605	0.624	13.42
910121	1300	0.53	0.49	0.21	60.0	90.0	0.230	0.230	0.430	0.403	0.403	13.30
910121	1900	1.45	1.37	0.48	38.0	90.0	0.162	0.171	0.351	0.300	0.379	13.68

(Continued)

(Continued)

Date	Time EST	Wave Height H_{mo} m	$H_{mo,i}$ m	$H_{mo,r}$ m	Direction $\theta_{p,i}$ deg	$\theta_{p,r}$ deg	Frequency $f_{p,i}$ Hz	$f_{p,r}$ Hz	Reflection x_{mo}	$x_{p,i}$	$x_{p,r}$	Depth m
910122	0100	1.35	1.27	0.46	36.0	90.0	0.162	0.171	0.366	0.286	0.402	13.84
910122	0700	1.59	1.50	0.53	30.0	90.0	0.181	0.201	0.356	0.294	0.338	13.67
910122	1300	1.65	1.55	0.58	32.0	90.0	0.152	0.142	0.373	0.294	0.434	13.72
910122	1900	1.30	1.21	0.47	26.0	176.0	0.123	0.132	0.389	0.444	0.467	13.47
910123	0100	0.94	0.88	0.34	32.0	164.0	0.142	0.113	0.381	0.388	0.552	13.90
910123	0700	0.70	0.65	0.27	22.0	176.0	0.113	0.113	0.419	0.490	0.490	13.31
910123	1300	0.55	0.50	0.25	14.0	178.0	0.113	0.113	0.494	0.584	0.584	13.59
910123	1900	0.52	0.48	0.21	10.0	178.0	0.113	0.103	0.432	0.384	0.461	13.00
910124	0100	0.39	0.34	0.19	8.0	-172.0	0.103	0.113	0.549	0.509	0.649	13.71
910124	0700	0.36	0.32	0.16	2.0	-176.0	0.093	0.093	0.511	0.470	0.470	12.92
910124	1300	0.36	0.32	0.16	0.0	-174.0	0.093	0.093	0.506	0.476	0.476	13.45
910124	1900	0.36	0.32	0.16	-4.0	-178.0	0.093	0.093	0.504	0.492	0.492	12.79
910125	0100	0.36	0.32	0.15	-2.0	-172.0	0.093	0.093	0.472	0.500	0.500	13.86
910125	0700	1.84	1.79	0.44	40.0	90.0	0.162	0.181	0.243	0.154	0.269	13.22
910125	1300	1.57	1.49	0.49	32.0	90.0	0.181	0.181	0.328	0.370	0.370	13.74
910125	1900	1.10	1.05	0.33	22.0	90.0	0.132	0.132	0.312	0.324	0.324	12.96
910126	0100	0.90	0.85	0.31	22.0	170.0	0.152	0.142	0.362	0.373	0.419	13.91
910126	0700	0.75	0.72	0.22	10.0	180.0	0.123	0.113	0.313	0.309	0.365	13.18
910126	1300	0.68	0.64	0.23	10.0	-180.0	0.152	0.123	0.359	0.381	0.466	13.53
910126	1900	0.55	0.51	0.19	2.0	-180.0	0.132	0.132	0.375	0.377	0.377	12.95
910127	0100	0.45	0.41	0.17	0.0	-176.0	0.132	0.142	0.399	0.435	0.467	13.66
910127	0700	0.34	0.31	0.14	-8.0	-174.0	0.132	0.123	0.466	0.404	0.448	13.27
910127	1300	0.33	0.30	0.14	-6.0	-178.0	0.142	0.142	0.463	0.487	0.487	13.30
910127	1900	0.36	0.33	0.14	-16.0	-176.0	0.132	0.132	0.434	0.455	0.455	13.11
910128	0100	0.49	0.46	0.18	-14.0	-90.0	0.132	0.142	0.385	0.406	0.427	13.35
910128	0700	0.63	0.57	0.27	-8.0	-90.0	0.132	0.132	0.462	0.546	0.546	13.53
910128	1300	0.51	0.48	0.18	-12.0	-90.0	0.132	0.132	0.376	0.413	0.413	13.02
910128	1900	0.64	0.55	0.32	-12.0	-130.0	0.113	0.113	0.580	0.621	0.621	13.38
910129	0100	0.62	0.57	0.25	-8.0	-108.0	0.123	0.113	0.448	0.416	0.503	13.14
910129	0700	0.61	0.54	0.28	-12.0	-132.0	0.113	0.113	0.516	0.537	0.537	13.95
910129	1300	0.68	0.65	0.21	-10.0	-90.0	0.123	0.113	0.321	0.305	0.385	12.94
910129	1900	0.69	0.65	0.25	-4.0	-122.0	0.132	0.113	0.381	0.421	0.500	13.75
910130	0100	0.84	0.80	0.26	-6.0	-90.0	0.162	0.171	0.329	0.331	0.379	12.93
910130	0700	0.71	0.65	0.28	-6.0	-172.0	0.152	0.152	0.431	0.447	0.447	14.08
910201	1300	0.81	0.80	0.15	26.0	90.0	0.152	0.152	0.185	0.171	0.171	12.66
910201	1900	0.66	0.63	0.19	24.0	166.0	0.162	0.113	0.299	0.269	0.351	13.70
910202	0100	0.54	0.53	0.13	6.0	90.0	0.152	0.113	0.255	0.213	0.313	12.75
910202	0700	0.55	0.52	0.19	2.0	176.0	0.103	0.103	0.359	0.439	0.439	13.71
910202	1300	0.52	0.49	0.17	-2.0	-104.0	0.103	0.103	0.335	0.327	0.327	12.78
910202	1900	0.54	0.50	0.21	-12.0	-110.0	0.103	0.113	0.418	0.481	0.502	13.54
910203	0100	0.50	0.46	0.20	-12.0	-112.0	0.103	0.103	0.444	0.468	0.468	12.99
910203	0700	0.51	0.46	0.22	-8.0	-108.0	0.103	0.103	0.470	0.521	0.521	13.44
910203	1300	0.46	0.41	0.20	-10.0	-116.0	0.103	0.093	0.476	0.433	0.528	12.92
910203	1900	0.54	0.48	0.24	-16.0	-112.0	0.113	0.113	0.498	0.513	0.513	13.28
910204	0100	0.46	0.40	0.23	-20.0	-136.0	0.103	0.103	0.581	0.632	0.632	13.17
910204	0700	0.45	0.41	0.20	-10.0	-110.0	0.113	0.103	0.490	0.469	0.520	13.22
910204	1300	0.37	0.32	0.17	-10.0	-136.0	0.103	0.103	0.527	0.532	0.532	13.12

(Continued)

(Continued)

Date	Time EST	Wave Height H_{mo} m	$H_{mo,i}$ m	$H_{mo,r}$ m	Direction $\theta_{p,i}$ deg	$\theta_{p,r}$ deg	Frequency $f_{p,i}$ Hz	$f_{p,r}$ Hz	Reflection x_{mo}	$x_{p,i}$	$x_{p,r}$	Depth m
910204	1900	0.41	0.37	0.18	-16.0	-108.0	0.113	0.113	0.481	0.426	0.426	13.13
910205	0100	0.41	0.35	0.20	-24.0	-134.0	0.113	0.103	0.557	0.551	0.641	13.47
910205	0700	0.43	0.38	0.19	-28.0	-110.0	0.103	0.113	0.506	0.471	0.535	13.21
910205	1300	0.48	0.42	0.23	-14.0	-136.0	0.113	0.123	0.537	0.487	0.610	13.44
910205	1900	0.51	0.46	0.23	-14.0	-132.0	0.113	0.113	0.499	0.534	0.534	13.20
910206	0100	0.60	0.52	0.30	-16.0	-138.0	0.113	0.113	0.575	0.559	0.559	13.74
910206	0700	0.63	0.56	0.29	-20.0	-132.0	0.113	0.113	0.514	0.509	0.509	13.18
910206	1300	0.56	0.49	0.28	-18.0	-136.0	0.113	0.113	0.569	0.591	0.591	13.51
910206	1900	0.53	0.48	0.24	-14.0	-128.0	0.113	0.123	0.511	0.450	0.537	13.12
910207	0100	0.51	0.45	0.25	-16.0	-138.0	0.113	0.113	0.569	0.633	0.633	13.77
910207	0700	0.51	0.45	0.24	-12.0	-134.0	0.123	0.123	0.522	0.565	0.565	13.18
910207	1300	0.54	0.47	0.25	-12.0	-140.0	0.113	0.113	0.534	0.583	0.583	13.32
910207	1900	0.56	0.50	0.25	-6.0	-138.0	0.123	0.113	0.504	0.486	0.541	13.17
910208	0100	0.66	0.60	0.27	4.0	-144.0	0.113	0.113	0.446	0.512	0.512	13.92
910208	0700	1.99	1.90	0.59	30.0	90.0	0.171	0.171	0.308	0.330	0.330	13.42
910209	1300	1.33	1.26	0.43	18.0	90.0	0.210	0.123	0.340	0.336	0.435	13.53
910209	1900	0.90	0.85	0.29	16.0	180.0	0.123	0.142	0.341	0.342	0.426	13.22
910210	0100	0.71	0.66	0.26	10.0	178.0	0.123	0.123	0.386	0.457	0.457	13.67
910210	0700	0.67	0.63	0.24	2.0	-178.0	0.113	0.113	0.384	0.389	0.389	13.41
910211	1300	0.64	0.63	0.15	14.0	90.0	0.240	0.230	0.244	0.204	0.206	13.34
910211	1900	0.56	0.54	0.16	8.0	-180.0	0.162	0.162	0.294	0.280	0.280	13.48
910212	0100	1.11	1.07	0.31	26.0	90.0	0.210	0.210	0.286	0.277	0.277	13.48
910212	0700	1.69	1.64	0.42	30.0	90.0	0.152	0.171	0.258	0.212	0.281	13.84
910212	1300	1.16	1.13	0.27	28.0	90.0	0.162	0.171	0.244	0.219	0.270	13.29
910212	1900	0.91	0.87	0.26	26.0	170.0	0.152	0.142	0.292	0.216	0.309	13.58
910213	0100	0.64	0.61	0.18	16.0	174.0	0.123	0.123	0.302	0.322	0.322	13.13
910213	0700	0.49	0.46	0.16	0.0	174.0	0.132	0.103	0.344	0.277	0.350	13.59
910213	1300	0.35	0.33	0.11	-18.0	-90.0	0.201	0.103	0.349	0.320	0.356	12.81
910213	1900	0.27	0.25	0.09	-20.0	-90.0	0.103	0.083	0.367	0.361	0.519	13.49
910214	0100	0.41	0.38	0.15	-20.0	-106.0	0.132	0.132	0.399	0.408	0.408	12.95
910214	0700	0.62	0.55	0.30	-30.0	-124.0	0.132	0.093	0.553	0.524	0.683	13.74
910214	1300	0.66	0.61	0.27	-22.0	-90.0	0.083	0.083	0.451	0.467	0.467	12.81
910214	1900	0.63	0.56	0.29	-20.0	-132.0	0.093	0.103	0.527	0.539	0.608	13.77
910215	0100	0.53	0.49	0.22	-12.0	-104.0	0.103	0.093	0.452	0.419	0.505	12.94
910215	0700	0.41	0.36	0.19	-8.0	-152.0	0.083	0.083	0.513	0.503	0.503	13.88
910215	1300	0.39	0.36	0.13	-16.0	-102.0	0.093	0.093	0.420	0.494	0.494	12.81
910215	1900	0.85	0.81	0.26	66.0	90.0	0.201	0.240	0.319	0.241	0.403	13.83
910216	0100	0.95	0.90	0.29	60.0	90.0	0.201	0.240	0.316	0.293	0.426	12.91
910216	0700	0.95	0.91	0.27	60.0	90.0	0.181	0.230	0.301	0.252	0.380	13.92
910216	1300	0.79	0.76	0.21	62.0	90.0	0.191	0.240	0.276	0.245	0.401	12.84
910216	1900	0.66	0.63	0.19	54.0	90.0	0.181	0.171	0.300	0.292	0.302	13.81
910217	0100	0.39	0.37	0.11	-2.0	90.0	0.083	0.083	0.307	0.361	0.361	12.73
910217	0700	0.29	0.26	0.13	2.0	168.0	0.083	0.083	0.496	0.550	0.550	13.60
910217	1300	0.25	0.23	0.09	-12.0	176.0	0.093	0.064	0.392	0.303	0.581	12.52
910217	1900	0.29	0.26	0.13	-30.0	168.0	0.093	0.083	0.485	0.594	0.731	13.57

(Continued)

(Continued)

Date	Time EST	Wave Height H_{mo} m	$H_{mo,i}$ m	$H_{mo,r}$ m	Direction $\theta_{p,i}$ deg	$\theta_{p,r}$ deg	Frequency $f_{p,i}$ Hz	$f_{p,r}$ Hz	Reflection X_{mo}	$X_{p,i}$	$X_{p,r}$	Depth m
910218	0100	0.31	0.29	0.11	-24.0	-90.0	0.093	0.064	0.389	0.377	0.663	12.80
910218	0700	0.28	0.26	0.12	-10.0	170.0	0.083	0.093	0.473	0.592	0.661	13.61
910219	1300	0.46	0.43	0.16	-36.0	-90.0	0.181	0.083	0.378	0.369	0.559	13.08
910219	1900	0.47	0.44	0.17	-30.0	-90.0	0.181	0.083	0.377	0.376	0.527	13.51
910220	0100	0.44	0.41	0.15	-18.0	-90.0	0.171	0.171	0.364	0.400	0.400	13.28
910220	0700	0.44	0.41	0.15	-28.0	-90.0	0.171	0.171	0.361	0.324	0.324	13.10
910220	1300	0.40	0.38	0.15	-34.0	-90.0	0.152	0.152	0.387	0.372	0.372	12.97
910220	1900	0.39	0.37	0.12	-30.0	-90.0	0.152	0.152	0.324	0.260	0.260	13.04
910221	0100	0.40	0.37	0.14	-30.0	-90.0	0.142	0.142	0.369	0.389	0.389	13.48
910221	0700	0.57	0.55	0.14	2.0	-90.0	0.152	0.152	0.249	0.266	0.266	13.05
910221	1300	0.66	0.64	0.17	12.0	-90.0	0.152	0.171	0.263	0.244	0.334	13.32
910221	1900	0.58	0.56	0.16	12.0	-90.0	0.113	0.113	0.280	0.386	0.386	12.99
910222	0100	0.66	0.62	0.23	6.0	-130.0	0.171	0.113	0.372	0.327	0.455	13.65
910222	0700	0.52	0.50	0.16	-8.0	-90.0	0.113	0.103	0.311	0.338	0.376	12.86
910222	1300	0.43	0.40	0.18	-14.0	-138.0	0.113	0.103	0.442	0.507	0.536	13.38
910222	1900	0.37	0.34	0.12	-14.0	-104.0	0.113	0.113	0.361	0.366	0.366	12.78
910223	0100	1.02	0.95	0.36	20.0	90.0	0.230	0.240	0.376	0.396	0.419	13.89
910223	0700	2.29	2.24	0.48	30.0	90.0	0.152	0.171	0.216	0.159	0.301	13.22
910223	1300	2.19	2.12	0.56	32.0	90.0	0.152	0.171	0.265	0.188	0.365	13.82
910223	1900	2.41	2.36	0.49	18.0	90.0	0.142	0.171	0.207	0.171	0.266	13.14
910224	0100	1.58	1.53	0.40	18.0	90.0	0.152	0.171	0.260	0.236	0.322	13.97
910224	0700	1.38	1.35	0.29	12.0	90.0	0.152	0.171	0.218	0.192	0.259	13.15
910224	1300	1.42	1.37	0.37	8.0	176.0	0.142	0.142	0.272	0.281	0.281	13.58
910224	1900	1.81	1.75	0.47	-2.0	-90.0	0.113	0.113	0.266	0.299	0.299	13.05
910225	0100	1.68	1.60	0.52	2.0	178.0	0.113	0.113	0.322	0.394	0.394	13.81
910225	0700	1.22	1.16	0.38	10.0	-178.0	0.113	0.113	0.324	0.430	0.430	13.35
910225	1300	1.26	1.21	0.33	14.0	178.0	0.132	0.132	0.276	0.290	0.290	13.48
910225	1900	1.10	1.05	0.33	12.0	180.0	0.132	0.132	0.310	0.355	0.355	13.27
910226	0100	1.02	0.98	0.29	8.0	174.0	0.142	0.132	0.293	0.295	0.346	13.57
910226	0700	1.64	1.58	0.45	20.0	90.0	0.201	0.181	0.285	0.296	0.299	13.66
910226	1300	1.44	1.40	0.36	20.0	90.0	0.171	0.171	0.261	0.256	0.256	13.41
910226	1900	1.07	1.02	0.31	20.0	160.0	0.171	0.181	0.308	0.320	0.334	13.62
910227	0100	0.80	0.76	0.23	18.0	176.0	0.132	0.132	0.302	0.284	0.284	13.30
910227	0700	0.82	0.77	0.30	28.0	166.0	0.113	0.123	0.385	0.428	0.467	13.87
910227	1300	0.57	0.55	0.16	22.0	170.0	0.123	0.123	0.293	0.304	0.304	13.05
910227	1900	0.44	0.41	0.16	30.0	166.0	0.113	0.113	0.388	0.443	0.443	13.79
910228	0100	0.37	0.34	0.13	12.0	-90.0	0.113	0.103	0.395	0.382	0.485	12.95
910228	0700	0.30	0.28	0.13	6.0	-90.0	0.103	0.103	0.455	0.456	0.456	13.91
910228	1300	0.35	0.32	0.13	8.0	174.0	0.103	0.103	0.419	0.404	0.404	12.78
910228	1900	0.47	0.42	0.22	12.0	-180.0	0.093	0.093	0.519	0.589	0.589	13.82
910301	0100	0.44	0.42	0.15	8.0	110.0	0.093	0.093	0.357	0.335	0.335	12.77
910301	0700	0.67	0.61	0.27	-20.0	-90.0	0.181	0.181	0.442	0.513	0.513	13.94
910301	1300	0.62	0.59	0.19	-8.0	-90.0	0.103	0.103	0.324	0.340	0.340	12.74
910301	1900	0.66	0.60	0.26	-6.0	-90.0	0.103	0.103	0.429	0.437	0.437	13.98
910302	0100	1.10	1.05	0.32	-16.0	-90.0	0.142	0.142	0.307	0.313	0.313	12.73
910302	0700	1.38	1.28	0.51	-14.0	-90.0	0.123	0.123	0.394	0.401	0.401	13.80
910302	1300	1.16	1.11	0.35	-10.0	-90.0	0.113	0.113	0.312	0.309	0.309	12.58

(Continued)

(Continued)

Date	Time EST	Wave Height H_{mo} m	$H_{mo,i}$ m	$H_{mo,r}$ m	Direction $\theta_{p,i}$ deg	$\theta_{p,r}$ deg	Frequency $f_{p,i}$ Hz	$f_{p,r}$ Hz	Reflection X_{mo}	$X_{p,i}$	$X_{p,r}$	Depth m
910302	1900	1.02	0.94	0.39	-12.0	-112.0	0.113	0.113	0.416	0.458	0.458	13.80
910303	0100	0.93	0.89	0.27	-6.0	-90.0	0.113	0.113	0.307	0.299	0.299	12.74
910303	0700	1.01	0.93	0.40	-6.0	-90.0	0.113	0.113	0.435	0.428	0.428	13.66
910303	1300	0.87	0.83	0.26	-6.0	-90.0	0.113	0.113	0.316	0.310	0.310	12.74
910303	1900	1.34	1.24	0.51	-8.0	-116.0	0.113	0.113	0.415	0.450	0.450	13.65
910304	0100	1.29	1.22	0.42	-12.0	-116.0	0.103	0.093	0.345	0.292	0.339	12.82
910304	0700	1.18	1.09	0.44	-8.0	-118.0	0.093	0.093	0.404	0.417	0.417	13.39
910304	1300	1.15	1.07	0.41	-10.0	-90.0	0.093	0.093	0.387	0.324	0.324	12.79
910304	1900	1.11	0.98	0.52	-10.0	-134.0	0.093	0.093	0.533	0.523	0.523	13.53
910305	0100	0.98	0.88	0.43	-16.0	-124.0	0.093	0.083	0.485	0.434	0.535	13.23
910305	0700	0.96	0.87	0.39	-6.0	-140.0	0.093	0.093	0.450	0.470	0.470	13.52
910305	1300	0.88	0.81	0.34	-4.0	-136.0	0.093	0.093	0.424	0.416	0.416	13.24
910305	1900	0.87	0.80	0.36	-2.0	-138.0	0.103	0.103	0.454	0.485	0.485	13.46
910306	0100	0.77	0.69	0.36	-2.0	-142.0	0.103	0.103	0.518	0.520	0.520	13.37
910306	0700	0.80	0.73	0.32	2.0	-138.0	0.103	0.103	0.439	0.412	0.412	13.19
910306	1300	0.78	0.70	0.34	2.0	-140.0	0.103	0.103	0.482	0.488	0.488	13.19
910307	0100	0.82	0.73	0.37	-4.0	-146.0	0.103	0.103	0.516	0.519	0.519	13.33
910307	0700	0.70	0.64	0.29	-4.0	-90.0	0.103	0.103	0.454	0.392	0.392	12.98
910307	1300	0.55	0.49	0.27	-2.0	-142.0	0.093	0.093	0.549	0.532	0.532	13.34
910307	1900	0.49	0.45	0.18	-4.0	-138.0	0.093	0.093	0.404	0.449	0.449	13.18
910308	0100	0.58	0.55	0.20	6.0	90.0	0.240	0.103	0.358	0.255	0.420	13.70
910308	0700	1.01	0.97	0.26	30.0	90.0	0.191	0.201	0.269	0.266	0.290	13.19
910308	1300	0.91	0.87	0.26	34.0	90.0	0.191	0.191	0.295	0.306	0.306	13.44
910308	1900	0.85	0.81	0.24	16.0	90.0	0.181	0.181	0.300	0.316	0.316	13.05
910309	0100	0.78	0.75	0.23	22.0	90.0	0.201	0.201	0.309	0.297	0.297	13.64
910309	0700	1.23	1.19	0.32	22.0	90.0	0.162	0.171	0.272	0.226	0.292	13.10
910309	1300	1.08	1.03	0.33	22.0	90.0	0.181	0.181	0.323	0.366	0.366	13.50
910309	1900	0.93	0.89	0.27	22.0	90.0	0.132	0.142	0.302	0.262	0.296	13.06
910310	0100	0.78	0.74	0.24	18.0	170.0	0.142	0.142	0.331	0.332	0.332	13.64
910310	0700	1.13	1.09	0.30	18.0	166.0	0.181	0.181	0.272	0.310	0.310	13.14
910310	1300	1.18	1.13	0.33	18.0	168.0	0.152	0.152	0.296	0.295	0.295	13.61
910310	1900	1.20	1.14	0.36	20.0	168.0	0.171	0.152	0.317	0.307	0.344	13.29
910311	0100	1.29	1.20	0.47	32.0	162.0	0.162	0.171	0.397	0.374	0.406	13.92
910311	0700	1.44	1.38	0.42	30.0	156.0	0.152	0.152	0.306	0.293	0.293	13.48
910311	1300	1.66	1.57	0.54	30.0	146.0	0.142	0.142	0.346	0.346	0.346	13.70
910311	1900	1.33	1.26	0.42	28.0	90.0	0.142	0.142	0.332	0.345	0.345	13.42
910312	0100	1.45	1.37	0.46	30.0	90.0	0.162	0.171	0.339	0.291	0.347	13.81
910312	0700	1.27	1.20	0.42	26.0	172.0	0.142	0.113	0.352	0.328	0.447	13.58
910312	1300	1.11	1.05	0.34	24.0	174.0	0.152	0.132	0.324	0.309	0.365	13.59
910312	1900	0.87	0.81	0.32	18.0	176.0	0.123	0.103	0.394	0.368	0.473	13.47
910313	0100	0.80	0.73	0.32	18.0	176.0	0.103	0.103	0.440	0.576	0.576	13.53
910313	0700	0.88	0.80	0.37	14.0	176.0	0.074	0.074	0.457	0.444	0.444	13.58
910313	1300	1.00	0.93	0.37	10.0	166.0	0.083	0.074	0.398	0.385	0.420	13.33
910313	1900	1.09	1.01	0.40	2.0	172.0	0.083	0.083	0.401	0.419	0.419	13.51
910314	0100	0.96	0.90	0.35	-2.0	-90.0	0.083	0.093	0.386	0.396	0.428	13.35
910314	0700	1.18	1.09	0.45	16.0	174.0	0.132	0.132	0.408	0.462	0.462	13.75
910314	1300	0.93	0.88	0.30	16.0	176.0	0.123	0.113	0.343	0.307	0.438	13.25

(Continued)

(Continued)

Date	Time EST	Wave Height H_{mo} m	$H_{mo,i}$ m	$H_{mo,r}$ m	Direction $\theta_{p,i}$ deg	$\theta_{p,r}$ deg	Frequency $f_{p,i}$ Hz	$f_{p,r}$ Hz	Reflection X_{mo}	$X_{p,i}$	$X_{p,r}$	Depth m
910314	1900	0.97	0.89	0.39	18.0	170.0	0.113	0.113	0.441	0.434	0.434	13.84
910315	0100	1.26	1.17	0.47	18.0	176.0	0.103	0.103	0.401	0.448	0.448	13.37
910315	0700	1.48	1.37	0.57	22.0	172.0	0.093	0.093	0.414	0.537	0.537	14.06
910315	1300	1.63	1.55	0.52	20.0	90.0	0.103	0.103	0.333	0.383	0.383	13.32
910315	1900	1.78	1.65	0.65	22.0	174.0	0.093	0.093	0.390	0.492	0.492	14.15
910316	0100	1.82	1.73	0.57	20.0	170.0	0.093	0.093	0.332	0.388	0.388	13.28
910316	0700	1.72	1.58	0.69	18.0	176.0	0.083	0.083	0.435	0.539	0.539	14.17
910316	1300	1.46	1.37	0.50	14.0	170.0	0.083	0.083	0.367	0.401	0.401	13.16
910316	1900	1.35	1.22	0.59	14.0	178.0	0.083	0.093	0.487	0.472	0.607	14.19
910317	0100	1.30	1.22	0.44	10.0	162.0	0.083	0.083	0.362	0.351	0.351	13.01
910317	0700	1.29	1.18	0.53	8.0	178.0	0.083	0.074	0.450	0.442	0.490	14.04
910317	1300	1.20	1.12	0.42	6.0	160.0	0.083	0.083	0.379	0.377	0.377	12.94
910317	1900	1.30	1.16	0.58	6.0	180.0	0.074	0.074	0.506	0.575	0.575	14.15
910318	0100	1.29	1.20	0.49	4.0	164.0	0.083	0.083	0.410	0.450	0.450	12.90
910318	0700	1.21	1.09	0.51	4.0	178.0	0.083	0.083	0.466	0.552	0.552	13.90
910318	1300	1.41	1.32	0.49	-2.0	-90.0	0.074	0.074	0.374	0.379	0.379	12.76
910318	1900	1.53	1.39	0.62	0.0	-144.0	0.083	0.083	0.446	0.443	0.443	14.06
910319	0100	1.20	1.12	0.44	0.0	-90.0	0.083	0.103	0.391	0.340	0.410	12.98
910319	0700	0.96	0.85	0.44	0.0	-144.0	0.103	0.103	0.517	0.513	0.513	13.83
910319	1300	0.96	0.89	0.35	-2.0	90.0	0.083	0.083	0.391	0.341	0.341	12.98
910319	1900	0.84	0.76	0.37	2.0	90.0	0.093	0.093	0.497	0.511	0.511	14.04
910320	0100	0.62	0.56	0.25	10.0	90.0	0.083	0.083	0.453	0.463	0.463	13.16
910320	0700	0.51	0.46	0.23	8.0	174.0	0.083	0.093	0.500	0.501	0.625	13.57
910320	1300	0.44	0.40	0.18	6.0	158.0	0.083	0.083	0.447	0.439	0.439	13.02
910320	1900	0.46	0.41	0.20	12.0	170.0	0.083	0.083	0.486	0.493	0.493	13.66
910321	0100	0.48	0.43	0.20	8.0	176.0	0.083	0.074	0.472	0.405	0.463	13.34
910321	0700	0.52	0.46	0.24	8.0	174.0	0.074	0.074	0.516	0.604	0.604	13.35
910321	1300	0.51	0.46	0.22	4.0	-180.0	0.074	0.074	0.467	0.469	0.469	13.21
910321	1900	0.51	0.46	0.23	2.0	162.0	0.083	0.083	0.492	0.481	0.481	13.33
910322	0100	0.48	0.43	0.23	4.0	-166.0	0.083	0.074	0.544	0.406	0.606	13.52
910322	0700	0.45	0.41	0.18	0.0	156.0	0.074	0.083	0.446	0.398	0.450	13.11
910323	1300	0.82	0.76	0.31	18.0	152.0	0.132	0.132	0.410	0.395	0.395	13.74
910323	1900	0.99	0.93	0.31	16.0	-90.0	0.113	0.113	0.335	0.363	0.363	13.08
910324	0100	0.87	0.79	0.38	14.0	174.0	0.103	0.103	0.479	0.496	0.496	13.94
910324	0700	0.81	0.76	0.28	10.0	-90.0	0.113	0.113	0.371	0.352	0.352	13.09
910324	1300	0.83	0.75	0.37	8.0	176.0	0.113	0.113	0.494	0.509	0.509	13.73
910324	1900	0.69	0.64	0.25	6.0	-90.0	0.113	0.113	0.393	0.347	0.347	13.05
910325	0100	0.92	0.88	0.27	22.0	90.0	0.230	0.230	0.309	0.303	0.303	13.98
910325	0700	0.90	0.87	0.25	26.0	90.0	0.171	0.162	0.287	0.302	0.339	13.11
910325	1300	0.69	0.66	0.21	10.0	166.0	0.103	0.103	0.313	0.415	0.415	13.69
910325	1900	0.48	0.46	0.15	12.0	162.0	0.093	0.103	0.334	0.394	0.427	13.09
910326	0100	0.49	0.45	0.17	8.0	174.0	0.093	0.093	0.385	0.420	0.420	13.86
910326	0700	0.43	0.40	0.16	10.0	166.0	0.093	0.083	0.409	0.395	0.503	13.37
910326	1300	0.55	0.50	0.22	6.0	176.0	0.093	0.093	0.445	0.512	0.512	13.68
910326	1900	0.54	0.49	0.22	8.0	-178.0	0.093	0.093	0.444	0.517	0.517	13.39
910327	0100	0.67	0.61	0.26	10.0	174.0	0.093	0.103	0.426	0.420	0.454	13.63

(Continued)

(Continued)

Date	Time EST	Wave Height H_{mo} m	$H_{mo,i}$ m	$H_{mo,r}$ m	Direction $\theta_{p,i}$ deg	$\theta_{p,r}$ deg	Frequency $f_{p,i}$ Hz	$f_{p,r}$ Hz	Reflection x_{mo}	$x_{p,i}$	$x_{p,r}$	Depth m
910327	0700	0.73	0.66	0.31	4.0	-178.0	0.093	0.093	0.468	0.488	0.488	13.47
910327	1300	0.80	0.75	0.30	2.0	162.0	0.093	0.093	0.407	0.419	0.419	13.35
910327	1900	0.73	0.65	0.33	0.0	-178.0	0.093	0.093	0.498	0.498	0.498	13.43
910328	0100	0.63	0.58	0.25	2.0	158.0	0.083	0.093	0.435	0.407	0.514	13.10
910328	0700	0.64	0.57	0.28	0.0	-174.0	0.083	0.083	0.485	0.499	0.499	13.43
910328	1300	0.55	0.51	0.21	-4.0	-90.0	0.083	0.093	0.400	0.374	0.436	12.95
910328	1900	0.52	0.46	0.23	-22.0	-150.0	0.093	0.083	0.507	0.515	0.533	13.59
910329	0100	0.47	0.44	0.18	-8.0	-90.0	0.093	0.083	0.410	0.405	0.478	12.90
910329	0700	0.51	0.45	0.23	-30.0	-90.0	0.093	0.093	0.499	0.520	0.520	13.66
910329	1300	0.69	0.64	0.27	-28.0	-90.0	0.142	0.240	0.431	0.380	0.546	12.86
910329	1900	0.76	0.67	0.37	-24.0	-90.0	0.132	0.132	0.547	0.575	0.575	13.85
910330	0100	0.81	0.75	0.32	-20.0	-90.0	0.132	0.132	0.424	0.431	0.431	12.84
910330	0700	0.86	0.76	0.40	-22.0	-130.0	0.103	0.093	0.528	0.543	0.592	13.94
910330	1300	1.84	1.76	0.55	32.0	90.0	0.171	0.171	0.314	0.298	0.298	13.18
910330	1900	1.59	1.50	0.53	22.0	90.0	0.132	0.132	0.352	0.423	0.423	14.30
910331	0100	1.09	1.04	0.31	10.0	146.0	0.123	0.103	0.300	0.239	0.340	13.04
910331	0700	1.15	1.09	0.37	12.0	164.0	0.123	0.132	0.343	0.347	0.433	14.01
910331	1300	1.19	1.15	0.29	14.0	90.0	0.201	0.201	0.253	0.269	0.269	13.01
910331	1900	1.28	1.22	0.40	16.0	166.0	0.171	0.181	0.326	0.320	0.351	14.15
910401	0100	1.03	1.00	0.27	14.0	168.0	0.113	0.113	0.271	0.305	0.305	12.98
910401	0700	1.02	0.94	0.39	10.0	172.0	0.123	0.123	0.416	0.430	0.430	13.85
910401	1300	0.79	0.76	0.23	10.0	160.0	0.113	0.093	0.304	0.269	0.343	12.90
910401	1900	0.66	0.60	0.28	14.0	174.0	0.093	0.093	0.473	0.524	0.524	13.96
910402	0100	0.64	0.60	0.21	8.0	176.0	0.103	0.103	0.347	0.378	0.378	12.99
910402	0700	0.78	0.73	0.27	8.0	174.0	0.113	0.113	0.377	0.445	0.445	13.72
910402	1300	0.56	0.53	0.18	8.0	-90.0	0.123	0.113	0.334	0.288	0.389	12.99
910402	1900	0.52	0.49	0.18	6.0	174.0	0.132	0.132	0.362	0.411	0.411	13.85
910403	0100	0.52	0.48	0.18	6.0	-180.0	0.103	0.103	0.374	0.411	0.411	13.14
910403	0700	0.57	0.53	0.19	4.0	174.0	0.113	0.103	0.361	0.411	0.435	13.58
910403	1300	0.50	0.47	0.17	4.0	180.0	0.113	0.113	0.367	0.386	0.386	13.13
910403	1900	0.53	0.50	0.18	0.0	166.0	0.113	0.113	0.360	0.379	0.379	13.63
910404	0100	0.56	0.53	0.18	-4.0	160.0	0.113	0.083	0.332	0.322	0.401	13.26
910404	0700	0.61	0.58	0.19	4.0	-90.0	0.093	0.093	0.336	0.468	0.468	13.31
910404	1300	0.55	0.52	0.18	-4.0	-102.0	0.093	0.093	0.341	0.417	0.417	13.18
910404	1900	0.57	0.54	0.20	-8.0	-90.0	0.093	0.093	0.364	0.442	0.442	13.43
910405	0100	0.53	0.48	0.22	-12.0	-148.0	0.093	0.093	0.447	0.520	0.520	13.36
910405	0700	0.53	0.49	0.19	-12.0	-90.0	0.093	0.093	0.380	0.364	0.364	13.10
910405	1300	0.56	0.51	0.23	-14.0	-140.0	0.093	0.093	0.464	0.490	0.490	13.20
910405	1900	0.51	0.47	0.19	-20.0	-90.0	0.093	0.093	0.406	0.415	0.415	13.13
910406	0100	0.45	0.40	0.19	-24.0	-146.0	0.093	0.093	0.472	0.496	0.496	13.38
910406	0700	0.44	0.41	0.15	-20.0	-90.0	0.093	0.093	0.359	0.367	0.367	12.96
910406	1300	0.50	0.46	0.21	-12.0	-90.0	0.103	0.103	0.459	0.510	0.510	13.31
910406	1900	0.50	0.47	0.18	-12.0	-100.0	0.103	0.103	0.395	0.370	0.370	13.09
910407	0100	0.48	0.43	0.22	-12.0	-144.0	0.103	0.103	0.504	0.549	0.549	13.52
910407	0700	0.40	0.37	0.16	-12.0	-90.0	0.103	0.103	0.424	0.439	0.439	12.97
910407	1300	0.36	0.33	0.15	-12.0	-144.0	0.103	0.113	0.468	0.455	0.533	13.41
910407	1900	0.35	0.32	0.14	-32.0	-100.0	0.113	0.113	0.429	0.396	0.396	13.03

(Continued)

(Continued)

Date	Time EST	Wave Height H_{mo} m	$H_{mo,i}$ m	$H_{mo,r}$ m	Direction $\theta_{p,i}$ deg	$\theta_{p,r}$ deg	Frequency $f_{p,i}$ Hz	$f_{p,r}$ Hz	Reflection X_{mo}	$X_{p,i}$	$X_{p,r}$	Depth m
910408	0100	0.36	0.33	0.14	-38.0	-108.0	0.113	0.113	0.431	0.464	0.464	13.57
910408	0700	0.34	0.31	0.12	-38.0	-90.0	0.113	0.113	0.398	0.373	0.373	12.94
910408	1300	0.33	0.31	0.14	-32.0	-106.0	0.113	0.113	0.443	0.479	0.479	13.47
910408	1900	0.35	0.32	0.13	-30.0	-90.0	0.113	0.113	0.412	0.377	0.377	13.00
910409	0100	0.38	0.35	0.16	-34.0	-90.0	0.113	0.113	0.461	0.437	0.437	13.57
910409	0700	0.48	0.44	0.17	-34.0	-90.0	0.162	0.162	0.395	0.418	0.418	12.93
910409	1300	0.51	0.47	0.19	-26.0	-90.0	0.162	0.152	0.403	0.416	0.482	13.43
910409	1900	0.51	0.48	0.18	-24.0	-90.0	0.113	0.113	0.377	0.367	0.367	12.95
910410	0100	0.52	0.46	0.23	-26.0	-90.0	0.142	0.142	0.487	0.489	0.489	13.44
910410	0700	0.45	0.42	0.17	-36.0	-90.0	0.142	0.142	0.411	0.388	0.388	12.94
910410	1300	0.39	0.36	0.15	-26.0	-90.0	0.113	0.113	0.428	0.457	0.457	13.42
910410	1900	0.38	0.35	0.15	-34.0	-90.0	0.113	0.113	0.422	0.414	0.414	13.17
910411	0100	0.69	0.66	0.22	44.0	90.0	0.240	0.240	0.340	0.336	0.336	13.61
910411	0700	1.82	1.74	0.52	42.0	90.0	0.162	0.171	0.299	0.214	0.365	13.52
910411	1300	0.99	0.94	0.29	24.0	162.0	0.162	0.171	0.311	0.276	0.387	13.59
910411	1900	0.55	0.52	0.19	10.0	164.0	0.162	0.152	0.367	0.387	0.477	13.38
910412	0100	0.49	0.46	0.15	4.0	-172.0	0.142	0.171	0.331	0.338	0.425	13.29
910412	0700	0.79	0.77	0.19	18.0	90.0	0.210	0.240	0.241	0.205	0.233	13.47
910412	1300	1.40	1.36	0.33	26.0	90.0	0.162	0.162	0.243	0.242	0.242	13.40
910412	1900	1.03	0.99	0.29	24.0	164.0	0.162	0.162	0.297	0.313	0.313	13.66
910413	0100	1.11	1.08	0.26	14.0	90.0	0.201	0.171	0.241	0.234	0.307	13.18
910413	0700	0.86	0.83	0.23	14.0	168.0	0.171	0.171	0.278	0.302	0.302	13.54
910413	1300	0.80	0.78	0.20	6.0	-90.0	0.162	0.162	0.256	0.283	0.283	13.14
910413	1900	0.83	0.79	0.26	2.0	-90.0	0.152	0.142	0.328	0.283	0.369	13.81
910414	0100	0.78	0.75	0.21	0.0	-90.0	0.152	0.171	0.285	0.268	0.293	13.00
910414	0700	0.65	0.61	0.22	-14.0	-90.0	0.162	0.162	0.369	0.395	0.395	13.78
910414	1300	0.53	0.51	0.15	-12.0	-90.0	0.093	0.093	0.302	0.364	0.364	13.16
910414	1900	1.50	1.41	0.52	22.0	158.0	0.132	0.132	0.372	0.417	0.417	14.25
910415	0100	1.33	1.30	0.29	14.0	90.0	0.113	0.103	0.224	0.204	0.245	13.00
910415	0700	1.28	1.22	0.40	14.0	176.0	0.113	0.113	0.325	0.365	0.365	13.87
910415	1300	1.00	0.96	0.26	6.0	-90.0	0.113	0.083	0.270	0.236	0.283	12.88
910415	1900	0.84	0.77	0.32	0.0	178.0	0.123	0.113	0.415	0.411	0.445	14.10
910416	0100	0.71	0.68	0.20	-4.0	-90.0	0.103	0.113	0.294	0.258	0.283	12.76
910416	0700	0.68	0.62	0.28	-12.0	-90.0	0.113	0.103	0.452	0.426	0.616	13.84
910416	1300	0.53	0.50	0.16	-10.0	-90.0	0.123	0.123	0.327	0.334	0.334	12.81
910416	1900	0.62	0.58	0.21	2.0	-90.0	0.123	0.132	0.352	0.346	0.405	14.12
910417	0100	0.57	0.55	0.15	-12.0	-90.0	0.132	0.162	0.277	0.224	0.267	12.75
910417	0700	0.59	0.55	0.20	-12.0	-90.0	0.162	0.123	0.356	0.355	0.412	13.68
910417	1300	0.47	0.44	0.14	-18.0	-90.0	0.[illegible]2	0.064	0.312	0.290	0.534	12.73
910417	1900	0.47	0.43	0.19	-22.0	-90.0	0.132	0.064	0.450	0.420	0.784	13.98
910418	0700	1.03	1.00	0.28	18.0	90.0	0.240	0.240	0.277	0.255	0.255	13.82
910418	1300	1.70	1.65	0.42	32.0	90.0	0.171	0.171	0.253	0.251	0.251	13.37
910418	1900	1.66	1.60	0.45	30.0	90.0	0.152	0.152	0.281	0.280	0.280	14.11
910419	0100	1.78	1.73	0.43	22.0	90.0	0.171	0.171	0.247	0.282	0.282	13.63
910419	0700	1.74	1.68	0.43	20.0	90.0	0.171	0.171	0.254	0.248	0.248	13.71
910419	1300	1.53	1.47	0.39	14.0	90.0	0.103	0.103	0.267	0.290	0.290	13.50
910419	1900	1.59	1.53	0.41	10.0	90.0	0.103	0.103	0.267	0.295	0.295	13.72

(Continued)

(Continued)

Date	Time EST	Wave Height H_{mo} m	$H_{mo,i}$ m	$H_{mo,r}$ m	Direction $\theta_{p,i}$ deg	$\theta_{p,r}$ deg	Frequency $f_{p,i}$ Hz	$f_{p,r}$ Hz	Reflection X_{mo}	$X_{p,i}$	$X_{p,r}$	Depth m
910420	0100	1.60	1.55	0.40	8.0	-90.0	0.142	0.103	0.258	0.211	0.271	13.84
910420	0700	1.84	1.79	0.42	4.0	-90.0	0.142	0.142	0.234	0.223	0.223	13.45
910420	1300	2.58	2.52	0.55	0.0	-90.0	0.113	0.113	0.217	0.209	0.209	13.77
910420	1900	3.07	2.99	0.70	12.0	90.0	0.123	0.240	0.234	0.155	0.445	13.57
910421	0100	2.17	2.08	0.62	16.0	90.0	0.123	0.113	0.299	0.266	0.315	14.11
910421	0700	1.66	1.59	0.48	18.0	90.0	0.123	0.103	0.302	0.250	0.313	13.33
910421	1300	1.36	1.25	0.52	24.0	-178.0	0.123	0.123	0.417	0.378	0.378	13.92
910421	1900	0.85	0.79	0.32	20.0	-178.0	0.123	0.113	0.401	0.325	0.394	13.22
910422	0100	0.61	0.55	0.26	18.0	180.0	0.123	0.113	0.475	0.516	0.523	13.99
910422	0700	0.45	0.41	0.17	6.0	-180.0	0.123	0.123	0.422	0.423	0.423	13.00
910422	1300	0.48	0.43	0.21	4.0	-90.0	0.113	0.113	0.484	0.506	0.506	13.75
910422	1900	0.49	0.45	0.20	-4.0	-90.0	0.113	0.113	0.440	0.422	0.422	12.90
910423	0100	0.57	0.50	0.27	2.0	-140.0	0.113	0.113	0.533	0.585	0.585	13.80
910423	0700	0.47	0.43	0.18	2.0	-90.0	0.113	0.103	0.422	0.360	0.435	12.97
910423	1300	0.46	0.41	0.21	6.0	176.0	0.123	0.113	0.519	0.478	0.558	13.82
910423	1900	0.47	0.43	0.19	4.0	168.0	0.123	0.123	0.430	0.373	0.373	13.06
910424	0100	0.51	0.46	0.23	0.0	174.0	0.123	0.123	0.492	0.452	0.452	13.72
910424	0700	0.54	0.50	0.21	2.0	-90.0	0.123	0.093	0.415	0.342	0.449	13.05
910425	1300	0.47	0.44	0.15	6.0	90.0	0.240	0.093	0.345	0.306	0.476	13.54
910425	1900	0.45	0.42	0.17	10.0	-180.0	0.083	0.093	0.401	0.440	0.491	13.53
910426	0100	0.46	0.44	0.15	10.0	176.0	0.093	0.093	0.345	0.369	0.369	13.33
910426	0700	0.47	0.43	0.18	2.0	-180.0	0.093	0.093	0.429	0.498	0.498	13.48
910426	1300	0.50	0.47	0.18	-2.0	176.0	0.142	0.103	0.382	0.374	0.482	13.32
910426	1900	0.43	0.39	0.18	-2.0	180.0	0.093	0.093	0.451	0.492	0.492	13.72
910427	0100	0.42	0.39	0.15	-4.0	172.0	0.093	0.093	0.378	0.515	0.515	13.09
910427	0700	0.43	0.39	0.17	0.0	176.0	0.093	0.093	0.435	0.443	0.443	13.59
910427	1300	0.54	0.50	0.19	2.0	-90.0	0.093	0.093	0.374	0.432	0.432	13.11
910427	1900	0.56	0.50	0.24	-2.0	174.0	0.093	0.093	0.470	0.509	0.509	13.86
910428	0100	0.63	0.59	0.23	2.0	168.0	0.074	0.074	0.391	0.479	0.479	12.91
910428	0700	0.60	0.53	0.26	0.0	172.0	0.083	0.083	0.495	0.547	0.547	13.66
910428	1300	0.56	0.52	0.21	0.0	166.0	0.083	0.083	0.394	0.371	0.371	12.97
910428	1900	0.53	0.49	0.20	-26.0	-90.0	0.083	0.083	0.406	0.435	0.435	14.04
910429	0100	0.52	0.48	0.19	-30.0	-90.0	0.093	0.083	0.396	0.377	0.645	13.04
910429	0700	0.80	0.76	0.25	-14.0	-90.0	0.162	0.162	0.323	0.345	0.345	13.91
910430	1300	0.64	0.61	0.20	6.0	-90.0	0.132	0.074	0.323	0.275	0.417	13.00
910430	1900	0.53	0.49	0.20	4.0	180.0	0.074	0.074	0.413	0.472	0.472	14.00
910501	0100	0.46	0.42	0.18	2.0	168.0	0.074	0.074	0.427	0.591	0.591	13.00
910501	0700	0.41	0.37	0.16	4.0	172.0	0.074	0.074	0.435	0.603	0.603	13.74
910501	1300	0.40	0.37	0.16	8.0	168.0	0.074	0.074	0.444	0.579	0.579	13.08
910501	1900	0.38	0.35	0.15	-4.0	180.0	0.083	0.083	0.414	0.546	0.546	13.96
910502	0100	0.33	0.29	0.14	-2.0	176.0	0.083	0.083	0.492	0.555	0.555	13.13
910502	0700	0.33	0.31	0.12	2.0	172.0	0.083	0.074	0.394	0.386	0.506	13.65
910502	1300	0.34	0.31	0.14	-2.0	172.0	0.083	0.074	0.436	0.446	0.588	13.15
910502	1900	0.37	0.34	0.13	-4.0	172.0	0.074	0.074	0.390	0.493	0.493	13.80
910503	0100	0.38	0.35	0.14	-2.0	176.0	0.132	0.074	0.401	0.298	0.501	13.24
910503	0700	0.31	0.29	0.11	0.0	172.0	0.083	0.074	0.394	0.401	0.624	13.47

(Continued)

(Continued)

Date	Time EST	Wave Height H_{mo} m	$H_{mo,i}$ m	$H_{mo,r}$ m	Direction $\theta_{p,i}$ deg	$\theta_{p,r}$ deg	Frequency $f_{p,i}$ Hz	$f_{p,r}$ Hz	Reflection X_{mo}	$X_{p,i}$	$X_{p,r}$	Depth m
910503	1300	0.42	0.39	0.14	18.0	90.0	0.240	0.240	0.346	0.328	0.328	13.30
910503	1900	0.57	0.55	0.15	46.0	90.0	0.191	0.201	0.270	0.238	0.263	13.66
910504	0100	0.41	0.40	0.11	36.0	166.0	0.181	0.181	0.288	0.256	0.256	13.39
910504	0700	0.30	0.28	0.10	4.0	-90.0	0.240	0.083	0.352	0.267	0.486	13.36
910504	1300	0.30	0.29	0.09	-6.0	-90.0	0.191	0.191	0.325	0.367	0.367	13.37
910504	1900	0.30	0.29	0.09	-2.0	-90.0	0.201	0.093	0.304	0.261	0.523	13.45
910505	0100	0.40	0.39	0.11	14.0	-90.0	0.171	0.171	0.286	0.284	0.284	13.47
910505	0700	0.40	0.39	0.10	18.0	-90.0	0.191	0.191	0.270	0.249	0.249	13.20
910505	1300	0.37	0.35	0.11	-14.0	-90.0	0.230	0.083	0.310	0.274	0.378	13.48
910505	1900	0.41	0.39	0.12	-8.0	-90.0	0.191	0.191	0.299	0.307	0.307	13.39
910506	0100	0.49	0.46	0.16	-18.0	-90.0	0.201	0.201	0.352	0.385	0.385	13.69
910506	0700	0.68	0.64	0.21	-18.0	-90.0	0.181	0.181	0.319	0.333	0.333	13.17
910506	1900	0.39	0.38	0.12	-14.0	-90.0	0.171	0.132	0.317	0.248	0.372	13.15
910507	0100	0.40	0.37	0.14	-22.0	-138.0	0.162	0.152	0.386	0.343	0.381	13.62
910507	0700	0.35	0.33	0.12	-20.0	-90.0	0.152	0.142	0.361	0.320	0.348	13.11
910507	1300	0.68	0.66	0.18	62.0	90.0	0.240	0.240	0.278	0.262	0.262	13.77
910507	1900	0.50	0.48	0.14	28.0	90.0	0.210	0.220	0.283	0.239	0.330	13.17
910508	0100	0.45	0.43	0.14	0.0	-90.0	0.210	0.083	0.336	0.211	0.537	13.68
910508	0700	0.41	0.39	0.12	0.0	150.0	0.142	0.093	0.305	0.246	0.351	13.00
910508	1300	0.40	0.38	0.14	0.0	180.0	0.093	0.093	0.358	0.435	0.435	13.71
910508	1900	0.40	0.39	0.13	-8.0	-90.0	0.162	0.093	0.325	0.282	0.412	13.08
910509	0100	0.42	0.40	0.14	-10.0	-144.0	0.181	0.171	0.363	0.359	0.410	13.66
910509	0700	0.42	0.40	0.12	-14.0	-90.0	0.191	0.093	0.298	0.230	0.460	12.98
910509	1300	0.38	0.36	0.12	-14.0	174.0	0.191	0.093	0.336	0.296	0.485	13.73
910509	1900	0.40	0.38	0.10	-12.0	-90.0	0.103	0.103	0.266	0.288	0.288	13.18
910510	0100	0.47	0.44	0.14	-10.0	-90.0	0.201	0.201	0.312	0.290	0.290	13.66
910510	0700	0.47	0.45	0.13	-18.0	-90.0	0.201	0.191	0.295	0.254	0.326	13.08
910510	1300	0.45	0.41	0.16	-14.0	-144.0	0.132	0.132	0.397	0.491	0.491	13.67
910510	1900	0.39	0.37	0.15	-18.0	-142.0	0.132	0.132	0.408	0.480	0.480	13.33
910511	0100	0.93	0.91	0.21	10.0	90.0	0.220	0.201	0.230	0.193	0.289	13.55
910511	0700	0.95	0.93	0.20	10.0	90.0	0.191	0.191	0.217	0.206	0.206	13.28
910511	1300	0.93	0.89	0.25	8.0	148.0	0.123	0.123	0.284	0.305	0.305	13.57
910511	1900	0.69	0.66	0.20	2.0	172.0	0.123	0.123	0.302	0.329	0.329	13.51
910512	0100	0.74	0.71	0.22	2.0	166.0	0.103	0.113	0.305	0.343	0.345	13.20
910512	0700	0.73	0.68	0.28	-4.0	-148.0	0.113	0.113	0.412	0.413	0.413	13.31
910512	1300	0.78	0.73	0.27	-6.0	-146.0	0.103	0.103	0.377	0.409	0.409	13.23
910512	1900	0.62	0.56	0.27	-6.0	-148.0	0.103	0.103	0.474	0.465	0.465	13.67
910513	0100	0.59	0.56	0.19	-8.0	162.0	0.103	0.103	0.337	0.323	0.323	12.90
910513	0700	0.52	0.47	0.22	-4.0	178.0	0.093	0.103	0.471	0.440	0.479	13.46
910515	1300	0.27	0.25	0.09	-42.0	-90.0	0.171	0.103	0.365	0.300	0.557	12.76
910515	1900	0.29	0.27	0.09	-52.0	-90.0	0.181	0.191	0.329	0.336	0.346	14.27
910516	0100	0.37	0.36	0.10	-38.0	-90.0	0.240	0.152	0.277	0.219	0.353	12.92
910516	0700	0.54	0.51	0.18	20.0	90.0	0.220	0.210	0.352	0.309	0.356	13.88
910516	1300	0.48	0.47	0.12	10.0	90.0	0.230	0.230	0.262	0.251	0.251	12.85
910516	1900	0.59	0.57	0.17	-6.0	176.0	0.171	0.162	0.306	0.332	0.342	14.13
910517	0100	0.46	0.44	0.11	-6.0	-90.0	0.162	0.171	0.250	0.228	0.242	13.01

(Continued)

(Continued)

Date	Time KST	Wave Height H_{mo} m	$H_{mo,i}$ m	$H_{mo,r}$ m	Direction $\theta_{p,i}$ deg	$\theta_{p,r}$ deg	Frequency $f_{p,i}$ Hz	$f_{p,r}$ Hz	Reflection X_{mo}	$X_{p,i}$	$X_{p,r}$	Depth m
910517	0700	0.44	0.42	0.13	-4.0	-90.0	0.201	0.210	0.301	0.267	0.304	13.70
910517	1300	0.36	0.35	0.10	-12.0	-90.0	0.171	0.103	0.285	0.218	0.455	12.97
910517	1900	0.38	0.36	0.12	-6.0	-90.0	0.191	0.181	0.335	0.289	0.326	13.80
910518	0100	0.32	0.30	0.10	-12.0	-90.0	0.113	0.113	0.345	0.347	0.347	13.19
910518	0700	0.31	0.29	0.11	0.0	-90.0	0.113	0.123	0.364	0.394	0.429	13.40
910518	1300	1.40	1.37	0.28	18.0	90.0	0.201	0.201	0.203	0.236	0.236	13.42
910518	1900	2.21	2.16	0.46	22.0	90.0	0.142	0.142	0.213	0.186	0.186	13.87
910519	0100	2.22	2.17	0.48	20.0	90.0	0.113	0.113	0.223	0.243	0.243	13.95
910519	0700	2.48	2.44	0.42	12.0	90.0	0.152	0.171	0.171	0.150	0.180	13.63
910519	1300	2.31	2.26	0.48	14.0	90.0	0.142	0.142	0.210	0.197	0.197	13.92
910519	1900	1.87	1.83	0.36	12.0	90.0	0.162	0.171	0.199	0.191	0.207	13.55
910520	0100	1.65	1.60	0.39	6.0	176.0	0.093	0.093	0.242	0.199	0.199	14.04
910520	0700	1.54	1.51	0.32	2.0	-90.0	0.093	0.171	0.210	0.179	0.243	13.30
910521	1300	1.00	0.95	0.29	-4.0	-90.0	0.123	0.152	0.310	0.279	0.325	13.84
910521	1900	0.92	0.88	0.26	-4.0	-90.0	0.123	0.162	0.294	0.230	0.352	12.97
910522	0100	0.86	0.80	0.31	-6.0	-90.0	0.132	0.132	0.385	0.392	0.392	13.76
910522	0700	0.75	0.72	0.22	-8.0	-90.0	0.123	0.142	0.307	0.256	0.311	12.84
910522	1300	0.67	0.62	0.25	-8.0	-144.0	0.132	0.113	0.400	0.392	0.482	13.79
910522	1900	0.57	0.54	0.20	-8.0	-90.0	0.113	0.123	0.371	0.323	0.360	12.96
910523	0100	0.57	0.52	0.24	-6.0	-144.0	0.142	0.123	0.469	0.465	0.496	13.59
910523	0700	0.47	0.43	0.17	-20.0	-140.0	0.123	0.113	0.402	0.326	0.389	12.91
910523	1300	0.48	0.43	0.22	-26.0	-144.0	0.123	0.123	0.518	0.567	0.567	13.76
910523	1900	0.40	0.36	0.17	-24.0	-138.0	0.123	0.113	0.479	0.442	0.516	13.24
910524	0100	0.40	0.36	0.17	-28.0	-106.0	0.123	0.123	0.455	0.445	0.445	13.62
910524	0700	0.42	0.38	0.17	-26.0	-138.0	0.123	0.132	0.437	0.394	0.455	13.23
910524	1300	0.46	0.42	0.19	-22.0	-142.0	0.132	0.132	0.442	0.478	0.478	13.68
910524	1900	0.41	0.38	0.17	-12.0	-136.0	0.123	0.123	0.444	0.449	0.449	13.41
910525	0100	0.50	0.46	0.20	-12.0	-102.0	0.132	0.132	0.434	0.468	0.468	13.28
910525	0700	0.53	0.49	0.20	-12.0	-144.0	0.142	0.132	0.419	0.381	0.413	13.21
910525	1300	0.51	0.47	0.21	-28.0	-138.0	0.142	0.064	0.444	0.438	1.034	13.31
910525	1900	0.47	0.43	0.19	-24.0	-138.0	0.142	0.142	0.449	0.453	0.453	13.49
910526	0100	0.53	0.49	0.21	-24.0	-90.0	0.132	0.142	0.421	0.383	0.398	13.04
910526	0700	0.55	0.50	0.23	-22.0	-140.0	0.142	0.142	0.465	0.494	0.494	13.34
910526	1300	0.51	0.47	0.21	-22.0	-106.0	0.142	0.074	0.449	0.455	0.657	13.18
910526	1900	0.47	0.43	0.20	-34.0	-112.0	0.142	0.142	0.476	0.498	0.498	13.74
910527	0100	0.47	0.43	0.19	-32.0	-90.0	0.142	0.074	0.451	0.397	0.622	13.06
910527	0700	0.47	0.43	0.19	-32.0	-90.0	0.142	0.142	0.442	0.475	0.475	13.60
910529	1300	0.37	0.33	0.16	-28.0	-100.0	0.074	0.083	0.491	0.535	0.551	13.01
910529	1900	0.37	0.34	0.15	-14.0	-90.0	0.083	0.083	0.427	0.451	0.451	13.99
910530	0100	0.36	0.33	0.15	-8.0	-138.0	0.083	0.083	0.464	0.441	0.441	12.97
910530	0700	0.40	0.36	0.16	-6.0	-140.0	0.083	0.083	0.451	0.478	0.478	13.70
910530	1300	0.38	0.35	0.15	-16.0	-136.0	0.083	0.083	0.443	0.479	0.479	12.97
910530	1900	0.34	0.31	0.14	-14.0	-144.0	0.083	0.083	0.451	0.537	0.537	13.85
910531	0100	0.32	0.29	0.15	-24.0	-136.0	0.083	0.083	0.512	0.551	0.551	12.91
910531	0700	0.33	0.31	0.12	-22.0	-100.0	0.093	0.083	0.403	0.409	0.431	13.57
910531	1300	0.34	0.31	0.14	-14.0	-104.0	0.093	0.083	0.434	0.448	0.517	13.03

(Continued)

(Concluded)

Date	Time EST	Wave Height H_{mo} m	$H_{mo,i}$ m	$H_{mo,r}$ m	Direction $\theta_{p,i}$ deg	$\theta_{p,r}$ deg	Frequency $f_{p,i}$ Hz	$f_{p,r}$ Hz	Reflection x_{mo}	$x_{p,i}$	$x_{p,r}$	Depth m
910531	1900	0.35	0.33	0.13	-12.0	-90.0	0.093	0.103	0.397	0.354	0.406	13.79
910601	0100	0.33	0.30	0.14	-8.0	-178.0	0.093	0.093	0.466	0.453	0.455	13.13
910601	0700	0.32	0.30	0.11	-8.0	-90.0	0.093	0.093	0.373	0.360	0.360	13.58
910601	1300	0.32	0.29	0.12	-10.0	-90.0	0.093	0.093	0.425	0.424	0.424	13.20
910601	1900	0.29	0.27	0.11	-4.0	-172.0	0.093	0.093	0.411	0.410	0.410	13.75
910602	0100	0.31	0.28	0.12	-4.0	178.0	0.093	0.093	0.430	0.478	0.478	13.29

Appendix B: Time Series Graphs of Bulk Spectral Parameters

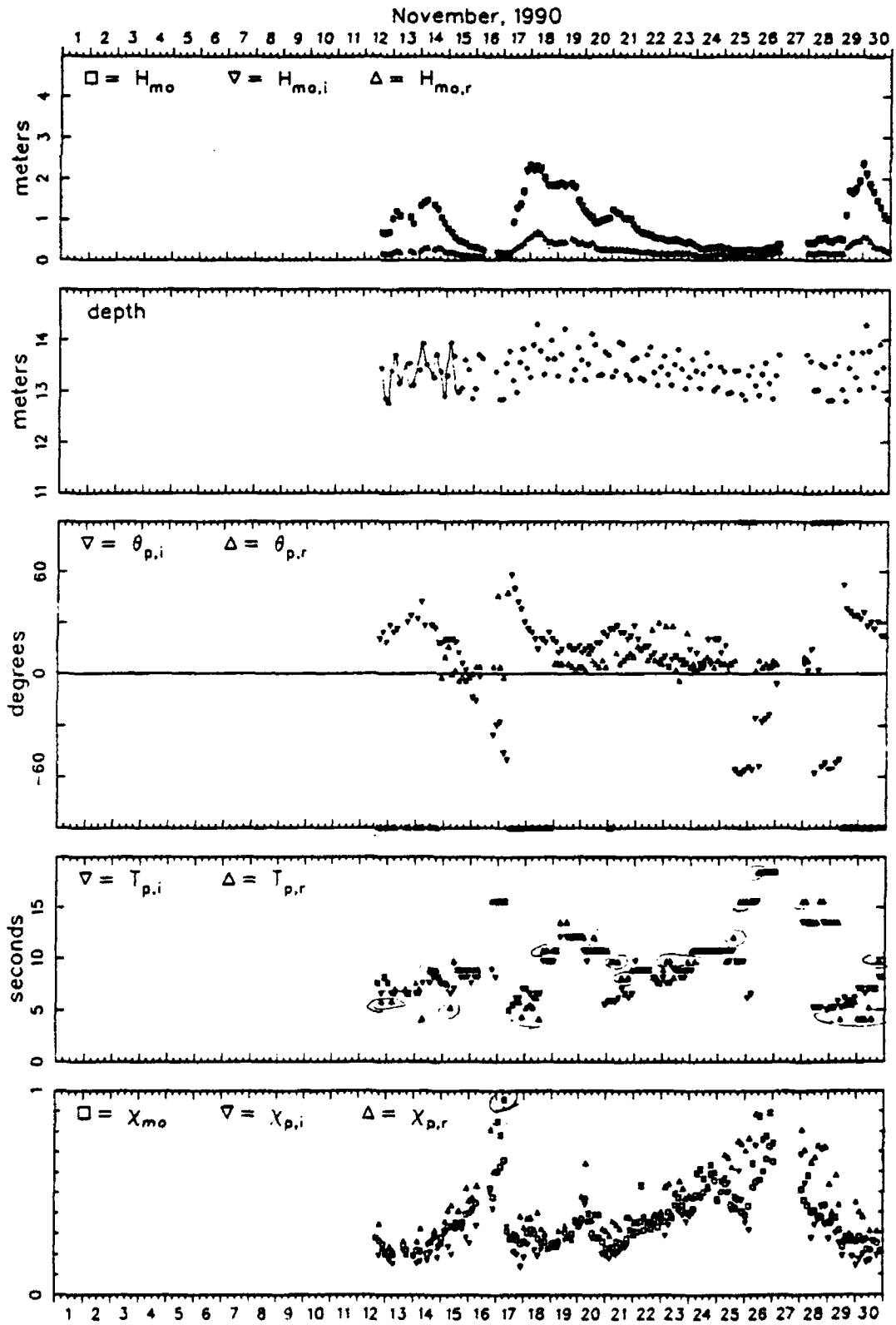

I can believe Δ @ low T we need a threshold

Figure B1. Bulk data for November 1990

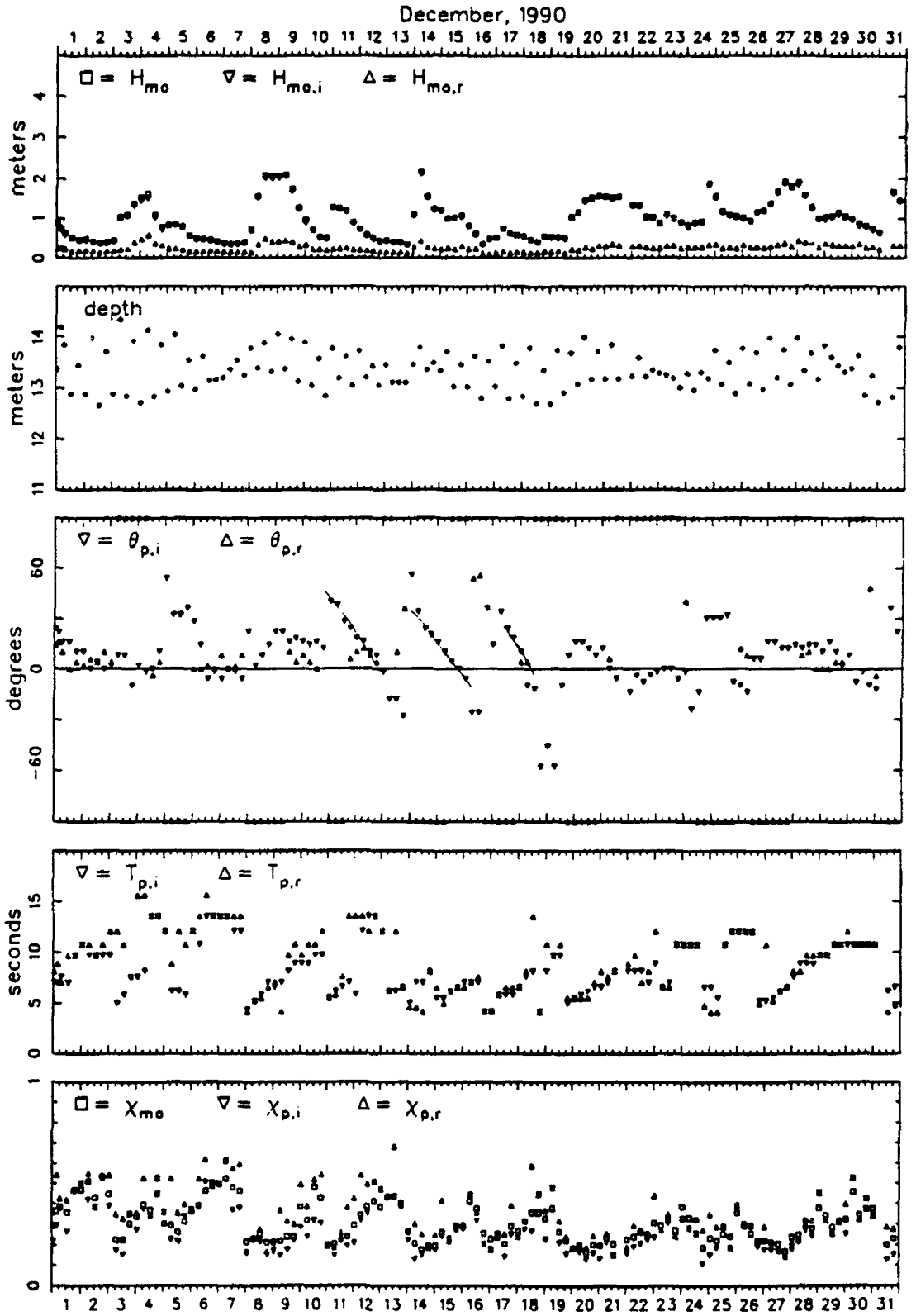

Figure B2. Bulk data for December 1990

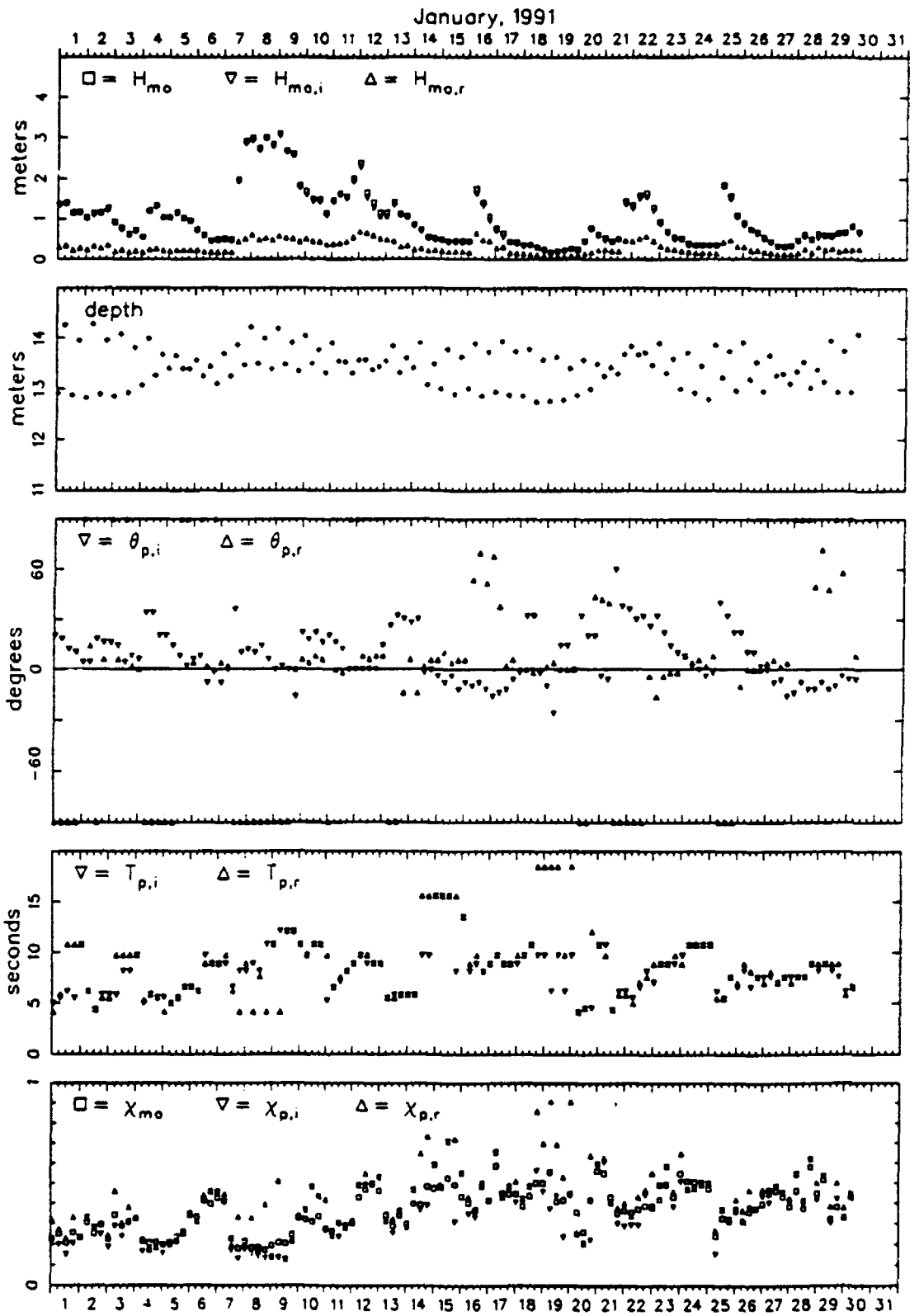

Figure B3. Bulk data for January 1991

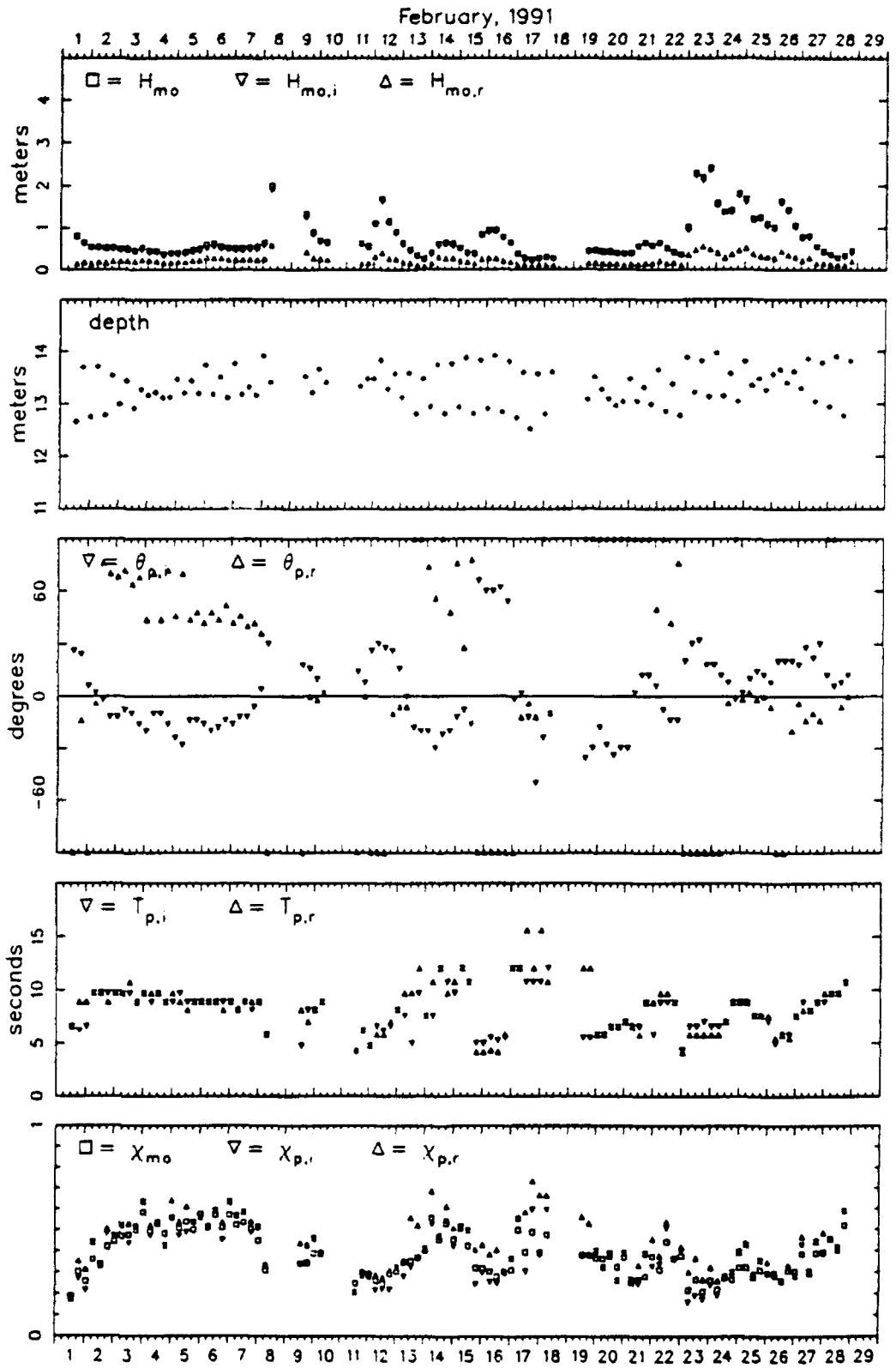

Figure B4. Bulk data for February 1991

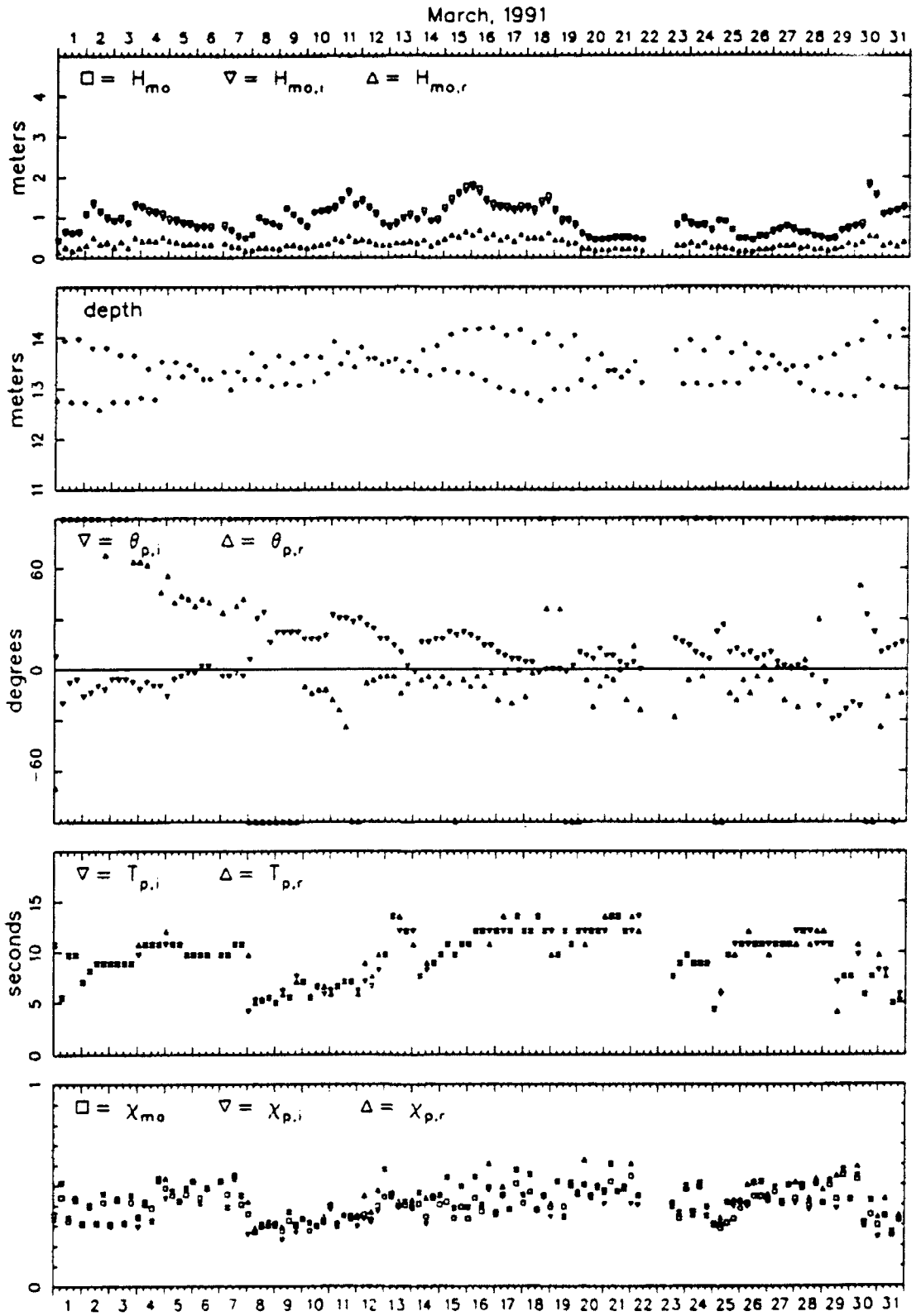

Figure B5. Bulk data for March 1991

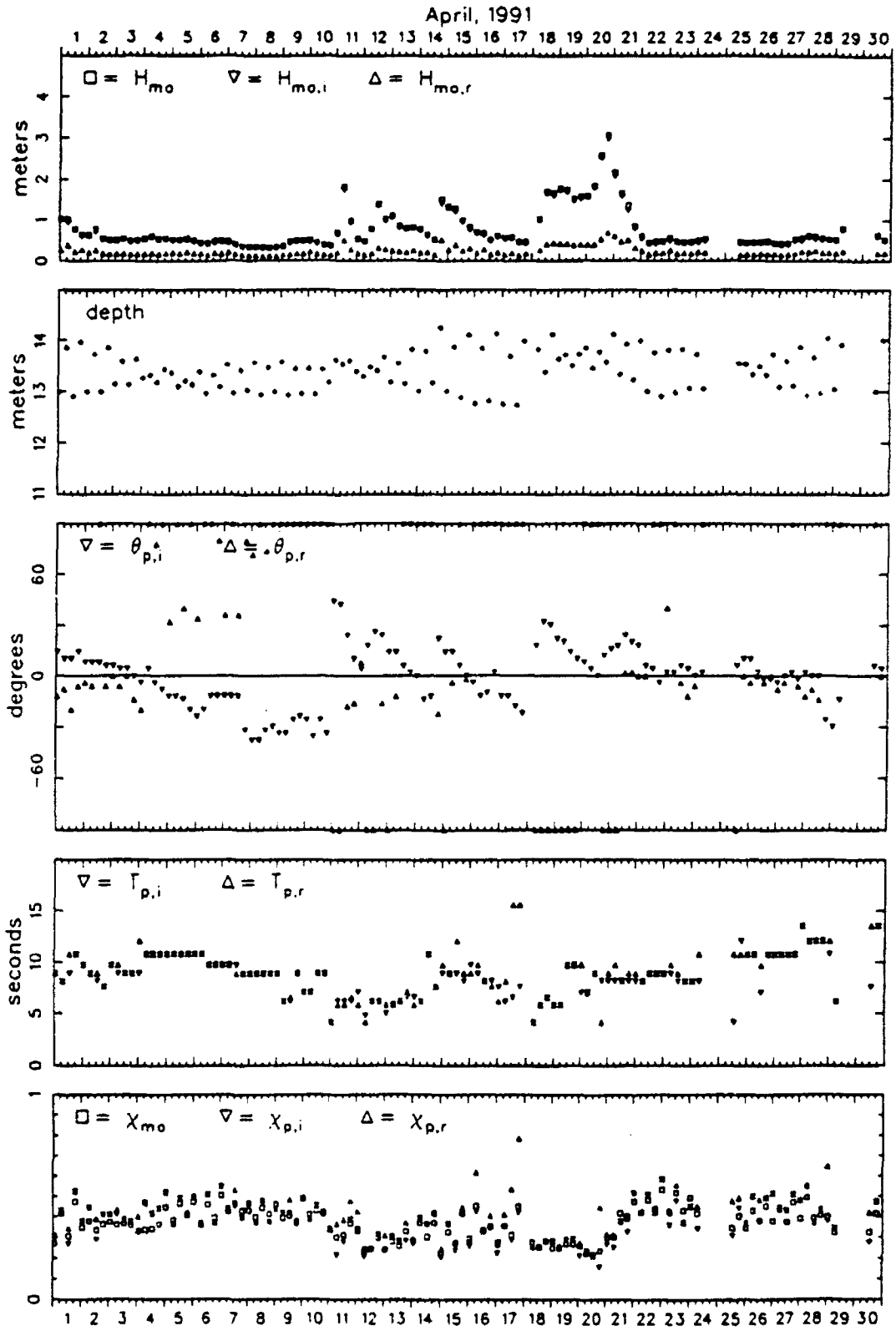

Figure B6. Bulk data for April 1991

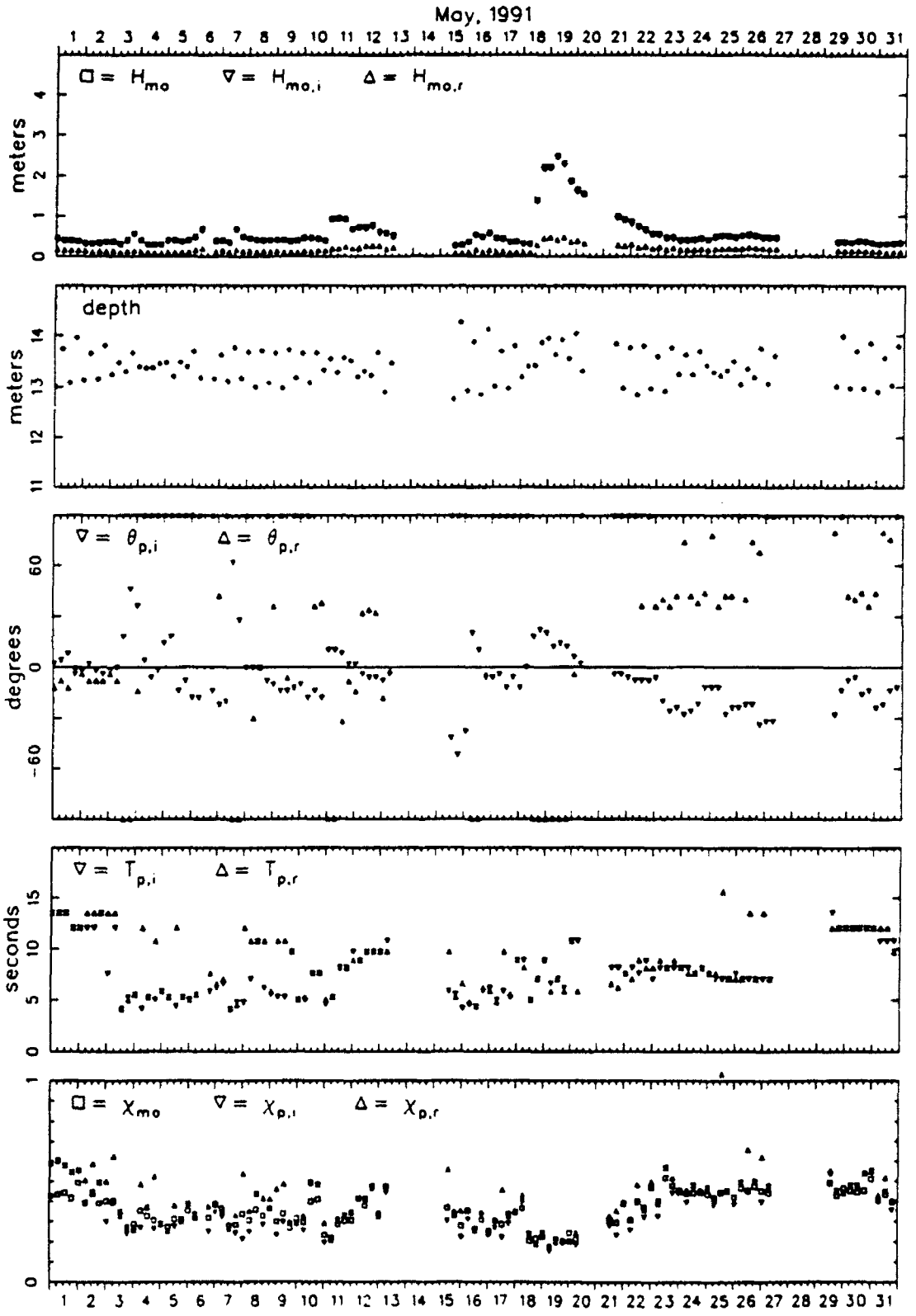

Figure B7. Bulk data for May 1991

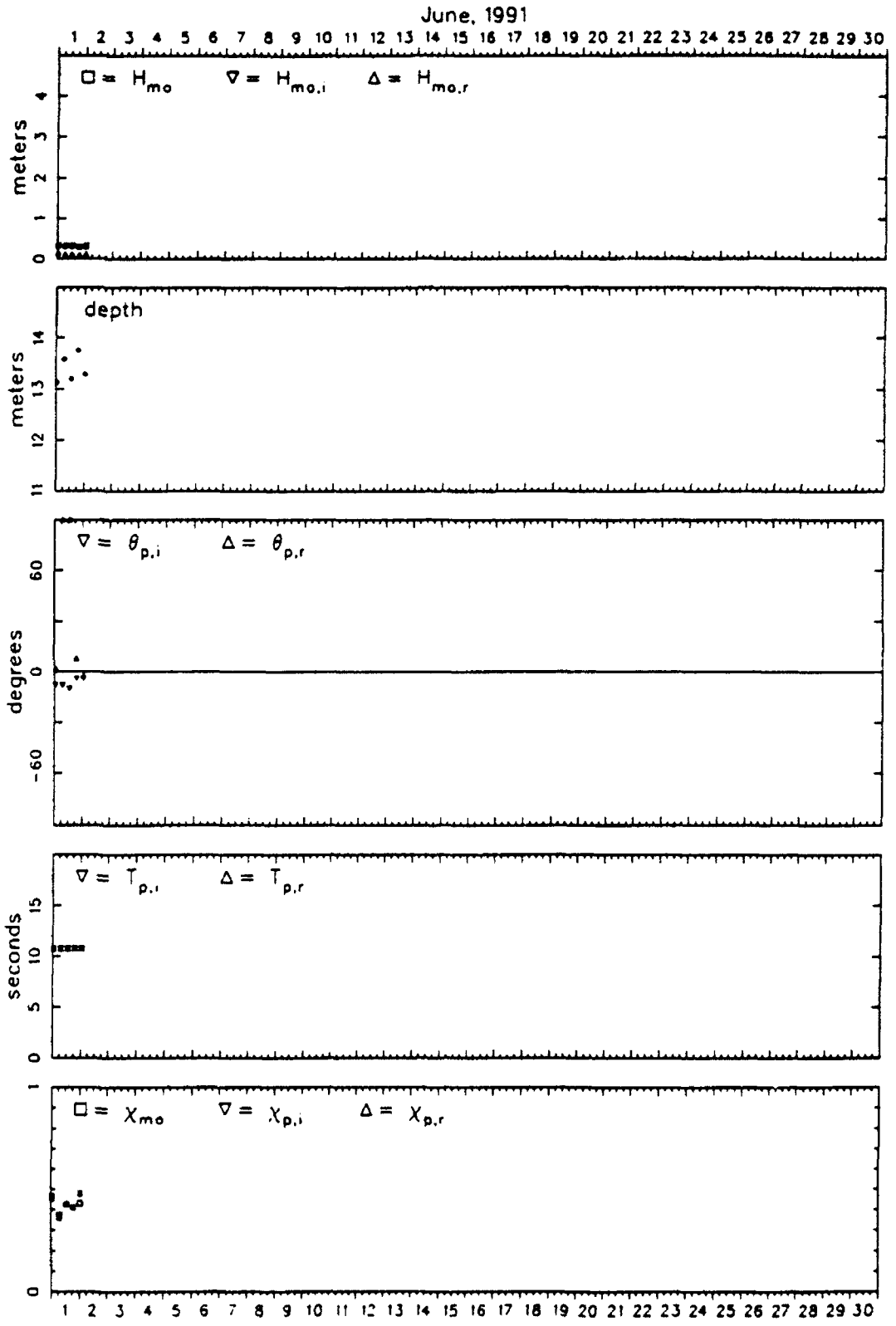

Figure B8. Bulk data for June 1991

Appendix C: A Derivation of the Maximum Likelihood Estimator

Appendix C: A Derivation of the Maximum Likelihood Estimator

1. Under ideal circumstances, a single train of ocean surface waves can be represented as a sinusoid in the form*

$$\eta(x,y,t) = a\cos(k\cos\theta\, x + k\sin\theta\, y - \sigma t + \epsilon) \tag{C1}$$

where x and y are right-handed coordinates in a horizontal plane (at elevation $z = 0$, where z is the vertical coordinate directed positive upward from the mean sea surface), t is time, a is the wave amplitude, k is radian wavenumber, θ is the direction toward which the wave propagates and is measured counterclockwise (looking downward) from the positive x-axis, σ is radian wave frequency, and ϵ is an initial phase. When linear wave theory is used, wavenumber and frequency are, for a given depth of water, uniquely related by the linear wave dispersion relation

$$\sigma^2 = gk\tanh kd \tag{C2}$$

where g is gravitational acceleration, and d is water depth. A natural sea can be considered an infinite sum of such waves so that sea surface displacement is represented generally as

$$\eta(x,y,t) = \sum_{n=1}^{\infty} a_n\cos(k_n\cos\theta_n x + k_n\sin\theta_n y - \sigma_n t + \epsilon_n) \tag{C3}$$

For each index n, there is a unique set of a_n, σ_n, θ_n and ϵ_n that, for a given depth, completely determine the nature of the n^{th} wave train (note that k_n is dictated by σ_n and d through the dispersion relation).

2. Because it can be rather awkward keeping track of this infinite number of four-variable sets, it is useful to have a form of book-keeping that is compact enough that even a very complicated sea can be quantified and depicted in a simple way. A common form of such book-keeping is the frequency-direction spectrum. In this method, a plane is gridded in even steps of the orthogonal coordinates σ and θ, with each cell in the grid being of infinitesimal dimension $\Delta\sigma$ by $\Delta\theta$. There is then a cell that corresponds to the σ_n and θ_n of the n^{th} wave train so that the other two properties a_n and ϵ_n of this wave train can be associated with that cell. Above the gridded σ-θ plane can be constructed surfaces that represent wave

---

* A notation for this appendix is included in Appendix D

train properties. The most common of these is variance of sea surface displacement (which by linear wave theory is proportional to mean energy of a wave train) normalized by grid cell area. This variance density (sometimes called energy density) together with its coordinates in σ-θ space is the frequency-direction spectrum of sea surface variance $E(\sigma,\theta)$, which is most commonly sought. One could also build spectra of wave amplitude or phase, but wave energy is usually of greatest interest.

3. The variance of a single sinusoidal wave train of amplitude a_n is half the amplitude squared. By definition, this is the volume under the spectrum over one grid cell. This relation can be written

$$\frac{1}{2}a_n^2 = \int_{\theta_n-\frac{1}{2}\Delta\theta}^{\theta_n+\frac{1}{2}\Delta\theta} \int_{\sigma_n-\frac{1}{2}\Delta\sigma}^{\sigma_n+\frac{1}{2}\Delta\sigma} E(\sigma,\theta)\, d\sigma\, d\theta \qquad (C4)$$

The primary effort in most directional spectral estimation is the determination of $E(\sigma,\theta)$ from time series of sea surface displacement at a few points in space, i.e., from a sparse sample of the left side of Equation C3 to an estimate of the integrand on the right side of Equation C4.

4. Preliminary theoretical considerations involve computation of a Fourier frequency transform of the covariance between the model sea surface at location x,y and time t and the sea surface at arbitrarily displaced coordinates $x+X,y+Y$ and displaced time $t+T$. This process yields a useful relationship between the measurable frequency cross-spectra between two points in space and an integral with respect to direction of the frequency-direction spectrum. A good discussion of this process is given by Munk, et al. (1963)*, and the following is based on insights gained therefrom.

5. The covariance $R(X,Y,T)$ between spatially and temporally separated sea surface displacements is found from the average over large reaches of space and long durations the product of the model for $\eta(x,y,t)$ with the model for $\eta(x+X,y+Y,t+T)$. This can be expressed as

$$R(X,Y,T) = \lim_{\substack{A\to\infty \\ B\to\infty \\ C\to\infty}} \frac{1}{ABC} \int_{-\frac{C}{2}}^{\frac{C}{2}} \int_{-\frac{B}{2}}^{\frac{B}{2}} \int_{0}^{A} \eta(x,y,t)\, \eta(x+X,y+Y,t+T)\, dt\, dx\, dy \qquad (C5)$$

When the model Equation C3 is substituted, this expression becomes a triple

---

* References for this appendix are listed in the main body of the report

integral of the product of two infinite sums. Its evaluation is time consuming but straightforward, and results in the rather simple expression

$$R(X,Y,T) = \sum_{n=1}^{\infty} \frac{1}{2} a_n^2 \cos(k_n \cos\theta_n X + k_n \sin\theta_n Y - \sigma_n T) \tag{C6}$$

The variance within the sum can be replaced with its spectral definition given by Equation C4, which leads to

$$R(X,Y,T) = \sum_{n=1}^{\infty} \left[\int_{\theta_n - \frac{1}{2}\Delta\theta}^{\theta_n + \frac{1}{2}\Delta\theta} \int_{\sigma_n - \frac{1}{2}\Delta\sigma}^{\sigma_n + \frac{1}{2}\Delta\sigma} E(\sigma,\theta)\, d\sigma\, d\theta \right] \cos(k_n \cos\theta_n X + k_n \sin\theta_n Y - \sigma_n T) \tag{C7}$$

The summation covers all conceivable bins in the infinitesimally gridded σ-θ domain and effectively links the edges of each integration region to form a continuous double integral over the bounds ($0 \le \theta \le 2\pi$, $0 \le \sigma \le \infty$) of frequency-direction space. Hence, the covariance function becomes

$$R(X,Y,T) = \int_0^{2\pi} \int_0^{\infty} E(\sigma,\theta) \cos(k\cos\theta\, X + k\sin\theta\, Y - \sigma T)\, d\sigma\, d\theta \tag{C8}$$

The trigonometric identity for the cosine of the sum of two angles can be used to isolate terms in σT in Equation C8. If that result is regrouped and the order of integration reversed, the result is

$$\begin{aligned} R(X,Y,T) = &\int_0^{\infty} \left[\int_0^{2\pi} E(\sigma,\theta) \cos(k\cos\theta\, X + k\sin\theta\, Y)\, d\theta \right] \cos\sigma T\, d\sigma \\ &+ \int_0^{\infty} \left[\int_0^{2\pi} E(\sigma,\theta) \sin(k\cos\theta\, X + k\sin\theta\, Y)\, d\theta \right] \sin\sigma T\, d\sigma \end{aligned} \tag{C9}$$

The bracketed term in the first integral on the right side of Equation C9 is the usual definition of the coincident spectrum, denoted $C(X,Y,\sigma)$, and the bracketed term in the second integral on the right side of Equation C9 is the quadrature spectrum $Q(X,Y,\sigma)$. The covariance function then becomes

$$R(X,Y,T) = \int_0^{\infty} [C(X,Y,\sigma) \cos\sigma T + Q(X,Y,\sigma) \sin\sigma T]\, d\sigma \tag{C10}$$

A Fourier transform of the covariance function acts to isolate the coincident and quadrature spectra in the form

$$\int_{-\infty}^{\infty} R(X,Y,T)\, e^{-i\sigma T}\, dT = C(X,Y,\sigma) - i\,Q(X,Y,\sigma) \tag{C11}$$

If the integral definitions of these spectra are substituted, one obtains

$$C(X,Y,\sigma) - iQ(X,Y,\sigma)$$

$$= \int_0^{2\pi} E(\sigma,\theta)\cos(k\cos\theta X + k\sin\theta Y)\,d\theta - i\int_0^{2\pi} E(\sigma,\theta)\sin(k\cos\theta X + k\sin\theta Y)\,d\theta \quad \text{(C12)}$$

$$= \int_0^{2\pi} E(\sigma,\theta)\left[\cos(k\cos\theta X + k\sin\theta Y) - i\sin(k\cos\theta X + k\sin\theta Y)\right]d\theta$$

$$= \int_0^{2\pi} E(\sigma,\theta)\, e^{-i(k\cos\theta X + k\sin\theta Y)}\,d\theta$$

6. The cross-spectra can usually be estimated from measurements because samples can be obtained often enough that frequency content is well-resolved. If samples could be obtained in space with equivalent coverage, Equation C12 could be Fourier transformed spatially to isolate the frequency-direction spectrum. The problem is that it is very difficult to obtain spatial sampling with sufficient density for Fourier transformation and only a few (order 10) spatial points are measured. An alternative approach is to create a model of $E(\sigma,\theta)$ and employ the sparse available measurements to determine the model parameters. There are several ways to formulate such a model. Maximum Likelihood Estimation (MLE) is one of them.

7. In MLE, the combined amplitude and phase of a single wave train are modeled. This wave train has a unique frequency and direction, and so has a unique location in the frequency-direction plane used to define spectral elements. Spectral density is computed from the amplitude of this wave train. MLE is somewhat unique in that continuous distributions of energy density are not found. The estimator "looks" along a single discrete direction at a time to find, for each of a set of discrete frequencies, the most likely (maximum likelihood) amplitude of a wave moving in that direction. By looking along a number of adjacent discrete directions, an estimated directional spectrum can be constructed. Some features of this method, including its direction resolving ability, its ability to distinguish multiple wave trains and its behavior in relation to the number and spacing of the observing gages, must be deduced empirically by analyzing synthetic data imposed on a particular array design.

8. The purpose here is to outline the reasoning and mathematical underpinnings of MLE as applied to wave directional estimation. What follows is an expansion of what is covered in just a few lines in each of two papers

used for reference. One is by Davis and Regier (1977) and the other is by Oltman-Shay and Guza (1984).

9. The frequency-direction spectrum is found by trying to isolate the amplitudes of single plane waves, one wave train at a time. A single plane wave can be defined by Equation C1, but for the present method, it is desired to rewrite this expression using the Euler notation definition of cosine [$\cos x = (e^{ix} + e^{-ix})/2$] so that Equation C1 becomes

$$\begin{aligned}\eta(x,y,t) &= a\frac{1}{2}\left[e^{i(k\cos\theta x + k\sin\theta y - \sigma t + \epsilon)} + e^{-i(k\cos\theta x + k\sin\theta y - \sigma t + \epsilon)}\right] \\ &= \frac{1}{2}a\,e^{i\epsilon}\,e^{i(k\cos\theta x + k\sin\theta y - \sigma t)} + \frac{1}{2}a\,e^{-i\epsilon}\,e^{-i(k\cos\theta x + k\sin\theta y - \sigma t)} \qquad \text{(C13)} \\ &= \frac{1}{2}D\,e^{i(k\cos\theta x + k\sin\theta y - \sigma t)} + \frac{1}{2}D^{*}e^{-i(k\cos\theta x + k\sin\theta y - \sigma t)}\end{aligned}$$

where $D = ae^{i\epsilon}$ is known as the *complex amplitude* and the asterisk means complex conjugate. Because this is only a change in notation and not in substance, wave train properties given above will remain the same, but the notation will change. Where a squared amplitude appeared (as in covariance estimates) previously as a^2, it will now be DD^{*}. The infinite suite of wave trains that defines a sea surface has the notation

$$\eta(x,y,t) = \sum_{n=1}^{\infty} \frac{1}{2}D_n e^{i(k_n\cos\theta_n x + k_n\sin\theta_n y - \sigma_n t)} + \frac{1}{2}D_n^{*}e^{-i(k_n\cos\theta_n x + k_n\sin\theta_n y - \sigma_n t)} \qquad \text{(C14)}$$

Then the variance of the n^{th} component wave is from Equation C4

$$\frac{1}{2}a_n^2 = \frac{1}{2}D_nD_n^{*} \qquad \text{(C15)}$$

and the covariance function $R(X,Y,T)$ is

$$R(X,Y,T) = \sum_{n=1}^{\infty} \frac{1}{2}D_nD_n^{*}\cos(k_n\cos\theta_n X + k_n\sin\theta_n Y - \sigma_n T) \qquad \text{(C16)}$$

All subsequent expressions, including those for the continuous frequency-direction spectrum and the cross-spectra, will be identical to those given above.

10. Data are expected to be some measure of sea surface displacement η which may be direct measurements or derived from surface corrected time series of pressure recorded at some level in the water column. Here it is assumed

that direct measurements have been made. There will be in general a set of N gages, indexed $n = 1,2,\ldots,N$, from each of which is collected an R-point time series sampled at time interval Δt for a duration of $R\Delta t$. Gages are deployed in a two-dimensional array in a pattern that follows, in two dimensions, the guidance given quite nicely by Davis and Regier (1977) for one dimensional arrays. The frequency content of the data is needed, so a conventional discrete Fourier transform is computed. For the n^{th} gage, located at horizontal position x_n, y_n, the Fourier transform at the q^{th} frequency is, in accordance with procedures given by Bendat and Piersol (1971) or Jenkins and Watts (1968),

$$X_q(x_n,y_n) = \sum_{r=1}^{R} \eta_r(x_n,y_n)\, e^{-i2\pi qr/R} \qquad q=1,2,\ldots,\frac{R}{2} \tag{C17}$$

where η_r is the data value at the r^{th} time step. The model of wave amplitude D is based on the coefficients of the Fourier series representation of sea surface displacement. Fourier series coefficients can be found directly from Fourier transforms. For the q^{th} frequency σ_q of the transformed data at location x_n, y_n, the Fourier coefficient can be written

$$A_q(x_n,y_n) - iB_q(x_n,y_n) = \frac{2}{R} X_q(x_n,y_n) \tag{C18}$$

which is valid at all frequencies except zero and the Nyquist, which two cases are ignored with very little penalty in this derivation.

11. The heart of the maximum likelihood method is finding an expression to represent the complex amplitude $D = ae^{i\epsilon}$ of a single wave train at frequency σ_q (as dictated in practice by the Fourier transform above) and traveling in the single look direction α. Because Fourier coefficients intrinsically contain amplitude and phase information on a frequency-by-frequency basis, it is reasonable to formulate a model for $ae^{i\epsilon}$ as a linear combination of the N Fourier series coefficients at frequency σ_q determined from the N gages in the array. A linear combination means a weighted sum, so the model takes the form

$$\begin{aligned} D = ae^{i\epsilon} &= \sum_{n=1}^{N} w_n(\alpha)\,[A_q(x_n,y_n) - iB_q(x_n,y_n)] \\ &= \sum_{n=1}^{N} w_n(\alpha)\,\frac{2}{R} X_q(x_n,y_n) \end{aligned} \tag{C19}$$

where the $w_n(\alpha)$ are a set of N complex weights unique to the look direction α, which will be determined by the optimization scheme described below. The variance of the modeled wave train is given by Equation C15, and, if the model Equation C19 is substituted, the variance becomes

$$\frac{1}{2}a^2 = \frac{1}{2}\left[\sum_{n=1}^{N} w_n(\alpha)\,\frac{2}{R}\,X_q(x_n,y_n)\right]\left[\sum_{m=1}^{N} w_m(\alpha)\,\frac{2}{R}\,X_q(x_m,y_m)\right]^* \tag{C20}$$

where the summing index is changed on the second sum to distinguish the various terms after the multiplication is carried out. Taking the complex conjugate of the second sum, carrying out the term-by-term multiplication and recombining the results leads to

$$\begin{aligned}\frac{1}{2}a^2 &= \frac{1}{2}\left[\sum_{n=1}^{N} w_n(\alpha)\,\frac{2}{R}\,X_q(x_n,y_n)\right]\left[\sum_{m=1}^{N} w_m^*(\alpha)\,\frac{2}{R}\,X_q^*(x_m,y_m)\right] \\ &= \frac{1}{2}\sum_{n=1}^{N}\sum_{m=1}^{N} w_n(\alpha)\,w_m^*(\alpha)\,\frac{4}{R^2}\,X_q(x_n,y_n)X_q^*(x_m,y_m)\end{aligned} \tag{C21}$$

The contribution of this variance to the frequency-direction spectrum is unique in that it represents that piece of the total variance in a region of area $\Delta\theta$ by $\Delta\sigma$ centered at direction α and frequency σ_q in the frequency-direction plane. When normalized by the incremental area $\Delta\sigma\Delta\theta$ of the frequency-direction plane, an estimate of the frequency-direction spectrum $\hat{E}(\sigma_q,\alpha)$ due to this wave train can be written

$$\begin{aligned}\hat{E}(\sigma_q,\alpha) &= \frac{\frac{1}{2}a^2}{\Delta\sigma\Delta\theta} \\ &= \frac{1}{2\Delta\sigma\Delta\theta}\sum_{n=1}^{N}\sum_{m=1}^{N} w_n(\alpha)\,w_m^*(\alpha)\,\frac{4}{R^2}\,X_q(x_n,y_n)X_q^*(x_m,y_m) \\ &= \frac{1}{\Delta\theta}\sum_{n=1}^{N}\sum_{m=1}^{N} w_n(\alpha)\,w_m^*(\alpha)\left[\frac{2}{R^2\Delta\sigma}\,X_q(x_n,y_n)X_q^*(x_m,y_m)\right]\end{aligned} \tag{C22}$$

where the hat ($\hat{}$) means an estimate, and terms in the last equality have simply been regrouped.

12. The bracketed term in Equation C22 is a conventional discrete frequency cross-spectrum, denoted $E_{mn}(\sigma_q)$ and identically equal to $C_{mn}(\sigma_q) - iQ_{mn}(\sigma_q)$, as described by Bendat and Piersol (1971). Within the brackets, the first Fourier transform term $X_q(x_n,y_n)$ is from a time series collected from gage n of the array. The second Fourier transform term $X_q^*(x_m,y_m)$ is the conjugate of the transform of a time series collected from gage m, which is generally different from gage n. The frequency increment $\Delta\sigma$ is known from conventional discrete Fourier transformation to be $\Delta\sigma = 2\pi/R\Delta t$. With these substitutions, the bracketed term in Equation C22 becomes

$$\frac{2}{R^2\Delta\sigma} X_q(x_n,y_n)X_q^*(x_m,y_m) = E_{mn}(\sigma_q) = C_{mn}(\sigma_q) - iQ_{mn}(\sigma_q) \tag{C23}$$

and the estimate $\hat{E}(\sigma_q,\alpha)$ becomes

$$\hat{E}(\sigma_q,\alpha) = \frac{1}{\Delta\theta}\sum_{n=1}^{N}\sum_{m=1}^{N} w_n(\alpha)\,w_m^*(\alpha)\left[C_{mn}(\sigma_q) - iQ_{mn}(\sigma_q)\right] \tag{C24}$$

13. It is important to note at this point that a variance density estimate has been formulated from a basic Fourier transform definition and a more reliable estimate must be formed to avoid arithmetic problems later. Cross-spectral estimates formed from raw Fourier transforms have broad confidence intervals, i.e., alone they have rather high uncertainty. Confidence is improved by obtaining long time series, segmenting records before transformation, computing cross-spectral estimates for corresponding pairs of segments, and averaging segment estimates together. Further reliability is obtained when estimates from adjacent frequency bands are also averaged together. The trade-off is that the final resolution frequency bandwidth is broader than for the raw estimates. However, sampling strategies can usually keep the new bandwidth tolerably narrow. These smoothing methods are standard procedures in spectral estimation. The point here is that it is essential for smoothed estimates to be used in maximum likelihood estimation.

14. In this derivation, smoothing can take place as soon as products of Fourier transforms are formed. Hence, one can smooth any of Equations C21 to C24, under the assumption that the weights $w(\alpha)$ are not affected by this process. If only segment averaging is done, the meaning of the notation in

the rest of this derivation is unchanged. If band averaging is done, subsums of terms will be computed over small ranges of the subscript q and the normalizing bandwidth $\Delta\sigma$ will be larger (equal to the number of bands averaged times the raw bandwidth $2\pi/R\Delta t$). If, for the remainder of this derivation, subscript q is considered to be the index of this new set of frequency bands, then the notation need not be changed.

15. A logical next step is to define $\Delta\theta$, but this is difficult to do at this stage. Hypothetically, the method seeks a single wave train having a single propagation direction α. Under ideal conditions, the arc of direction in the frequency-direction domain represented by this wave train is of zero width, i.e., the spectrum is a spike or delta function at direction α. However, directional resolving ability is limited by the number of observations available, so there is a finite arc width associated with the fitted wave train, just as there is a finite bandwidth in the frequency domain. Because of the intricate arithmetic and dependence on the number and separation of gages, it is usually not possible to assign a resolution arc width until the estimator is completely derived. At that time, a resolution arc width can be found empirically by examining the minimum angular separation of two wave trains that can, by some criterion, be distinguished with the estimator. This procedure is usually done with artificial wave signals, solving the estimator equations for a large number of individual look directions (α's) and then deciding how small an arc is required for estimates from adjacent look directions to be reasonably statistically independent. Results will be a function of frequency (long waves are more difficult to resolve) and may be a function of direction, depending on the geometry of the gage array.

16. Given that, for now, $\Delta\theta$ is not defined, the working entity is the frequency-direction spectrum times an unspecified arc width. Hence, multiplying both sides of Equation C24 by $\Delta\theta$ results in what is essentially the q^{th} element of a slice of a direction-bounded frequency spectrum of arc width $\Delta\theta$ centered along look direction α, or

$$\hat{E}(\sigma_q,\alpha)\,\Delta\theta = \sum_{n=1}^{N}\sum_{m=1}^{N} w_n(\alpha)\,w_m^*(\alpha)\left[C_{nm}(\sigma_q) - i\,Q_{nm}(\sigma_q)\right]$$
$$= \sum_{n=1}^{N}\sum_{m=1}^{N} w_n(\alpha)\,w_m^*(\alpha)\,E_{nm}(\sigma_q) \qquad \text{(C25)}$$

The model is a weighted sum of the frequency cross-spectra of sea surface displacement at frequency σ_q between all possible pairs of gages n and m , where the weights are unique to the single direction α . Weights are determined based on reasoning derived from consideration of ideal spectra.

17. Complete, ideal cross-spectra are related to the true frequency-direction spectrum $E(\sigma,\theta)$ (no hat) by Equation C12. If this expression is adapted to an array of gages positioned arbitrarily (for now) in x,y coordinates, separations between gages m and n are

$$\begin{aligned} X &= x_m - x_n \\ Y &= y_m - y_n \end{aligned} \tag{C26}$$

Use of Equations C26 in Equation C12 gives an expression for cross-spectra of sea surface displacement in terms of gage separation

$$\begin{aligned} C_{mm}(\sigma_q) - i\,Q_{mm}(\sigma_q) &= C(x_m-x_n, y_m-y_n, \sigma_q) - i\,Q(x_m-x_n, y_m-y_n, \sigma_q) \\ &= \int_0^{2\pi} E(\sigma_q,\theta)\, e^{-ik_q[(x_m-x_n)\cos\theta + (y_m-y_n)\sin\theta]}\, d\theta \end{aligned} \tag{C27}$$

18. The next step is to isolate that part of the spectrum near look direction α . This is done by asserting that the total directional spectrum at frequency σ_q is made up of two parts: a spike or delta function at the look direction α that represents a single, signal-containing wave train, and a "noise" spectrum that represents some true noise, but also the rest of the true spectrum that is to have minimum influence on the estimate at look direction α . That is, a kind of filter is enforced that only allows information near look direction α . The two parts of $E(\sigma_q,\theta)$ can be written

$$E(\sigma_q,\theta) = H(\theta-\alpha,\Delta\theta)\,E(\sigma_q,\alpha) + E_N(\sigma_q,\theta) \tag{C28}$$

where $E(\sigma_q,\alpha)$ is the desired piece of the total spectrum, $E_N(\sigma_q,\theta)$ is the rest of the spectrum the influence of which is to be minimized, and $H(\theta-\alpha,\Delta\theta)$ is an isolating function. The isolating function has a value of 1 in a region $\Delta\theta$ wide about direction α and is zero elsewhere. Its effect is to allow an artificial distribution of the energy in the spike of $E(\sigma_q,\alpha)$ over a finite arc width $\Delta\theta$.

19. If Equation C28 is substituted into the integral of Equation C27, one obtains

$$C_{mn}(\sigma_q) - iQ_{mn}(\sigma_q) = \int_0^{2\pi} \left[H(\theta-\alpha,\Delta\theta)\, E(\sigma_q,\alpha) + E_N(\sigma_q,\theta) \right] e^{-ik_q[\cos\theta\,(x_m-x_n) + \sin\theta\,(y_m-y_n)]}\, d\theta$$

$$= \int_0^{2\pi} H(\theta-\alpha,\Delta\theta)\, E(\sigma_q,\alpha)\, e^{-ik_q[\cos\theta\,(x_m-x_n) + \sin\theta\,(y_m-y_n)]}\, d\theta$$

$$+ \int_0^{2\pi} E_N(\sigma_q,\theta)\, e^{-ik_q[\cos\theta\,(x_m-x_n) + \sin\theta\,(y_m-y_n)]}\, d\theta \qquad \text{(C29)}$$

$$= E(\sigma_q,\alpha) \int_0^{2\pi} H(\theta-\alpha,\Delta\theta)\, e^{-ik_q[\cos\theta\,(x_m-x_n) + \sin\theta\,(y_m-y_n)]}\, d\theta$$

$$+ \int_0^{2\pi} E_N(\sigma_q,\theta)\, e^{-ik_q[\cos\theta\,(x_m-x_n) + \sin\theta\,(y_m-y_n)]}\, d\theta$$

Some effort is required to evaluate the first integral on the right side of the last equality. The function $H(\theta-\alpha,\Delta\theta)$ has the simple effect of resetting the limits on the integral so that one can write

$$\int_0^{2\pi} H(\theta-\alpha,\Delta\theta)\, e^{-ik_q[\cos\theta\,(x_m-x_n) + \sin\theta\,(y_m-y_n)]}\, d\theta$$

$$= \int_{\alpha-\frac{1}{2}\Delta\theta}^{\alpha+\frac{1}{2}\Delta\theta} e^{-ik_q[\cos\theta\,(x_m-x_n) + \sin\theta\,(y_m-y_n)]}\, d\theta \qquad \text{(C30)}$$

The integrand can be expanded as infinite sums of the products of Bessel functions of the gage separations and sinusoidal functions of θ. The sinusoids can be integrated and, if $\Delta\theta$ is small enough, results can be expressed as products of $\Delta\theta$ and sinusoids of α. The infinite sums of the resulting products of Bessel functions of the gage separations and sinusoidal functions of α can then be contracted to an exponential function. Equation C30 then becomes the approximate expression

$$\int_{\alpha-\frac{1}{2}\Delta\theta}^{\alpha+\frac{1}{2}\Delta\theta} e^{-ik_q[(x_m-x_n)\cos\theta + (y_m-y_n)\sin\theta]}\, d\theta \approx e^{-ik_q[(x_m-x_n)\cos\alpha + (y_m-y_n)\cos\alpha]}\, \Delta\theta \qquad \text{(C31)}$$

The expression for the frequency cross-spectra then takes the form

$$C_{mn}(\sigma_q) - iQ_{mn}(\sigma_q) \approx E(\sigma_q,\alpha)\, \Delta\theta\, e^{-ik_q[(x_m-x_n)\cos\alpha + (y_m-y_n)\sin\alpha]}$$

$$+ \int_0^{2\pi} E_N(\sigma_q,\theta)\, e^{-ik_q[(x_m-x_n)\cos\theta + (y_m-y_n)\sin\theta]}\, d\theta \qquad \text{(C32)}$$

20. If the frequency cross-spectra of Equation C32 are substituted into the model Equation C25, one obtains

$$\begin{aligned}
\hat{E}(\sigma_q,\alpha)\,\Delta\theta &= \sum_{n=1}^{N}\sum_{m=1}^{N} w_n(\alpha)\,w_m^*(\alpha)\Big[\,E(\sigma_q,\alpha)\,\Delta\theta\; e^{-ik_q[(x_m-x_n)\cos\alpha + (y_m-y_n)\sin\alpha]} \\
&\qquad + \int_0^{2\pi} E_N(\sigma_q,\theta)\; e^{-ik_q[(x_m-x_n)\cos\theta + (y_m-y_n)\sin\theta]}\,d\theta\Big] \\
&= E(\sigma_q,\alpha)\,\Delta\theta \sum_{n=1}^{N}\sum_{m=1}^{N} w_n(\alpha)\,w_m^*(\alpha)\; e^{-ik_q[(x_m-x_n)\cos\alpha + (y_m-y_n)\sin\alpha]} \\
&\qquad + \sum_{n=1}^{N}\sum_{m=1}^{N} w_n(\alpha)\,w_m^*(\alpha) \int_0^{2\pi} E_N(\sigma_q,\theta)\; e^{-ik_q[(x_m-x_n)\cos\theta + (y_m-y_n)\sin\theta]}\,d\theta \\
&= E(\sigma_q,\alpha)\,\Delta\theta \left[\sum_{n=1}^{N}\sum_{m=1}^{N} w_n(\alpha)\,w_m^*(\alpha)\; e^{-ik_q[(x_m-x_n)\cos\alpha + (y_m-y_n)\sin\alpha]}\right] \\
&\qquad + \int_0^{2\pi} \left[\sum_{n=1}^{N}\sum_{m=1}^{N} w_n(\alpha)\,w_m^*(\alpha)\; e^{-ik_q[(x_m-x_n)\cos\theta + (y_m-y_n)\sin\theta]}\right] E_N(\sigma_q,\theta)\,d\theta
\end{aligned} \tag{C33}$$

In the second equality of Equation C33, $E(\sigma_q,\alpha)\Delta\theta$ was moved outside the double sum because it does not explicitly depend on m or n. In the third equality, the double sum and weights are moved inside the integral because the computation can be done in any order. Also in the third equality, the weights and the exponential functions are bracketed together with the double summation signs, thereby grouping the summation dependent terms.

21. The bracketed terms in the last equality of Equation C33 are called *window functions*, the general form of which is denoted $W(\alpha,\theta)$ and defined by

$$W(\alpha,\theta) = \sum_{n=1}^{N}\sum_{m=1}^{N} w_n(\alpha)\,w_m^*(\alpha)\; e^{-ik_q[(x_m-x_n)\cos\theta + (y_m-y_n)\sin\theta]} \tag{C34}$$

and the special form where $\alpha = \theta$ is

$$W(\alpha,\alpha) = \sum_{n=1}^{N}\sum_{m=1}^{N} w_n(\alpha)\,w_m^*(\alpha)\; e^{-ik_q[(x_m-x_n)\cos\alpha + (y_m-y_n)\sin\alpha]} \tag{C35}$$

Using the window function notation, the estimated spectrum from the last equality of Equation C33 becomes

$$\hat{E}(\sigma_q,\alpha)\,\Delta\theta \approx E(\sigma_q,\alpha)\,\Delta\theta\,W(\alpha,\alpha) + \int_0^{2\pi} W(\alpha,\theta)\,E_N(\sigma_q,\theta)\,d\theta \tag{C36}$$

22. A constraint on the problem arises where there is no "noise" spectrum and the true spectrum is all that exists. That is, if $E_N(\sigma_q,\alpha) = 0$, it is required that $\hat{E}(\sigma_q,\alpha)\Delta\theta = E(\sigma_q,\alpha)\Delta\theta$. For this expression to be true, $W(\alpha,\alpha) = 1$. Note that the expression for $W(\alpha,\alpha)$ can be factored as follows

$$\begin{aligned}
W(\alpha,\alpha) &= \sum_{n=1}^{N}\sum_{m=1}^{N} w_n(\alpha)\,w_m^*(\alpha)\,e^{-ik_q[(x_m-x_n)\cos\alpha + (y_m-y_n)\sin\alpha]} \\
&= \sum_{n=1}^{N}\sum_{m=1}^{N} w_n(\alpha)\,w_m^*(\alpha)\,e^{-ik_q(x_m\cos\alpha + y_m\sin\alpha)}\,e^{ik_q(x_n\cos\alpha + y_n\sin\alpha)} \\
&= \sum_{n=1}^{N}\sum_{m=1}^{N} w_n(\alpha)\,e^{ik_q(x_n\cos\alpha + y_n\sin\alpha)}\,w_m^*(\alpha)\,e^{-ik_q(x_m\cos\alpha + y_m\sin\alpha)} \\
&= \sum_{n=1}^{N} w_n(\alpha)\,e^{ik_q(x_n\cos\alpha + y_n\sin\alpha)} \sum_{m=1}^{N} w_m^*(\alpha)\,e^{-ik_q(x_m\cos\alpha + y_m\sin\alpha)} \\
&= \left[\sum_{n=1}^{N} w_n(\alpha)\,e^{ik_q(x_n\cos\alpha + y_n\sin\alpha)}\right]\left[\sum_{m=1}^{N} w_m(\alpha)\,e^{ik_q(x_m\cos\alpha + y_m\sin\alpha)}\right]^*
\end{aligned} \tag{C37}$$

Because the term in the second bracket of the last equality is simply the complex conjugate of the term in the first bracket, Equation C37 can be written

$$W(\alpha,\alpha) = \left|\sum_{n=1}^{N} w_n(\alpha)\,e^{ik_q(x_n\cos\alpha + y_n\sin\alpha)}\right|^2 \tag{C38}$$

and it is seen that the window is always a positive and real. The constraint that $W(\alpha,\alpha) = 1$ is satisfied (not necessarily uniquely) if

$$\sum_{n=1}^{N} w_n(\alpha)\,e^{ik_q(x_n\cos\alpha + y_n\sin\alpha)} = \sum_{n=1}^{N} w_n^*(\alpha)\,e^{-ik_q(x_n\cos\alpha + y_n\sin\alpha)} = 1 \tag{C39}$$

The more general window $W(\alpha,\theta)$ can also be disassembled and rewritten as

$$W(\alpha,\theta) = \left| \sum_{n=1}^{N} w_n(\alpha)\, e^{ik_q(x_n\cos\theta + y_n\sin\theta)} \right|^2 \qquad \text{(C40)}$$

and it is noted that, because it is a magnitude squared, its values are real and positive or zero for all directions θ .

23. With $W(\alpha,\alpha) = 1$, our estimated spectrum from Equation C36 becomes

$$\hat{E}(\sigma_q,\alpha)\,\Delta\theta \approx E(\sigma_q,\alpha)\,\Delta\theta + \int_0^{2\pi} W(\alpha,\theta)\, E_N(\sigma_q,\theta)\, d\theta \qquad \text{(C41)}$$

To minimize the contribution from the "noise" spectrum, the integral in Equation C41 must be made as small as possible. It is noted that $E(\sigma_q,\alpha)$ is of fixed value and positive, that $W(\alpha,\theta)$ is positive by Equation C40 and that $E_N(\sigma_q,\theta)$ is positive, so that everything on the right side of Equation C41 is positive. Making the integral as small as possible is then equivalent to making $\hat{E}(\sigma_q,\alpha)$ as small as possible. That can be done for any expression defining $\hat{E}(\sigma_q,\alpha)$. Instead of minimizing Equation C41, one can minimize Equation C25, which is a more basic model definition. At the same time one must satisfy the window constraint of Equation C39.

24. Minimization means finding the derivatives of Equations C25 and C39 with respect to the real and imaginary parts of the complex weights w_n , setting the derivatives equal to zero and solving the subsequent set of simultaneous equations for the weights. Use of these minimizing weights in the model Equation C25 yields a maximum likelihood estimate of the spectral density at frequency σ_q and direction α . Direction binwidth $\Delta\theta$ continues to be undefined until the minimization has been completed.

25. Minimization of Equations C25 and C39 at the same time entails use of a method known as Lagrange multipliers, a subject covered in most advanced calculus texts of which Hildebrand (1965) is one. To set it up, it is noted that if Equation C39 is true then

$$1 - \sum_{n=1}^{N} w_n(\alpha)\, e^{ik_q(x_n\cos\alpha + y_n\sin\alpha)} = 0 \qquad \text{(C42)}$$

and Equation C42 can be added, with a coefficient, to the right side of Equation C25 without changing the truth of Equation C25 or Equation C39. This procedure gives us

$$\hat{E}(\sigma_q,\alpha)\,\Delta\theta = \sum_{n=1}^{N}\sum_{m=1}^{N} w_n(\alpha)\,w_m^*(\alpha)\,E_{nm}(\sigma_q) + \lambda\left[1 - \sum_{n=1}^{N} w_n(\alpha)\,e^{ik_q(x_n\cos\alpha + y_n\sin\alpha)}\right] \quad \text{(C43)}$$

The coefficient λ is called a Lagrange multiplier. Upon zeroing the derivatives of Equation C43 with respect to the real and imaginary parts of the w_n, one will obtain $2N$ equations (N equations for the real parts and N for the imaginary parts) that will yield the w_n in terms of λ. If these weights are used in Equation C39, another equation is obtained that can be used to solve for λ.

26. To illustrate this procedure, consider an array of 3 non-collinear wave gages. The analysis will work with any larger number of gages, but the bookkeeping takes longer to write. By showing the derivation for a 3-gage array, one can see the generalization for a larger array. With 3 gages, there are (N =) 3 time series, so that for each frequency σ_q, there are 3 Fourier coefficients and three weights w_n to find. Each weight is complex. The real and imaginary parts of the weights are identified by defining

$$w_n = w_{nR} + iw_{nI} \quad \text{(C44)}$$

and its complex conjugate

$$w_n^* = w_{nR} - iw_{nI} \quad \text{(C45)}$$

Products of weights as they appear in Equation C43 take the form

$$\begin{aligned} w_n w_m^* &= (w_{nR} + iw_{nI})(w_{mR} - iw_{mI}) \\ &= (w_{nR}w_{mR} + w_{nI}w_{mI}) + i(w_{nI}w_{mR} - w_{nR}w_{mI}) \end{aligned} \quad \text{(C46)}$$

To save space, the parentheses and the independent variables they carried have been dropped for now. They will be replaced at the end of the derivation.

27. The six differentiations required to minimize Equation C43 can be written as

$$\frac{\partial}{\partial w_{nR}}\hat{E}(\sigma_q,\alpha)\Delta\theta = \frac{\partial}{\partial w_{nI}}\hat{E}(\sigma_q,\alpha)\Delta\theta = 0 \qquad n = 1,2,3 \quad \text{(C47)}$$

or, using the right side of Equation C43 and expanding the differentials,

$$\begin{matrix} \frac{\partial}{\partial w_{1R}} \\ \frac{\partial}{\partial w_{2R}} \\ \frac{\partial}{\partial w_{3R}} \\ \frac{\partial}{\partial w_{1I}} \\ \frac{\partial}{\partial w_{2I}} \\ \frac{\partial}{\partial w_{3I}} \end{matrix} \left\{ \sum_{n=1}^{3} \sum_{m=1}^{3} w_n w_m^* E_{nm} + \lambda \left[1 - \sum_{n=1}^{3} w_n e^{ik_0(x_n \cos\alpha + y_n \sin\alpha)} \right] \right\} = 0 \qquad \text{(C48)}$$

where the terms in the curly brackets expand to

$$\begin{aligned} &(w_{1R}^2 + w_{1I}^2)E_{11} + [(w_{1R}w_{2R} + w_{1I}w_{2I}) + i(w_{1I}w_{2R} - w_{1R}w_{2I})]E_{21} \\ &\quad + [(w_{1R}w_{3R} + w_{1I}w_{3I}) + i(w_{1I}w_{3R} - w_{1R}w_{3I})]E_{31} \\ &\quad + [(w_{2R}w_{1R} + w_{2I}w_{1I}) + i(w_{2I}w_{1R} - w_{2R}w_{1I})]E_{12} \\ &+ (w_{2R}^2 + w_{2I}^2)E_{22} + [(w_{2R}w_{3R} + w_{2I}w_{3I}) + i(w_{2I}w_{3R} - w_{2R}w_{3I})]E_{32} \\ &\quad + [(w_{3R}w_{1R} + w_{3I}w_{1I}) + i(w_{3I}w_{1R} - w_{3R}w_{1I})]E_{13} \\ &+ [(w_{3R}w_{2R} + w_{3I}w_{2I}) + i(w_{3I}w_{2R} - w_{3R}w_{2I})]E_{23} + (w_{3R}^2 + w_{3I}^2)E_{33} \\ &+ \lambda\Big[1 - (w_{1R} + iw_{1I})e^{ik_0(x_1\cos\alpha + y_1\sin\alpha)} - (w_{2R} + iw_{2I})e^{ik_0(x_2\cos\alpha + y_2\sin\alpha)} \\ &\qquad - (w_{3R} + iw_{3I})e^{ik_0(x_3\cos\alpha + y_3\sin\alpha)} \Big] \end{aligned} \qquad \text{(C49)}$$

Taking the partial differential of Expression C48 with respect to w_{1R} and setting it equal to zero yields

$$2w_{1R}E_{11} + (w_{2R}-iw_{2I})E_{21} + (w_{3R}-iw_{3I})E_{31} + (w_{2R}+iw_{2I})E_{12} + (w_{3R}+iw_{3I})E_{13} - \lambda e^{ik_0(x_1\cos\alpha + y_1\sin\alpha)} = 0 \quad \text{(C50)}$$

Similarly the partials with respect to w_{2R} and w_{3R} lead, respectively, to

$$(w_{1R}+iw_{1I})E_{21} + (w_{1R}-iw_{1I})E_{12} + 2w_{2R}E_{22} + (w_{3R}-iw_{3I})E_{32} + (w_{3R}+iw_{3I})E_{23} - \lambda e^{ik_0(x_2\cos\alpha + y_2\sin\alpha)} = 0 \quad \text{(C51)}$$

$$(w_{1R}+iw_{1I})E_{31} + (w_{2R}+iw_{2I})E_{32} + (w_{1R}-iw_{1I})E_{13} + (w_{2R}-iw_{2I})E_{23} + 2w_{3R} - \lambda e^{ik_0(x_3\cos\alpha + y_3\sin\alpha)} = 0 \quad \text{(C52)}$$

The partials with respect to w_{1I} , w_{2I} and w_{3I} yield, respectively,

$$2w_{1I}E_{11} + (w_{2I}+iw_{2R})E_{21} + (w_{3I}+iw_{3R})E_{31} + (w_{2I}-iw_{2R})E_{12} + (w_{3I}-iw_{3R})E_{13} - i\lambda e^{ik_0(x_1\cos\alpha + y_1\sin\alpha)} = 0 \quad \text{(C53)}$$

$$(w_{1I}-iw_{1R})E_{21} + (w_{1I}+iw_{1R})E_{12} + 2w_{2I}E_{22} + (w_{3I}+iw_{3R})E_{32} + (w_{3I}-iw_{3R})E_{23} - i\lambda e^{ik_0(x_2\cos\alpha + y_2\sin\alpha)} = 0 \quad \text{(C54)}$$

$$(w_{1I}-iw_{1R})E_{31} + (w_{2I}-iw_{2R})E_{32} + (w_{1I}+iw_{1R})E_{13} + (w_{2I}+iw_{2R})E_{23} + 2w_{3I}E_{33} - i\lambda e^{ik_0(x_3\cos\alpha + y_3\sin\alpha)} = 0 \quad \text{(C55)}$$

Equations C50, C51 and C52 can be written in more abbreviated form by using the definitions of Equations C44 and C45. If terms containing λ are also moved to the right sides of the equations, one obtains

$$2w_{1R}E_{11} + w_2^*E_{21} + w_3^*E_{31} + w_2E_{12} + w_3E_{13} = \lambda e^{ik_0(x_1\cos\alpha + y_1\sin\alpha)} \quad \text{(C56)}$$

$$w_1E_{21} + w_1^*E_{12} + 2w_{2R}E_{22} + w_3^*E_{32} + w_3E_{23} = \lambda e^{ik_0(x_2\cos\alpha + y_2\sin\alpha)} \quad \text{(C57)}$$

$$w_1E_{31} + w_2E_{32} + w_1^*E_{13} + w_2^*E_{23} + 2w_{3R}E_{33} = \lambda e^{ik_0(x_3\cos\alpha + y_3\sin\alpha)} \tag{C58}$$

If Equation C53 is multiplied by i and terms are rearranged, the following sequence is induced

$$\begin{aligned}
&2iw_{1I}E_{11} + i(w_{2I}+iw_{2R})E_{21} + i(w_{3I}+iw_{3R})E_{31} \\
&\qquad + i(w_{2I}-iw_{2R})E_{12} + i(w_{3I}-iw_{3R})E_{13} - i^2\lambda e^{ik_0(x_1\cos\alpha + y_1\sin\alpha)} \\
&= 2iw_{1I}E_{11} + (iw_{2I}-w_{2R})E_{21} + (iw_{3I}-w_{3R})E_{31} \\
&\qquad + (iw_{2I}+w_{2R})E_{12} + (iw_{3I}+w_{3R})E_{13} + \lambda e^{ik_0(x_1\cos\alpha + y_1\sin\alpha)} \qquad \text{(C59)} \\
&= 2iw_{1I}E_{11} - (w_{2R}-iw_{2I})E_{21} - (w_{3R}-iw_{3I})E_{31} \\
&\qquad + (w_{2R}+iw_{2I})E_{12} + (w_{3R}+iw_{3I})E_{13} + \lambda e^{ik_0(x_1\cos\alpha + y_1\sin\alpha)} \\
&= 0
\end{aligned}$$

Writing Equation C59 in abbreviated form (using Equations C44 and C45) and putting the term containing λ on the right side results in

$$2iw_{1I}E_{11} - w_2^*E_{21} - w_3^*E_{31} + w_2E_{12} + w_3E_{13} = -\lambda e^{ik_0(x_1\cos\alpha + y_1\sin\alpha)} \tag{C60}$$

The same set of operations applied to Equations C54 and C55 provides, respectively,

$$w_1E_{21} - w_1^*E_{12} + 2iw_{2I}E_{22} - w_3^*E_{32} + w_3E_{23} = -\lambda e^{ik_0(x_2\cos\alpha + y_2\sin\alpha)} \tag{C61}$$

$$w_1E_{31} + w_2E_{32} - w_1^*E_{13} - W_2^*E_{23} + 2iw_{3I}E_{33} = -\lambda e^{ik_0(x_3\cos\alpha + y_3\sin\alpha)} \tag{C62}$$

If Equation C60 is subtracted from Equation C56, there results

$$(2w_{1R} - 2iw_{1I})E_{11} + 2w_2^*E_{21} + 2w_3^*E_{31} = 2\lambda e^{ik_0(x_1\cos\alpha + y_1\sin\alpha)} \tag{C63}$$

or, upon putting the first term on the left in simplified form and dividing by 2,

$$w_1^*E_{11} + w_2^*E_{21} + w_3^*E_{31} = \lambda e^{ik_0(x_1\cos\alpha + y_1\sin\alpha)} \tag{C64}$$

Similarly, subtracting Equation C61 from Equation C57 leads to

$$w_1^* E_{12} + w_2^* E_{22} + w_3^* E_{32} = \lambda e^{ik_q(x_2\cos\alpha + y_2\sin\alpha)} \tag{C65}$$

and Equation C62 taken from Equation C58 yields

$$w_1^* E_{13} + w_2^* E_{23} + w_3^* E_{33} = \lambda e^{ik_q(x_3\cos\alpha + y_3\sin\alpha)} \tag{C66}$$

Equations C64, C65 and C66 are very similar in form and the left side of each can be written as a sum. On doing this, the equation set is expressed

$$\sum_{m=1}^{3} w_m^* E_{mn} = \lambda e^{ik_q(x_n\cos\alpha + y_n\sin\alpha)} \qquad \text{for } n = 1,2,3 \tag{C67}$$

If one multiplies Equation C64 by w_1, Equation C65 by w_2 and Equation C66 by w_3, there is obtained a new set of equations that can be expressed in the summation form of Equation C67 as the product of both sides with w_n, i.e.,

$$w_n \sum_{m=1}^{3} w_m^* E_{mn} = w_n \lambda e^{ik_q(x_n\cos\alpha + y_n\sin\alpha)} \qquad \text{for } n = 1,2,3 \tag{C68}$$

or, upon moving w_n inside the sum because the sum is only over index m,

$$\sum_{m=1}^{3} w_n w_m^* E_{mn} = \lambda w_n e^{ik_q(x_n\cos\alpha + y_n\sin\alpha)} \qquad \text{for } n = 1,2,3 \tag{C69}$$

If all three equations are now added together, a very simple and useful result is obtained. Adding the equations in the summation expression is the same as taking the sum over index n of both sides of Equation C69, or

$$\begin{aligned} \sum_{n=1}^{3}\sum_{m=1}^{3} w_n w_m^* E_{mn} &= \sum_{n=1}^{3} \lambda w_n e^{ik_q(x_n\cos\alpha + y_n\sin\alpha)} \\ &= \lambda \sum_{n=1}^{3} w_n e^{ik_q(x_n\cos\alpha + y_n\sin\alpha)} \end{aligned} \tag{C70}$$

The double sum on the left side of Equation C70 is recognized as the estimate of the frequency-direction spectrum defined in Equation C25. The sum on the right side of Equation C70 is identified as satisfying the window constraint expressed by Equation C39 so that the sum can be replaced by 1. Equation C70 reduces to the simple expression

$$\hat{E}(\sigma_q, \alpha)\,\Delta\theta = \lambda \tag{C71}$$

Hence, if λ can be found, the estimator will be complete. Note that while the number of gages has been limited to 3 to keep the bookkeeping simple, all operations so far have been linear. Extension of this derivation to more gages is straightforward, consisting mostly of changing the upper limit on the summations. This derivation will continue to assume 3 gages, again for bookkeeping simplicity, but the result is more general.

28. To find λ, it is noted that Equations C64, C65 and C66 form a set of simultaneous equations in the conjugates of the weights w_n. These equations can be written in matrix form as

$$\begin{bmatrix} E_{11} & E_{21} & E_{31} \\ E_{12} & E_{22} & E_{32} \\ E_{13} & E_{23} & E_{33} \end{bmatrix} \begin{bmatrix} w_1^* \\ w_2^* \\ w_3^* \end{bmatrix} = \lambda \begin{bmatrix} e^{ik_q(x_1\cos\alpha + y_1\sin\alpha)} \\ e^{ik_q(x_2\cos\alpha + y_2\sin\alpha)} \\ e^{ik_q(x_3\cos\alpha + y_3\sin\alpha)} \end{bmatrix} \tag{C72}$$

To find the weights, both sides of Equation C72 must be multiplied by the inverse of the matrix E_{mn}. This inverse is computed by following any recipe for matrix inversion. On finding the inverse and doing the multiplication, Equation C72 becomes

$$\begin{bmatrix} w_1^* \\ w_2^* \\ w_3^* \end{bmatrix} = \lambda \begin{bmatrix} E_{11}^{-1} & E_{21}^{-1} & E_{31}^{-1} \\ E_{12}^{-1} & E_{22}^{-1} & E_{32}^{-1} \\ E_{13}^{-1} & E_{23}^{-1} & E_{33}^{-1} \end{bmatrix} \begin{bmatrix} e^{ik_q(x_1\cos\alpha + y_1\sin\alpha)} \\ e^{ik_q(x_2\cos\alpha + y_2\sin\alpha)} \\ e^{ik_q(x_3\cos\alpha + y_3\sin\alpha)} \end{bmatrix} \tag{C73}$$

which can be written as individual equations by doing the matrix multiplication to form

$$w_1^* = \lambda\left[E_{11}^{-1} e^{ik_q(x_1\cos\alpha + y_1\sin\alpha)} + E_{21}^{-1} e^{ik_q(x_2\cos\alpha + y_2\sin\alpha)} + E_{31}^{-1} e^{ik_q(x_3\cos\alpha + y_3\sin\alpha)}\right] \tag{C74}$$

$$w_2^* = \lambda\left[E_{12}^{-1} e^{ik_q(x_1\cos\alpha + y_1\sin\alpha)} + E_{22}^{-1} e^{ik_q(x_2\cos\alpha + y_2\sin\alpha)} + E_{32}^{-1} e^{ik_q(x_3\cos\alpha + y_3\sin\alpha)}\right] \tag{C75}$$

$$w_3^* = \lambda\left[E_{13}^{-1} e^{ik_q(x_1\cos\alpha + y_1\sin\alpha)} + E_{23}^{-1} e^{ik_q(x_2\cos\alpha + y_2\sin\alpha)} + E_{33}^{-1} e^{ik_q(x_3\cos\alpha + y_3\sin\alpha)}\right] \tag{C76}$$

Equations C74, C75 and C76 are of forms involving sums of similar terms. They can be compressed into a single summation equation that looks like

$$w_n^* = \lambda \sum_{m=1}^{3} E_{mn}^{-1} e^{ik_q(x_m\cos\alpha + y_m\sin\alpha)} \qquad \text{for } n = 1,2,3 \tag{C77}$$

This expression is readily manipulated to isolate λ . If both sides of Equation C77 are multiplied by $e^{ik_q(x_n\cos\alpha + y_n\sin\alpha)}$, there results

$$\begin{aligned} w_n^* e^{-ik_q(x_n\cos\alpha + y_n\sin\alpha)} &= e^{-ik_q(x_n\cos\alpha + y_n\sin\alpha)} \lambda \sum_{m=1}^{3} E_{mn}^{-1} e^{ik_q(x_m\cos\alpha + y_m\sin\alpha)} \\ &= \lambda \sum_{m=1}^{3} E_{mn}^{-1} e^{ik_q(x_m\cos\alpha + y_m\sin\alpha)} e^{-ik_q(x_n\cos\alpha + y_n\sin\alpha)} \\ &= \lambda \sum_{m=1}^{3} E_{mn}^{-1} e^{ik_q[(x_m-x_n)\cos\alpha + (y_m-y_n)\sin\alpha]} \qquad \text{for } n = 1,2,3 \end{aligned} \tag{C78}$$

where the exponential multiplier can go inside the summation because the sum is only over index m , and the exponents are combined in the last equality. If the 3 equations represented by Equation C78 are added together, i.e., summed on both sides over index n , the result is

$$\begin{aligned} \sum_{n=1}^{3} w_n^* e^{-ik_q(x_n\cos\alpha + y_n\sin\alpha)} &= \sum_{n=1}^{3} \lambda \sum_{m=1}^{3} E_{mn}^{-1} e^{ik_q[(x_m-x_n)\cos\alpha + (y_m-y_n)\sin\alpha]} \\ &= \lambda \sum_{n=1}^{3} \sum_{m=1}^{3} E_{mn}^{-1} e^{ik_q[(x_m-x_n)\cos\alpha + (y_m-y_n)\sin\alpha]} \end{aligned} \tag{C79}$$

The left side of Equation C79 satisfies the window constraint of Equation C39 so that it equals 1 . This result leaves

$$1 = \lambda \sum_{n=1}^{3} \sum_{m=1}^{3} E_{mn}^{-1} e^{ik_q[(x_m-x_n)\cos\alpha + (y_m-y_n)\sin\alpha]} \tag{C80}$$

or

$$\lambda = \frac{1}{\sum_{n=1}^{3}\sum_{m=1}^{3} E_{mn}^{-1}\, e^{ik_q[(x_m-x_n)\cos\alpha + (y_m-y_n)\sin\alpha]}} \tag{C81}$$

Hence, an expression for λ has been found, and, by virtue of Equation C71, so has an estimate of the frequency-direction spectrum, i.e.,

$$\hat{E}(\sigma_q,\alpha)\,\Delta\theta = \frac{1}{\sum_{n=1}^{3}\sum_{m=1}^{3} E_{mn}^{-1}\, e^{ik_q[(x_m-x_n)\cos\alpha + (y_m-y_n)\sin\alpha]}} \tag{C82}$$

This is the result being sought, a maximum likelihood estimate of the wave variance per frequency increment at frequency σ_q and look direction α.

29. The angle increment $\Delta\theta$ still has not been defined, however. This definition can be found, symbolically at least, by noting that, in practice, Equation C82 is commonly solved for a number of evenly spaced, discrete look angles θ_r defined by

$$\theta_r = r\Delta\theta \qquad \text{for } r = 1,2,\ldots,R \tag{C83}$$

such that, for the 360 degrees or 2π radians of arc that can be examined with a two-dimensional array,

$$\theta_R = R\Delta\theta = 2\pi \tag{C84}$$

from which $\Delta\theta = 2\pi/R$. With this definition of $\Delta\theta$ and the set of discrete directions given by Equation C83, the frequency-direction spectral estimate at frequency σ_q and direction θ_r is

$$\hat{E}(\sigma_q,\theta_r) = \frac{1}{\frac{2\pi}{R}\sum_{n=1}^{3}\sum_{m=1}^{3} E_{mn}^{-1}\, e^{ik_q[(x_m-x_n)\cos\theta_r + (y_m-y_n)\sin\theta_r]}} \tag{C85}$$

Again, nothing has been done in this derivation that precludes adding more gages to the array. Discussion was limited to three gages, mostly so the equation sets and matrix inversion equations would fit into a reasonable amount of space. Extension of the result given by Equation C85 is achieved symbolically by simply changing the upper limits on the sums, so a more general result is

$$\hat{E}(\sigma_q,\theta_r) = \frac{1}{\frac{2\pi}{R}\sum_{n=1}^{N}\sum_{m=1}^{N} E_{mn}^{-1}\, e^{ik_q[(x_m-x_n)\cos\theta_r + (y_m-y_n)\sin\theta_r]}} \qquad \text{(C86)}$$

where N is the number of gages, as before.

30. One must still do some empirical work to pin down $\Delta\theta$ (or R), because the directional resolution of the estimator depends very strongly on both the array design and the nature of the true spectrum that governs the data collected with the set of gages. One should use synthetic data, for which the true spectrum is known, to examine the response of a particular array design. From such results, one can determine the extent to which the array can resolve various wave approach directions, including cases where waves come from several directions at the same frequency. Some very good guidance on proper placement of gages in array design is given by Davis and Regier (1977).

31. Once an array is designed and deployed such that data are obtained, one applies this method by computing the cross-spectra between all gage pairs, forming the cross-spectral matrix E_{mn} for each frequency σ_q, computing the inverse of the cross-spectral matrix, and applying the estimator Equation C86 for each discrete direction θ_r.

32. This method is <u>not</u> constrained to conserve total variance, so when the frequency-direction spectral estimates are integrated with respect to direction, the frequency spectrum is not necessarily recovered completely. There are two common ways to deal with this. The simplest one is to perform the integration with respect to direction at frequency σ_q, compute the ratio of the variance from the frequency spectrum to the result of the integration, and multiply all values of the frequency-direction spectrum at this frequency by the computed ratio. This form of correction distributes the error as a uniform percentage over the entire directional distribution. A second correction method, known as Iterativ. Maximum Likelihood Estimation, is based on a method derived by Pawka (1983). The reasoning of Pawka's method is that if the MLE result is fed back into the estimation algorithm, the result of the second pass tends to be an attenuated form of the first pass. If results from the first pass are multiplied, direction-by-direction, by the ratio of first pass results to second pass results, the new estimate tends to be closer to the true spectrum than the first pass results. Extensive empirical tests by

Pawka indicate that repeated application of this procedure tends to produce an estimator that is much better than the single-pass MLE, not only giving better fidelity to the total variance, but also sharpening resolution in the detailed structure of the directional distribution of variance. The mathematics of this procedure are not discussed here because they are rather well described by Pawka (1983) and by Oltman-Shay and Guza (1984).

33. Thus, this appendix has outlined some of the reasoning and some of the mathematical detail of maximum likelihood estimation of wave directionality when used with a two-dimensional array. Equation C86 was used identically to estimate the frequency-direction spectra discussed in the body of this report.

Appendix D: Notation

Appendix D: Notation

$[\ ]^*$	Complex conjugate of [ ]
a	Wave amplitude
a_n	Amplitude of n^{th} component wave
A	Duration of time
A_q	Fourier series cosine coefficient at q^{th} frequency
B	Span along x-direction
B_q	Fourier series sine coefficient at q^{th} frequency
C	Span along y-direction
C_{mn}	Coincident spectral density between gages m and n
d	Water depth
dd	Mnemonic for two-digit day of the month
D	Complex wave amplitude
$D(f_n, \theta_m)$	Element of directional distribution function at n^{th} frequency and m^{th} direction
D_n	Complex amplitude of n^{th} component wave
E	Frequency-direction spectral density
$\hat{E}$	Estimate of frequency-direction spectral density
E_{mn}	Cross-spectral density between gages m and n
E^{-1}_{mn}	Element of row m and column n of matrix inverse of E_{mn}
E_N	Noise component of frequency-direction spectrum
f	Cyclic frequency
f_n	Cyclic frequency of n^{th} component wave
f_p	Spectral peak frequency
$f_{p,i}$	Peak frequency of incident spectrum
$f_{p,r}$	Peak frequency of reflected spectrum

g	Gravitational acceleration
H	Isolating function
H_{mo}	Spectrum-based characteristic wave height
$H_{mo,i}$	Characteristic height of incident spectrum
$H_{mo,r}$	Characteristic height of reflected spectrum
k	Radian wavenumber
k_n	Wavenumber of n^{th} component wave
m	Index integer
mm	Mnemonic for two-digit representation of month in a calender year
M	Upper limit of indices denoted m
n	Index integer
N	Upper limit of indices denoted n
q	Index integer
Q	Quadrature spectral density
Q_{mn}	Quadrature spectral density between gages m and n
r	Index integer
R	Upper limit of indices denoted r Covariance function
S	Spectral density
$S(f)$	Frequency spectral density
$S(f_n)$	Frequency spectral density at n^{th} discrete frequency
$S(f_n, \theta_m)$	Frequency-direction spectral density at n^{th} discrete frequency and m^{th} discrete direction
$S(\theta)$	Direction spectral density
$S_i(f_n)$	Incident frequency spectral density at n^{th} discrete frequency
$S_r(f_n)$	Reflected frequency spectral density at n^{th} discrete frequency
t	Time

T	Arbitrary displacement in time
T_p	Spectral peak period
$T_{p,i}$	Peak period of incident spectrum
$T_{p,r}$	Peak period of reflected spectrum
w_m	Complex weighting function for Fourier coefficient contribution from gage m
w_{mI}	Imaginary part of w_m
w_{mR}	Real part of w_m
w_n	Complex weighting function for Fourier coefficient contribution from gage n
w_{nI}	Imaginary part of w_n
w_{nR}	Real part of w_n
W	Window function
x	Horizontal cross-shore coordinate
x_m	Cross-shore coordinate of gage m
x_n	Cross-shore coordinate of gage n
X	Displacement or lag in x-direction
X_q	Element of discrete Fourier transform at q^{th} frequency
y	Horizontal longshore coordinate
yy	Mnemonic for two-digit representation of year
yymmdd	Date mnemonic, a concatenation of year, month, and day mnemonics
y_m	Longshore coordinate of gage m
y_n	Longshore coordinate of gage n
Y	Displacement or lag in y-direction
α	Wave direction as fitted by maximum likelihood estimation
Δt	Increment or step in time
$\Delta\sigma$	Increment of radian frequency
$\Delta\theta$	Increment of wave direction

ϵ	Initial wave phase
ϵ_n	Initial phase of n^{th} component wave
η	Sea surface displacement
η_r	Element of sea surface displacement time series at r^{th} time step
λ	Wavelength Lagrange multiplier
θ	Wave direction
θ_m	Element m of a discrete set of wave directions
θ_n	Direction of n^{th} component wave
θ_p	Peak wave direction
$\theta_{p,i}$	Peak direction of incident wave spectrum
$\theta_{p,r}$	Peak direction of reflected wave spectrum
σ	Radian wave frequency
σ_n	Radian frequency of n^{th} component wave
σ_q	Element q of a set of discrete radian wave frequencies
χ	Reflection coefficient based on wave heights
χ_{mo}	Reflection coefficient based on characteristic wave heights
$\chi_{p,i}$	Reflection coefficient at the peak frequency of the incident wave spectrum
$\chi_{p,r}$	Reflection coefficient at the peak frequency of the reflected wave spectrum